

Modeling, Simulation and Control of Rotary Blasthole Drills

Claude E. Aboujaoude

**Department of Electrical Engineering
McGill University, Montreal**

December 1991

**A thesis submitted to the Faculty of Graduate Studies and Research
in partial fulfillment of the requirements for the degree of
Masters of Engineering**

**December 1991
© Claude E. Aboujaoude**

In memory of my brother

Abstract

Few rotary blasthole drills presently used in open pit mines are equipped with automatic control systems. Those drilling control systems which do exist are based mainly on ladder programming techniques. This thesis is an investigation into a closed loop feedback control approach for drilling control.

A model for the plant consisting of the machine's actuators and the drilling process at the bit-rock interface is described based on physical assumptions and past research in this area. The model equations are further refined by experimental (field) testing. The instrumentation of a TAMROCK-DRILTECH D75K drill rig and the subsequent drilling tests aimed at refining the model equations are described, with an in-depth discussion of the field tests results. The analysis is based on regression techniques applied to empirical data, showing the dependencies between the cutting variables and ground conditions during actual drilling. The transfer functions of the mechanical actuators of the machine are also identified.

A strategy for automatic feed pressure control is proposed and developed as a software source code. The controller is tested and tuned by interfacing it to a software simulator of the plant which implements the relationships identified from field testing. The simulation results are discussed. They show that the proposed strategy is viable; however, it is subject to some limitations.

The thesis concludes with suggestions for future research and improvement of the proposed control approach.

Résumé

Le nombre de modèles de foreuses rotatives de très grandes puissance utilisées pour les trous de pré-clivage et dynamitage dans les mines à ciel ouvert présentement dotées d'un système à commande automatique demeure réduit. Cependant, les systèmes qui existent sont basés sur les techniques de programmation étagée (Ladder Programming). Cette thèse traite l'étude d'un nouveau système de commande qui utilise le principe de boucle à rétroaction fermée.

Un modèle mathématique du circuit composé des actionneurs mécaniques et du procédé de forage au niveau de l'interface foret-roche a été déduit des résultats de recherches antérieures dans ce domaine. Dans le but d'améliorer les équations décrites, une foreuse D75K de la compagnie TAMROCK-DRILTECH a été instrumentée et testée dans une mine de charbon à ciel ouvert. Les résultats de ces tests sont analysés en profondeur à l'aide de graphes qui montrent les différentes relations entre les variables concernées et la nature de la roche. Les fonctions de transfer des actionneurs mécaniques ont été également identifiés.

Une stratégie de commande automatique pour la force de pression est présentée sous forme de code source du logiciel C. Le système de commande a été réglé en l'enchainant à un logiciel de simulation du circuit qui incorpore le modèle amélioré, défini d'après les résultats des tests réels. Les résultats des simulations ont prouvé la viabilité de la stratégie proposée, mais ont dévoilé en même temps quelques failles qu'il faudrait contourner.

La thèse est conclue par des suggestions de recherches pour l'amélioration du système de commande proposé.

Acknowledgements

I would like to express my deepest gratitude and appreciation to Dr. Laeeque K. Daneshmend for supervision, guidance and encouragement during the course of this research work.

I am also indebted to Dr. Jonathan P. Peck, Laboratory Manager of the Canadian Center for Automation and Robotics in Mining at McGill University (CCARM-McGill) who administered this work from the beginning to the end. His devotion and hard work made field testing possible under severe time restrictions and budget limitations. His contribution to the success of this research is invaluable and greatly appreciated.

A special gratitude is expressed towards Mr. Rony Philippe who spent a long time developing and debugging the basic structures of the Simulator source code written within ACSL and the controller code written in C, based on initial physical assumptions. The source codes were later refined by the author to account for the continuous progress in empirical relationships and new control ideas and strategies devised during the research period.

I wish to thank TAMROCK-DRILTECH, Florida, USA, for providing financial support during the initial phase of this work and disclosing confidential technical information through the person of Mr. Kari Timperi, project manager. For the help in instrumenting the drill and assistance during field testing, I thank Mr. Jim Hester and Mr. Jim Hancock, the drill driver and expert who run the machine.

The AMAX Delta mine must also be thanked for providing the necessary commodities for field testing, and assistance whenever needed.

I am also grateful to personnel at the TAMROCK Technology center, Tampere, Finland, for highly constructive remarks and for their hospitality during my visit to Finland, June 1991. Specifically, Mr. Rolf Ström, vice president, Mr. Markku Kivipuru research manager, Mr. Pekka Salminen and Mr. Unto Mattero, research engineers.

At McGill university, I thank the McGill Research Center for Intelligent Machines (MCRCIM), the Canadian Center for Automation and Robotics in Mining (CCARM) and the people working there for providing an excellent working environment and computing facilities. The acknowledgement is also extended to the Mining Department.

I am grateful to Mr. Riadh Bouzaienne who patiently gathered the majority of the references, Mr. Andrew Trossman for assisting in hardware development, Dr. Carl Hendricks for his constructive criticism and Ms. Vicky Soltani CCARM's secretary for helping in typing and preparing transparencies used in my numerous presentations

Finally I wish to thank my parents whose endless support helped me throughout the hard times during this work, my girlfriend and all the friends and persons who directly and indirectly contributed to this project but are not mentioned here.

Note on the used Units of Measurements

Throughout this thesis, imperial units of measurements are used. Where appropriate and possible however, the S.I. metric equivalent have been provided. The reason for adopting imperial units is justified by the following:

1. This work is oriented towards technical advances in the drilling industry. However, the majority of the drill manufacturers are in the United States where imperial units are more commonly used.
2. Drilling equipment manufacturers are only recently using metric units. Most past guides and manuals are in imperial units.
3. Pressure gauges on the operator panel of the monitored drill were in both imperial and metric units. However, at the Delta mine, all drilling instructions were given in imperial units.
4. All past rotary drilling investigations and developed models were reported in imperial units.

On this basis, it was decided to maintain imperial units for all subsequent data presentation and calculations. The following page provides a *Table of Conversion* for imperial units to their metric equivalents.

Table of Conversion; Imperial to Metric

| Imperial | × factor | Metric |
|----------|----------|----------|
| ft | 0.3048 | m |
| in | 25.4 | mm |
| ft/hr | 0.3048 | m/hr |
| psi | 0.069 | MPa |
| lbs mass | 0.4536 | Kgs mass |
| rev/min | 0.1047 | rd/s |
| ft-lb | 1.36 | N.M |

Contents

| | |
|---|-----------|
| 1 INTRODUCTION | 1 |
| 1.1 Blasthole Drills | 1 |
| 1.2 Automatic Control Objectives: Problem Definition | 4 |
| 1.3 Methodology | 5 |
| 1.4 Thesis Overview | 6 |
| 2 LITERATURE SURVEY | 7 |
| 2.1 Overview | 7 |
| 2.2 Drilling Process Modeling | 7 |
| 2.2.1 Selected Models | 9 |
| 2.3 Blasthole Drilling Control | 9 |
| 2.3.1 Bucyrus-Erie Control system | 11 |
| 2.3.2 Gardner-Denver Control System | 12 |
| 2.3.3 Marion Control System | 13 |
| 2.4 Summary | 13 |
| 3 SYSTEM MODELING | 15 |
| 3.1 Rotary Drill Bits | 16 |
| 3.2 The "Perfect Cleaning" Model for Penetration Rate | 17 |
| 3.2.1 Penetration Rate Formula | 20 |
| 3.2.2 Imperfect Cleaning Relationship | 21 |

| | | |
|----------|--|-----------|
| 3.2.3 | More Recent Models for Penetration Rate | 22 |
| 3.3 | Modeling Torque | 23 |
| 3.3.1 | Energy Balance Concept | 23 |
| 3.3.2 | Force Balance Concept | 24 |
| 3.4 | System Identification Methodology | 27 |
| 4 | EXPERIMENTAL TESTING | 28 |
| 4.1 | Introduction | 28 |
| 4.1.1 | Objectives | 28 |
| 4.2 | Monitored Parameters | 29 |
| 4.3 | Experimental Testing Instrumentation | 38 |
| 4.3.1 | TEAC RD-200 PCM Data Recorder | 39 |
| 4.3.2 | Signal Conditioning Subsystem | 39 |
| 4.4 | Choice of Field Site | 41 |
| 4.4.1 | Geophysical Logging | 41 |
| 4.5 | Field Test Methodology | 43 |
| 4.5.1 | Machine Dynamics | 43 |
| 4.5.2 | Bit-Rock Interface Model | 44 |
| 5 | EXPERIMENTAL DATA ANALYSIS | 52 |
| 5.1 | Analysis Environment | 52 |
| 5.1.1 | Digitization Hardware | 52 |
| 5.1.2 | Analysis Software | 53 |
| 5.2 | Fitting a Model for Penetration Rate | 56 |
| 5.3 | Analysis of Penetration Rate Data | 58 |
| 5.4 | Analysis of Penetration Per Revolution Data | 63 |
| 5.4.1 | Computing Penetration Per Revolution | 64 |
| 5.4.2 | Graphical Analysis of Penetration Per Revolution | 64 |
| 5.5 | Fitting a Model for Torque | 66 |

| | | |
|----------|--|------------|
| 5.6 | Analysis of Disturbance Pressure Data | 71 |
| 5.7 | Conclusions | 77 |
| 6 | IDENTIFYING THE D75K DRILL DYNAMICS | 80 |
| 6.1 | Objectives | 80 |
| 6.2 | Rotary actuators dynamics | 80 |
| 6.2.1 | Effect of Bit Loading on Rotary Speed | 82 |
| 6.3 | Feed actuator Dynamics | 83 |
| 6.4 | Conclusion | 85 |
| 7 | CONTROLLER DESIGN | 86 |
| 7.1 | Formulation of The Control Strategy | 86 |
| 7.2 | Formulation of The High Bandwidth Inner Control Loop | 87 |
| 7.2.1 | Control Philosophy | 89 |
| 7.2.2 | Stability Considerations | 89 |
| 7.2.3 | Penetration Per Revolution Feedback Control Loop | 90 |
| 7.2.4 | Rotation Pressure Controller | 91 |
| 7.3 | Feedback Controllers Structure | 93 |
| 7.3.1 | Proportional Control | 94 |
| 7.3.2 | Integral Control | 94 |
| 7.3.3 | Derivative Control | 95 |
| 7.3.4 | PID Control | 95 |
| 7.3.5 | Controller Implementation | 95 |
| 7.4 | Controller Testing and Tuning | 97 |
| 7.5 | Simulating the Plant | 98 |
| 7.6 | Plant Block Diagram | 99 |
| 8 | SIMULATION RESULTS | 101 |
| 8.1 | Testing The Plant | 101 |
| 8.2 | Testing and Tuning Controller | 102 |

| | |
|--|------------|
| 8.3 Conclusion | 112 |
| 9 Conclusion | 113 |
| 9.1 Achievements | 113 |
| 9.2 Primary Research Contribution | 114 |
| 9.3 Industrial Relevance | 115 |
| 9.4 Recommendations for Further Work | 116 |

List of Figures

| | | |
|------|--|----|
| 1.1 | Elements of surface drilling | 2 |
| 1.2 | a) TAMROCK-DRILTECH D75K blasthole drill, b) Detail of drill mast and motor head assembly. | 3 |
| 1.3 | Control panel of the TAMROCK-DRILTECH D75K blasthole drill . . | 4 |
| 3.1 | Modeling the overall drilling process | 16 |
| 3.2 | Smith International Soft Formations tricone bit, model Q2J (after the Smith International 1989-1990 bit sales brochure) | 17 |
| 3.3 | Crater formation mechanism (after Maurer) | 18 |
| 3.4 | Analogy between rolling resistance of wheel and two dimensional cutter (after Warren) | 25 |
| 4.1 | D75K Feed system | 30 |
| 4.2 | Measurement of rotary speed | 32 |
| 4.3 | Measurement of rotary torque | 34 |
| 4.4 | Location of vibration sensors on the drill motor head assembly . . . | 37 |
| 4.5 | Block diagram showing experimental testing setup | 38 |
| 4.6 | Experimental Testing Instrumentation Layout | 40 |
| 4.7 | Test bench borehole layout; Delta Mine | 41 |
| 4.8 | Stratigraphy for borehole B3; Delta Mine | 43 |
| 4.9 | North-South sections of geology; Delta mine | 47 |
| 4.10 | East-West sections of geology; Delta mine | 48 |

| | | |
|------|---|----|
| 4.11 | Field Instrumentation. Top: Linear displacement (horizontal) and feed pressure (vertical) transducers; Bottom: Bailing air pressure transducer. | 49 |
| 4.12 | Top: Displacement transducer. (fixed on the upper horizontal frame); Bottom: The DAT recorder and the signal conditioning unit at the experiment site | 50 |
| 4.13 | TAMROCK-DRILTECH D75K during experimental testing at the Delta mine. | 51 |
| 5.1 | General Scheme for Office Data Digitization and Processing | 53 |
| 5.2 | Example of test signals | 55 |
| 5.3 | Young's Moduli for boreholes H2 and N5, as provided by the geophysical logging company | 57 |
| 5.4 | Penetration rate in Brereton and Bankston Fork Limestone plotted against feed pressure and rotary speed | 59 |
| 5.5 | Penetration rate in Sandy and Lawson Shales plotted against feed pressure and rotary speed | 60 |
| 5.6 | Penetration rate in Anvil Rock Sandstone plotted against feed pressure and rotary speed | 61 |
| 5.7 | $\frac{R}{N}$ in Brereton and Bankston Fork limestone plotted against feed pressure and rotary speed | 67 |
| 5.8 | $\frac{R}{N}$ in Sandy and Lawson Shales plotted against feed pressure and rotary speed | 68 |
| 5.9 | $\frac{R}{N}$ in Anvil Rock sandstone plotted against feed pressure and rotary speed | 69 |
| 5.10 | P_{dist} model for Bankston Fork Limestone, Brereton Limestone and Anvil Rock Sandstone | 72 |
| 5.11 | P_{dist} model for Sandy Shale and Lawson Shale | 73 |
| 5.12 | P_{dist} in Brereton and Bankston Fork Limestone plotted against feed pressure and rotary speed | 74 |

| | |
|---|-----|
| 5.13 P_{dist} in Sandy and Lawson Shales plotted against feed pressure and rotary speed | 75 |
| 5.14 P_{dist} in Anvil Rock Sandstone plotted against W and N | 76 |
| | |
| 6.1 Rotary actuators response with step inputs | 81 |
| 6.2 Rotary actuator response: actual and simulated | 82 |
| 6.3 Effect of bit loading on rotary speed | 83 |
| 6.4 Feed actuator response in two different rock types | 84 |
| | |
| 7.1 The Two Tier Control Strategy | 87 |
| 7.2 Penetration per revolution and rotation pressure controllers block diagram | 92 |
| 7.3 Block diagram of PID controller implementation | 97 |
| 7.4 The Blasthole Drilling Simulator Block Diagram | 98 |
| 7.5 Plant block diagram | 100 |
| | |
| 8.1 Actual and Simulated feed and rotation pressures in Anvil Rock Sandstone | 103 |
| 8.2 Actual and Simulated rotary speed and penetration rate in Anvil Rock Sandstone | 104 |
| 8.3 Simulation results of controller and plant at constant rotary speed, with $K_P = 4000$, $K_I = 500$ and $K_V = 50$ | 105 |
| 8.4 Simulation results of controller and plant at constant rotary speed, with $K_P = 7500$, $K_I = 1000$ and $K_V = 200$ | 107 |
| 8.5 Simulation results of controller and plant at variable rotary speed, with $K_P = 4000$, $K_I = 500$ and $K_V = 50$ | 109 |
| 8.6 Simulation results of controller and plant at variable rotary speed, with $K_P = 2000$, $K_I = 350$ and $K_V = 50$ | 111 |

List of Tables

| | | |
|-----|---|----|
| 4.1 | Test Sequence Followed in the field | 45 |
| 5.1 | Penetration rate fit in five different rock types | 58 |
| 5.2 | $\frac{R}{N}$ in five different rock types | 64 |
| 5.3 | P_{dist} evaluated in five different rock types, using Warren's model . . . | 71 |
| 5.4 | P_{dist} evaluated in five different rock types, using an arbitrary model . | 77 |

Chapter 1

INTRODUCTION

1.1 Blasthole Drills

The mining industry uses blasthole drills for drilling holes that can be loaded with explosives to fragment the rock. The fragmented material is then excavated by other mine equipment such as shovels, draglines, front end loaders etc. In addition, in certain operations where a knowledge of bench geology is required in advance of explosive loading, the holes are used to introduce various geophysical instrumentation (e.g. gamma, sonic and neutron logging) into the rock mass towards identifying variations in lithology along the hole length [10]. Such information is critical to the accurate placement of explosive charges within the hole. For example, in coal mining, it is important that explosives not be positioned adjacent to soft coal seams which would otherwise result in complete pulverization of the coal and dilution of it with the surrounding waste rock , rendering the ore irretrievable.

The drilling concept is illustrated in Fig. 1.1. A bit rotating under a feed force breaks the rock and generates small cuttings called *chips* that are removed from the hole by flushing air. In addition, percussion power could be used to assist in the breakage process. These basic concepts are implemented in modern drills, in a broad line of models and categories designed to meet the needs of individual mining

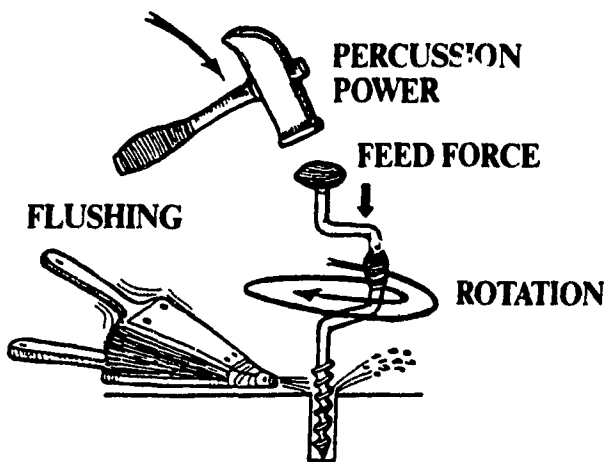


Figure 1.1: Elements of surface drilling

operations. For example, different machine design criteria apply to underground and open pit mines. Drills using percussion are called *percussive drills*, non percussive machines are referred to as *rotary drills*.

Figure 1.2a shows a rotary drill, model D75K from TAMROCK-DRILTECH (USA). Rotation is generated by two hydraulic motors fixed onto a frame (motor head assembly) that can slide along the length of the mast (see Fig. 1.2b). The motors drive a spindle sub (encircled, Fig. 1.2b) which connects to a steel rod via threading at one end, the other end threaded to the bit. The drill motor head assembly is pulled up and down by feed chains powered by two hydraulic cylinders. The pulldown force is controlled by adjusting the feed pressure to the hydraulic cylinders. The resulting vertical force at the bit level is the weight-on-bit. Three extra steel rods are stored in a carousel type rod changer. When the first steel rod is driven down the hole over its entire length, the driver disconnects it from the spindle sub by rotating the motors in reverse direction. He then moves the carousel into the loading position to add another steel rod on top of the previous one then resumes drilling. The steel column composed of one or more steel rods connecting the spindle sub to the bit is referred to as *drill string*.

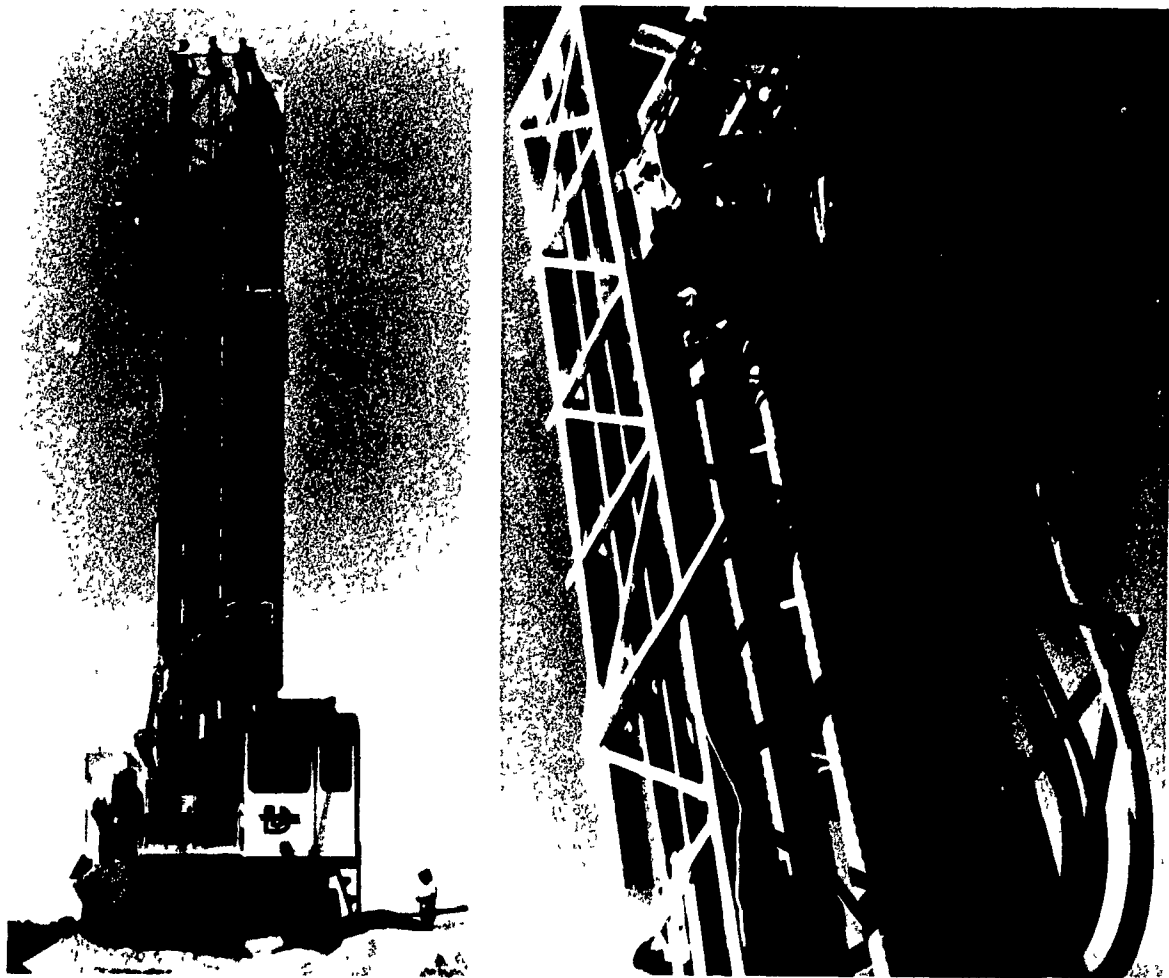


Figure 1.2: a) TAMROCK-DRILTECH D75K blasthole drill, b) Detail of drill mast and motor head assembly.

The *drilling cycle* consists of positioning the entire drill over the designed location of the blasthole and leveling the machine by lowering three independently controlled jacks. The operator then loads the first steel rod, pulls down the motor head assembly until the bit reaches ground level, starts rotation slowly while exerting a modest pulldown force (moderate feed pressure) until the bit reaches a depth of approximately fifteen feet (5 meters). The process of drilling smoothly the first 15 ft is called *collaring* the hole, and is essential to avoid deviation in the hole trajectory.

After collaring, the drill operator adjusts the rotary speed and the feed pres-

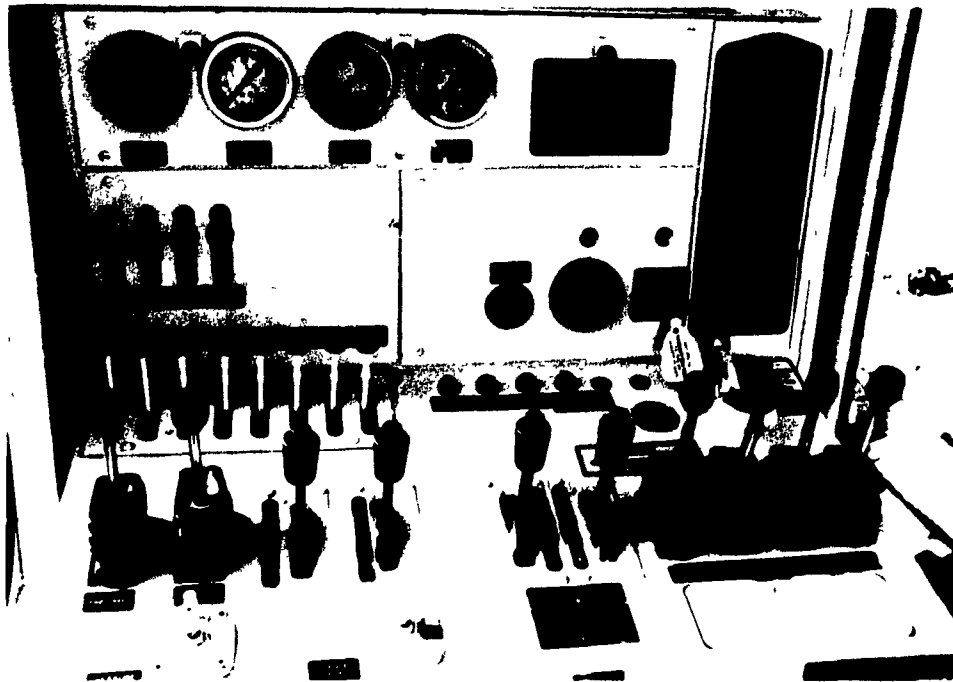


Figure 1.3: Control panel of the TAMROCK-DRILTECH D75K blasthole drill

sure to enable maximum production footage while trying to secure the longest possible bit life and keeping downtime and maintenance cost at a minimum. The driver's reaction is mainly based upon visual information from gauge displays of rotary speed, feed pressure, rotation pressure (which is responsible for torque generation), bailing air pressure, condition and size of flushed chips as well as noise and vibration levels.

1.2 Automatic Control Objectives: Problem Definition

The drilling industry is becoming increasingly competitive and the machine manufacturers are continuously exploring ways of reducing drilling costs and enhancing machine productivity through the application of automatic control.

The D75K drill as shown in Fig 1.3 is manually controlled. Upon examination of the various functions and motions performed by the blasthole rig, it has been clear

that the greatest demand for operator skill is during the actual drilling phase, where the operator is seen to continually adjust the feed pressure and rotary speed according to the changing nature of the material being drilled.

It had been proposed that an initial automatic control strategy would be oriented towards controlling the rotary drill during this drilling phase. This goal can be fulfilled by providing automatic control of rotary speed and feed pressure once the drill has been positioned and the hole has been collared.

The present thesis is focused towards the analysis and development of a viable control strategy, during the drilling phase. The behaviour of the D75K drill has been studied in depth, starting from theoretical assumptions up to experimental validation. A simulation model of the machine and the drilling process has been developed, based on experimental results, then implemented as a software program on a PC computer. A control strategy has been formulated and a control algorithm for controlling feed pressure has been devised. The control algorithm has been implemented as a C source code program, and interfaced with the drilling simulator for validation, fine tuning and testing. Simulation results are also included in this thesis.

The rotary speed remains manually controlled by the operator. At this stage, the proposed algorithm can be seen as a controller that simplifies the control action of the operator from adjusting feed pressure and rotary speed to just controlling rotary speed. The development of an algorithm for the control of rotary speed will be pursued as Ph.D. level research by the author.

1.3 Methodology

The methodology followed in the course of this research for developing and refining the control algorithms is centered on the concept of understanding the process to be controlled. This approach is summarized with the following points:

1. Derive fundamental models of the drilling process based on physical relationships and validate them with experimental data.
2. Based on the validated models, design control algorithms capable of meeting the specified objectives.
3. Validate and refine control algorithms through simulation, to stage of readiness for field trials.

1.4 Thesis Overview

The organization of this thesis is as follows: Chapter 2 surveys past work and achievements in drilling control, then chapter 3 describes a mathematical model of the drilling system. Chapter 4 deals with the instrumentation of a TAMROCK-DRILTECH D75K drill rig, for the purpose of validation and refinement of the proposed drilling models, concurrently enabling a thorough understanding of the D75K machine. The test methodology and actual experimentation involved are also explained in this chapter. Chapter 5 is concerned with the analysis of the experimental data related to variables at the bit-rock interface, while chapter 6 identifies the D75K actuator dynamics. Chapter 7 addresses the formulation and design of the control strategy, based on the results of experimental data analysis. The topic of building a blasthole drilling software simulator is also covered. Simulation results of the designed controller and simulator are discussed in chapter 8. Chapter 9 concludes the thesis and provides recommendation for improvement and further research areas.

Chapter 2

LITERATURE SURVEY

2.1 Overview

The main objectives of past attempts to develop control strategies for drills in the petroleum and mining industries were aimed at minimizing or eliminating human errors in the drilling cycle while maximizing production rates at minimum cost.

2.2 Drilling Process Modeling

Theoretical research into tricone rock drilling control and optimization attempted to develop a unified model of the drilling system. This approach was based upon the concept that the greater the knowledge and understanding of a system, then the better it can be controlled and optimized.

In the petroleum industry, results obtained from both laboratory and oil field testing were used to evaluate the relationships between the drilling variables of rotary speed, rotary torque, weight-on-bit and the rate of penetration. The formulated equations generally describe the dependent variables of penetration rate and torque in terms of the controlled variables of weight-on-bit and rotary speed for a given rock type. These equations can be used towards understanding the interdependence of

drilling variables and for simulating a drilling operation. Their scope, however, is limited to the particular geology, drill, bit type and flushing characteristics used in their definition. In all cases, the results should be considered to be specific to the set of assumptions and conditions on which these investigations were based. In addition, extensive field and/or laboratory tests and analyses are required to determine the correct coefficients for these equations.

Their findings can be grouped in three categories:

1. Transmission line effect with an end impedance section [14, 15].

The transmission line consists of surface structures, drill string, its interaction with the borehole and the flushing system. The end impedance model provides the rock/bit response to the applied weight-on-bit and rotary speed based on rock fracture energy concepts, and is represented as a "non-ideal" transformer. The whole system is described by a set of ordinary differential equations. This system is applicable to the petroleum industry and is not adequate for modeling blasthole drilling, due to the difference in hole length which results in diminished relevance of transmission line effects.

2. Rock/bit interaction and rock fracture behavior.

Theoretical approaches, based upon the stress and failure mechanisms of rock under applied load of individual bit inserts were attempted. From such studies, it was hoped that a prediction of rock failure could be made with subsequent derivation of a penetration rate. However, factors such as fracture mechanics, bit geometry, rock mass variation, flushing media properties, bit hydraulics, bit loads and additional operating influences that were known or unknown prevented the development of a single analytical model. Therefore, due to these drilling complexities, an approach based on empirical investigations combining both laboratory and field trials was followed. Several models based on this ap-

proach were proposed [6, 13, 18, 27, 36, 39]. Also included were considerations of bit-insert (tooth) wear and bottom hole cleaning [27].

3. Drill performance criteria based on specific energy. Teale [34] proposed the notion of specific energy E_s of a rock, defined as the minimum energy required to crush a unit volume of rock, which was considered a fundamental property of the rock. Several authors used this concept to account for bit torque and estimating the penetration rate by relating specific energy to the energy delivered by the bit [26, 31, 32, 33, 34]. However, based on experimental data, Warren [37] later showed that the efficiency factor relating the bit energy to the rock specific energy is not constant and depends on the rock type and other secondary factors.

2.2.1 Selected Models

The variability associated with ground conditions, degree of bit wear and efficiency of cutting removal makes it too complicated to describe the drilling process by a single static equation.

In the present thesis, the "perfect cleaning" model developed by Maurer (1962) [27] to estimate the penetration rate and the "force balance" model for torque derived by Warren (1984) [37] was selected as a preliminary and basic model of the drilling process due to their simplicity. Both models are explained in depth in the following chapter.

2.3 Blasthole Drilling Control

Little can be reported on blasthole drill rig control because not much has been done in this area. Thus, the work reported in this thesis is of pioneering nature, with the exception of the work undertaken by the manufacturers themselves.

The concept of automatic controls in the oil industry was introduced by Young (1969) [40] in his paper entitled "computerized drilling control", which stimulated the interest of the drilling industry in modernizing its methods by making use of new computer technology.

Control strategies for the oil industry were typically centered on the concept of minimum cost drilling. These theories were based upon a combination of historical data and empirical techniques for selecting optimum weight-on-bits and rotary speeds. This approach required a quantitative evaluation of the variables involved, i.e. drilling rate, bit bearing wear, tooth wear and cost. Rotary torque was also monitored at all times and maintained within preset maximum/minimum limits by continuously adjusting rotary speed and bit weight. The completed system was subsequently used by the Humble Oil Co.

A similar approach was followed in order to automate and control the performance of a diamond drill [16]. The strategy developed sought to maintain the drill and bit system within normal operating conditions in the face of changing rock mass properties, while attempting to maximize penetration rate and minimize bit wear. Their objective was not to demonstrate that automatic control would eliminate the need for an operator, but rather to improve the economics of diamond drilling. This would be achieved through the automation of several drill functions, thereby assisting operators to improve overall performance through increased productivity and reduced drill and bit wear. The control theory involved maintaining acceptable target levels of torque through continuous variation of rotary speed and weight-on-bit. Rate of penetration, monitored within the system, was kept at the maximum permitted without the drill operating outside the lower and upper limit ranges set previously for the other parameters (primarily torque).

In the mining industry and particularly for blasthole drills, these attempts resulted in the design of "automated drill control" packages by manufacturers (Bucyrus-

Erie, Gardner Denver, Marion) to fulfill the immediate needs of the mining industry. By the mid-seventies, these automated control packages were available, based on solid state electronic technology [8, 22, 24]. The control strategies used were constraint violation initiated, with "normal" operating conditions maintained through ad-hoc feedback control using appropriate sensors, current-limit devices and actuators. Operating limits were set by the mine, based on expected ground conditions, bit life and desired production rate.

2.3.1 Bucyrus-Erie Control system

A research program was conducted by Bucyrus-Erie to automate an electric rotary blasthole drill in northern Quebec in 1969 [8]. In limited field trials, a blasthole drill was modified for automated control during the drilling cycle. The automation mode began only after the drill had been positioned and leveled, and stopped when the bit reached its preset depth. Based on results from these trials it was concluded that:

1. Production footage using automation exceeded that from the past;
2. Bit costs per foot were significantly less than the best previous cost records in the same type of material;
3. Periods of severe vibration due to operator attempts to force progress through difficult ground were reduced.

It was indicated, however, that an overall increase in maintenance time occurred with the installed automation package. Further, longer term tests were seen to be necessary to refine the system (hardware and logic), towards eventually reducing downtime and increasing machine availability. The original system incorporated electronic transducers and current-limit devices which fed back drill performance data to a central controller. The system would respond to the monitored signals when preset

drilling and machine parameters were exceeded, through adjustments (individually or combined) to weight-on-bit and water injection rate, rotary speed and bailing air supply [8, 24]. This initial work formed the basis for the commercial development of an automated drilling control package by Bucyrus-Erie. This system was offered as an integral component on both 60R and 61R Series III drills as early as 1971.

A modern PLC-based automation package is currently being offered as a factory installed option on Bucyrus-Erie's new 49R drills. The new PLC systems offer enhanced hardware and software capabilities, a graphical display that replaces the old mechanical gauges, better resolution and scanning speeds, automatic stop at preset depth, a simple automatic leveling control and a system diagnosis feature.

The new PLC systems offer a powerful computing capability: however, since confidential information is not disclosed, it remains unclear whether closed loop continuous control is applied or not.

2.3.2 Gardner-Denver Control System

Similar systems were also developed by Gardner-Denver for their line of GD-120/130 rotary blasthole drills. The Gardner-Denver *programmed control package* offered several different hardware configurations depending upon the need of the customer. The basic control hardware operates by initially setting targets for variables such as rotary speed, weight-on-bit and feed rate to which the system would then seek to attain. The machine operator would set the drill bit on the bench, turn on the bailing air, set the desired depth of hole and initiate the automatic sequence. Once automatic control was set, the drill would collar for a preset number of minutes, then the system would attempt to achieve the target levels of the variables. As the weight-on-bit, rotary speed and feed rate increased at a controlled rate, the feedback of torque, vibration and bailing air pressure responses due to changing ground conditions, would result in modifications to the control system. If torque exceeded its preset value, while

weight-on-bit and feed rate were at acceptable levels, the controller would begin to reduce weight-on-bit at a controlled rate while allowing rotary speed to still seek its previously set value. If bailing air pressure began to rise, the controller would also reduce weight-on-bit and begin to limit feed rate. If vibration levels (measured in both axial and lateral directions) increased above preset thresholds, the rotary speed only would begin to be reduced at a controlled rate. The system would eventually stabilize at some value of rotary speed, weight-on-bit and feed rate which was as close to the originally preset limits as possible. This basic automation system is still available, not as retrofit equipment, but only as a factory installed option on new drills [5, 22].

2.3.3 Marion Control System

The Marion control system for the M-4 and M-5 crawler rig was based on consideration that automation of only the primary drill functions was necessary to optimize drill performance, and that such a system should serve to enhance rather than substitute for the driller's skills. The Marion system thus controls only the variables of weight-on-bit, bailing air pressure and torque. Limits for each of these are preset into the system, and are determined based upon ground conditions, projected rotary bit life and desired rate of production. The system was aimed at achieving maximum productivity in terms of increased drilling footage with lower downtime and maintenance costs, while reducing operator abuse of the equipment [22, 24]. An upgraded system, providing similar control functions to the original unit is available from Marion as an integral component on new drills.

2.4 Summary

In the systems reviewed above, complex control problems still appear to exist. Presently, experienced drill operators can identify, by "feel" the changing nature of the ground

being penetrated, and thus make adjustments to both the rotary speed and weight-on-bit in order to achieve optimum drill performance. However, if automation is to be successfully implemented, then the skills of the operator must be emulated by the control system, in order to modify the drilling functions. This logic can only be developed through detailed analysis and understanding of the interactions between the bit and the material through which it is penetrating.

Chapter 3

SYSTEM MODELING

It is essential to gain sufficient understanding of the overall drilling process and its behavior in order to design a control scheme which achieves some specific objectives. Thus, an appropriate model of the overall drilling process needs to be developed, allowing computer simulation.

A computer simulator is desirable in order to develop and initially validate any control scheme, particularly for a system that has complex dynamics which are difficult to characterize and assess analytically.

The break down of the overall "normal" drilling process is illustrated in Fig. 3.1. The machine operator is continuously changing the rotary speed and feed pressure inputs to the machine. These levels are transmitted to the bit, through the machine mechanics.

The bit-rock interface can be viewed as a multivariable system, where $P()$ is a function of ground conditions, rock type, bit type, bit wear, etc. The inputs to $P()$ are the weight-on-bit, rotary speed and bailing air pressure. The outputs will primarily consist of bit penetration rate, torque demand, vibration excitation, bailing air pressure rise if broken rocks are blocking the bit openings, and other secondary variables.

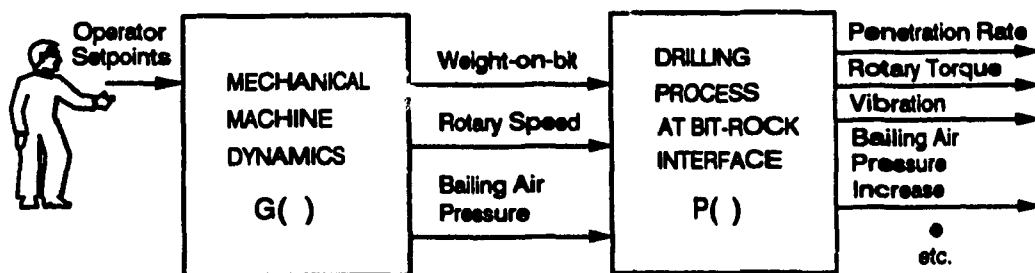


Figure 3.1: Modeling the overall drilling process

A starting point in developing a model for $P()$ is the analysis of the physics of the process. Such physical models tend to be overly complex in that it is often difficult to parameterize them for a restricted data set. Also, they often attempt to capture much finer details than are required for the purposes of controller design and evaluation.

3.1 Rotary Drill Bits

The following is an overview of the tricone bits used in rotary drilling.

Tricone bits consist of three conic shaped rollers each having arrays of tungsten-carbide inserts (teeth) aligned in several rows (usually four). The cones have different geometry and are designed to rotate about a fixed axis. The inserts are extremely resistant to abrasive wear and breakage and give consistent performance during the bit life. The insert length is usually row and cone dependant. Figure 3.2 shows a bit from Smith International, model Q2J.

These bits may have a slight shearing action in soft rock formations, but primarily operate to break the rock into chips by indentation of the inserts under an applied force (weight-on-bit) and rotating action. The distance between adjacent insert rows is designed to create a free surface which allows the chips to propagate



Figure 3.2: Smith International Soft Formations tricone bit, model Q2J (after the Smith International 1989–1990 bit sales brochure)

and be removed without being completely ground.

The bits differ from one another by geometry, diameter, shape of inserts and inserts length. Bits designed for hard rock formations have short ovoid-shaped inserts while soft formations bits have longer tooth-shaped inserts.

3.2 The "Perfect Cleaning" Model for Penetration Rate

There have been numerous drilling models presented in the literature over the years to relate the various mechanical factors involved in the drilling process to the penetration rate. These studies were mainly developed for the oil industry, where very long, deep holes were considered, with water used as flushing fluid, in contrast to compressed

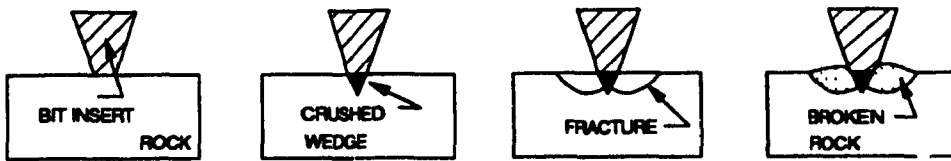


Figure 3.3: Crater formation mechanism (after Maurer)

air used in most rotary blasthole drills. The model selected here was presented by Maurer [27] in the context of petroleum engineering. Maurer proposed a "perfect cleaning" model based on studies of single-insert impacts.

Crater formation

When a bit insert impacts a rock, the rock is elastically deformed until the crushing strength of the rock is exceeded, at which time a wedge of crushed rock is formed below the insert [20, 30] (see Fig. 3.3 after Maurer [27]). As additional force is applied to the insert, the crushed material is compressed and exerts high lateral forces on the solid material surrounding the crushed wedge [17]. When these forces become sufficiently high, i.e. exceed the compressive strength of the rock, fractures are propagated to the free surface of the rock. The trajectories of these fractures intersect the principal stresses at a constant angle [7, 26, 30], as predicted by Mohr's and Griffith's theories of failure.

It has been experimentally shown [20, 26, 30, 38] that the volume of an impact crater V_c varies as:

$$V_c \propto E_c \quad (3.1)$$

where E_c is the total energy imparted to the rock during the formation of the crater. Maurer has also shown that for craters produced in rock by impacting spheres,

$$V_c \propto X^2 \quad (3.2)$$

where X is the depth of penetration, or crater depth. It has also been demonstrated

[30] that the same relationship holds for craters produced in by penetrating wedge-shaped chisels into rock.

The energy used in crater formation is given by:

$$E_v \propto \int_0^X F(u)du \quad (3.3)$$

where F is the force on the insert and u is a "dummy" variable. From Eqs. 3.1, 3.2 and 3.3,

$$X^2 \propto \int_0^X F(u)du \quad (3.4)$$

Differentiation of Eq. 3.4 with respect to X yields

$$X \propto F(X) \quad (3.5)$$

In the case of blunt inserts, a threshold force F_o is required before penetration begins, and the relationship in Eq. 3.5 becomes

$$\begin{cases} X \propto F - F_o & \text{for } F \geq F_o \\ X = 0 & \text{for } F \leq F_o \end{cases} \quad (3.6)$$

A good correlation has been found [19, 27] between the crater depth and the reciprocal of both the shear strength and the compressive strength of the rock. It is assumed that with constant force on the tooth,

$$X \propto \frac{1}{S} \quad (3.7)$$

where S is defined as the drillability strength of the rock. Combining Eqs. 3.2, 3.6 and 3.7,

$$\begin{cases} V_c \propto \frac{(F-F_o)^2}{S^2} & \text{for } F \geq F_o \\ V_c = 0 & \text{for } F \leq F_o \end{cases} \quad (3.8)$$

which shows that the crater volume varies directly as the effective force squared and inversely as the strength squared when the force on the tooth exceeds the threshold force.

3.2.1 Penetration Rate Formula

When the bit travels a distance Y , the total volume excavated is equivalent to the volume of a cylinder with height Y and base area equal to $\pi D^2/4$, where D is the diameter of the bit. The total volume V of rock removed is given by:

$$V = Y \frac{\pi D^2}{4} \quad (3.9)$$

Rearranging Eq. 3.9 and differentiating with respect to time, we get:

$$R = \frac{dY}{dt} = \frac{4}{\pi D^2} \frac{dV}{dt} \quad (3.10)$$

where R is the penetration rate and equivalent to dY/dt .

When all of the broken rock is removed from the craters between impacts,

$$V = nV_c \quad (3.11)$$

where n is the number of impacts. The condition where no regrinding occurs under the bit is defined by Maurer as *perfect cleaning*. The total volume of each crater as defined in Eq. 3.8 is independent of time. Thus,

$$\frac{dV}{dt} = \frac{dn}{dt} V_c \quad (3.12)$$

The rate at which the inserts are impacting is;

$$\frac{dn}{dt} = IN \quad (3.13)$$

where I is the number of impacts per revolution and N is the rotation speed. The effective force on the insert can be expressed as;

$$F - F_o = \frac{(W_{bit} - W_{bito})}{n_t} \quad (3.14)$$

where W_{bit} is the weight-on-bit, W_{bito} is the threshold weight required before the inserts penetrate the rock and n_t is the number of inserts in contact with the rock.

when there is maximum force per insert. From Eqs. 3.8 through 3.14,

$$\begin{cases} R \propto \frac{IN(W_{bit} - W_{bito})^2}{n_t^2 D^2 S^2} & \text{for } W_{bit} \geq W_{bito} \\ R = 0 & \text{for } W_{bit} \leq W_{bito} \end{cases} \quad (3.15)$$

The stipulation that $R = 0$ for $W_{bit} \leq W_{bito}$ is only a first approximation since some rock is removed by abrasion and R does not vanish completely until $W_{bit} = 0$. It is assumed that the constant I varies approximately as the area of the bit, and n_t varies as the bit diameter. The ratio I/n_t^2 will thus be assumed independent of bit size, and Eq. 3.15 becomes:

$$R \propto \frac{N(W_{bit} - W_{bito})^2}{D^2 S^2} \quad \text{for } W_{bit} \geq W_{bito} \quad (3.16)$$

Because of the large bit weights and the low strengths of soft and medium-hard formations, Maurer assumes that $W_{bit} \gg W_{bito}$, in which case Eq. 3.16 reduces to:

$$R = k \frac{NW_{bit}^2}{D^2 S^2} \quad (3.17)$$

Equation 3.17 is the penetration rate formula for *perfect cleaning*. The constant k has the dimensions of reciprocal distance, and depends upon several parameters such as rock properties, mud properties, pressure conditions, bit dullness and bit design. Maurer further suggests that for a given bit at a given depth, k should remain constant if *perfect cleaning* is obtained.

3.2.2 Imperfect Cleaning Relationship

According to Maurer, when a bit is drilling under imperfect cleaning conditions and the weight-on-bit or rotary speed is raised, the penetration rate increases. The increase in penetration rate is accompanied by a corresponding increase in broken rock and thus in the cleaning problem. For this reason the rate of increase in the penetration rate as a function of weight-on-bit or rotary speed is smaller than that which would be expected under perfect cleaning conditions.

After conducting a series of tests, Maurer concluded that

$$R \propto \frac{W_{bit}^x N^y}{D^z} \quad (3.18)$$

where x, y and z are adjustable constants, and should be smaller than the corresponding exponents in Eq. 3.17.

3.2.3 More Recent Models for Penetration Rate

Cunningham [6] (1978) suggested that a close correlation between compressive strength and penetration rate does not exist. He developed a *drilling strength* variable (σ_d) from experimental data, defined as a single physical property of formations drilled. The suggested model was as follows:

$$R = \frac{W_{bit}^x N}{0.424\sigma_d} \quad (3.19)$$

where $x = (0.178254 \ln \sigma_d + 1.09793)$.

Down hole field data reported by Cunningham indicate that penetration rate is nearly proportional to the weight-on-bit. However, for fixed weight-on-bit,

$$R \propto N^y \quad y < 1 \quad (3.20)$$

with y about 0.6 for very soft formations and about 0.85 for harder formations.

Warren [36] (1981) suggested that the deviation of field data from Maurer's model will occur under all reasonable hydraulic conditions for soft formations, not only because of inadequate hole cleaning. He also showed that Cunningham's model failed to match his experimental data, and consequently developed his own model presented as follows:

$$R = \left(\frac{aS^2 D^3}{N^b W_{bit}^2} + \frac{c}{ND} \right)^{-1} \quad (3.21)$$

where a, b, c are constants and S is representative of rock strength.

The model has been tested by the author and failed to fit the experimental data presented in this thesis.

Based on Eqs. 3.18, 3.19 and Warren's suggestions about the inherent imperfect cleaning problem, it can be concluded that within the same rock formation, using the same type of bit,

$$R = KW_{bit}^x N^y \quad (3.22)$$

where K is a constant which accounts for rock physical properties and bit type. The perfect cleaning model is a particular case of Eq. 3.22 when $x = 2$ and $y = 1$.

3.3 Modeling Torque

3.3.1 Energy Balance Concept

The literature has several references that discuss the energy utilized by a roller tricone bit in drilling rock [26, 31, 32, 33, 34]. These articles typically relate the mechanical work done by the bit to the energy required to crush a given volume of rock.

The energy E_v required to crush the volume of rock drilled in a unit increment of time is expressed as

$$E_v = \frac{\pi}{4} D^2 R E_s \quad (3.23)$$

where E_s is specific energy of the rock, D is hole diameter and R is penetration rate.

The total work done by the bit in the same unit time interval is given by

$$w_t = W_{bit} R + 2\pi N T \quad (3.24)$$

where W_{bit} is the weight-on-bit, N is rotary speed, and T is torque applied to the bit. The bit torque used in Eq. 3.24 is the time-averaged torque required to rotate the bit under steady state conditions.

Not all the energy applied to a bit is effective in creating new bore hole volume. The amount of energy used to crush a fixed volume of rock is strongly related to the size of chips generated [33]. Some energy is dissipated into the unbroken rock around the bore hole while the rock strength is being exceeded to form chips [31]. Energy may be used to further reduce the chip size (regrinding) and remove the broken rock from under the bit (bailing). Equations 3.23, 3.24 can therefore be equated by adding an efficiency factor η to account for nonproductive energy loss. The torque is then given by

$$T = \frac{\frac{D^2 E_s R}{\eta \pi} - WR}{2\pi N} \quad (3.25)$$

The usefulness of Eq. 3.25 depends largely on η having a reasonably constant value or at least a value that can be determined from other known parameters.

After conducting a series of controlled tests in two different rock materials, Warren [37] found that η increased by a factor of 3.7 in Carthage marble as the weight-on-bit increased from 5145 to 56,067 lbf (22.9 to 249.4 kN). An opposite effect was observed in Indiana Limestone as η decreased by a factor of 2.4 over a similar weight-on-bit increment. Warren concluded that Eq. 3.25 is not accurate enough for any practical use because of problems of quantifying both the specific energy for a particular rock and the drilling efficiency for a particular set of operating conditions.

3.3.2 Force Balance Concept

Warren proposed a different approach by considering a force balance concept rather than an energy balance approach. Bit torque, as used in his paper, is the time averaged torque required to rotate the bit under steady state conditions. The torque that is applied to the bit is resisted largely by the bit face rolling resistance, as shown in Fig. 3.4a. For an undamaged bit, the torque that results from bearing friction inside the cone and friction along the gage surface of the bit are assumed to be negligible.

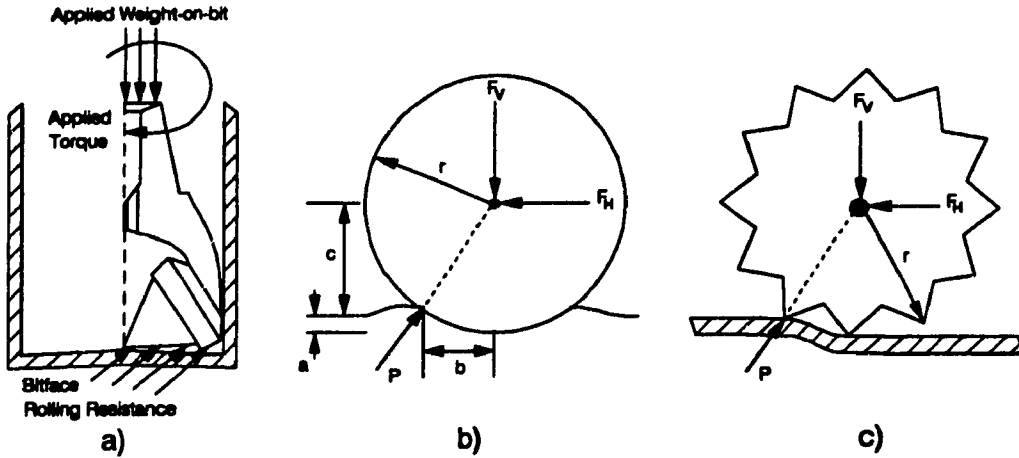


Figure 3.4: Analogy between rolling resistance of wheel and two dimensional cutter (after Warren)

Figure 3.4b is a diagram of the classical rolling resistance of a two-dimensional wheel. F_V is a vertical load applied through the center of the wheel, and a force F_H is required to cause the wheel to roll at a constant speed. The resistance to rolling is caused by a deformation of the wheel and/or the surface over which the wheel rolls. P is the contact reaction and is related to the surface deformation and the magnitude of the vertically applied load. P acts through the center of the wheel, and the frictional resistance at the bearing is assumed to be zero such that there is no moment about the wheel.

An analogy where a two dimensional cutter is represented as a wheel with rolling resistance is shown in Fig. 3.4c. In this case, the surface deformation is caused by the gap between inserts and by insert penetration below the surface.

From geometrical considerations, F_H can be computed as:

$$F_H = F_V \left(\frac{b}{c} \right) = F_V \frac{\sqrt{2ar - a^2}}{r - a} \quad (3.26)$$

The resistance to rolling occurs at the inserts because there is normally no contact between the cone shell and the rock. The analysis is simplified by assuming that three cones with discrete rows of inserts can be combined into a composite cone with

continuous inserts.

The total torque required to rotate the bit can be calculated by integrating the force acting on a circular cross section of the cone. Assuming the maximum radius of the cone is r_{max} and D the bit diameter, then the radius of the cone as a function of the distance x along the borehole radius is given by:

$$r = \frac{2xr_{max}}{D} \quad \text{for } 0 \leq x \leq \frac{D}{2}$$

The weight-on-bit is assumed uniformly distributed along the single cone, and the force dF_V acting on the element because of the applied weight is given by:

$$dF_V = \sin \theta \frac{2W_{bit}}{D} dx \quad (3.27)$$

where W_{bit} is the total applied weight-on-bit and $\sin \theta dx$ is the differential element thickness. Combining Eqs. 3.26, 3.27 and considering that the distance a is much less than the cone radius, we obtain the following expression for dF_H :

$$dF_H = \sin \theta \frac{2W_{bit}}{D} \sqrt{\frac{2a}{r}} dx \quad (3.28)$$

Warren further suggested that the effect of bit cone skew and of insert slip-page from both the cone skew and varying cone angle can be incorporated into the torque relationship by the addition of a constant in Eq. 3.28, as follows:

$$dF_H = \sin \theta \frac{2W_{bit}}{D} \left(C_1 + \sqrt{\frac{2a}{r}} \right) dx \quad (3.29)$$

The total torque that is required to roll the cone about its apex is then given by:

$$T = \sin \theta \frac{2W_{bit}}{D} \int_0^{\frac{D}{2}} \left(C_1 + \sqrt{\frac{2a}{r}} \right) dx \quad (3.30)$$

Assuming that a is proportional to the penetration per revolution and the maximum cone radius r_{max} is proportional to the bit diameter gives:

$$a = C_2 \frac{R}{N}; \quad r_{max} = C_5 D$$

Substituting for a and r_{max} in Eq. 3.30, then integrating and consolidating the constants gives:

$$T = \left[C_3 + C_4 \sqrt{\frac{R}{ND}} \right] W_{bit} D \quad (3.31)$$

where R is the penetration rate, T is torque, N is rotary speed, W_{bit} is weight-on-bit, D is bit diameter, C_3 and C_4 are constants.

Hence, based on the proposed equations, it appears that both penetration rate and torque will be more sensitive to variations in weight-on-bit rather than to variations in rotary speed.

3.4 System Identification Methodology

Since the objective of this project is control, the process modeling to be performed should be designed with respect to the relevant information required for controller analysis and design. The objectives in this case may be summarized as:

1. Model the D75K drill:

- Identify input-output transfer functions

2. Identify the process at the bit-rock interface:

- Identify static (gain) relationships between penetration rate, torque and other variables: input-output and coupling dependencies.
- Identify how the above static and dynamic relationships depend upon operating conditions: operator set-points and rock type.

The objectives mentioned above can be achieved by instrumenting a D75K drill and conducting several experimental tests.

Chapter 4

EXPERIMENTAL TESTING

4.1 Introduction

Experimental testing was considered essential to the development of a realistic model of the drilling process and thus in the building of a computer simulator to be interfaced with a control algorithm. During the period March — May 1990, a TAMROCK-DRILTECH D75K drill rig was instrumented by the author at the factory assembly line in Alachua, Florida. Subsequently, drilling tests were undertaken over a two week period in June 1990 at the AMAX Delta Mine in which data from 10 boreholes, each 140 feet (43 meters) deep, was recorded. The data thus obtained from these tests has been analyzed so as to more fully understand the response of this drill while operating in changing ground conditions.

4.1.1 Objectives

The objectives of the experimental testing may be restated as follows:

1. Determine the D75K hydraulic actuator dynamics.

2. Obtain a model for the process at the bit-rock interface, by attempting to validate the equations defined in the previous chapter using field test data, or to identify new empirical equations.
3. Acquire knowledge about the drilling process dynamics.
4. Acquire knowledge regarding the drill response for specified exceptional conditions.

The results would identify a model for the overall drilling process which can be integrated into a computer software simulator, enabling the design and simulation of the control system.

4.2 Monitored Parameters

It is apparent from earlier analysis that the parameters of interest are:

- Actual weight-on-bit
- Actual rotary speed
- Weight-on-bit set-point
- Rotary speed set-point
- Rotary torque at the bit-rock interface
- Depth
- Penetration rate
- Bailing Air Pressure
- Transverse, longitudinal and axial vibration of rotary motor head assembly

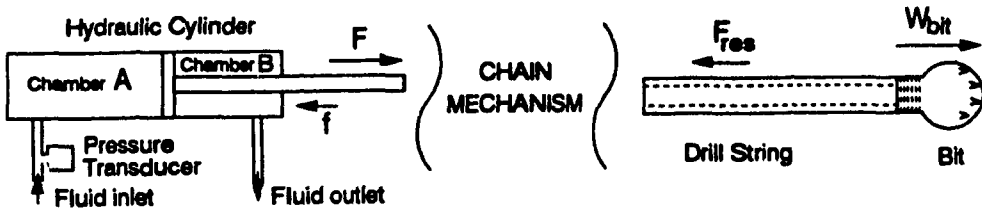


Figure 4.1: D75K Feed system

The bailing air pressure and the vibration data were monitored to study their behavior during normal drilling and to define thresholds values considered as "exceptions". However, these thresholds are not specified in this thesis.

Due to the nature of the drilling process, the majority of the parameters could not be measured at the bit-rock interface. However, other mechanical parameters related to them have been monitored at surface, as described in the following subsections.

Actual Weight-on-Bit

The vertical displacement of the bit is controlled by two hydraulic cylinders that drive the whole motor head assembly, drill string and bit through a chain-driven mechanism, as shown in Fig. 4.1. The feed force F produced by one feed cylinder is given by;

$$F = P_a A_a - P_b A_b - f \quad (4.1)$$

where P_a and P_b are the pressures in chambers A and B , A_a and A_b are the cross sectional areas of the piston at sides A and B , and f the frictional force between the cradle and the rail.

The weight-on-bit W_{bit} is computed from:

$$W_{bit} = F - F_{res} \quad (4.2)$$

where F_{res} is the sum of all forces opposing F and the motion of the piston.

Equating Eqs. 4.1 and 4.2, we obtain:

$$W_{bit} = P_a A_a - P_b A_b - f - F_{res} \quad (4.3)$$

One pressure transducer was installed to measure the pressure of the fluid at chamber A . At idle, with the bit standing still in air (i.e. no load), an average value of 200 psi was measured. Simultaneously, $W_{bit} = 0$ and both F_{res} and f can be neglected in the absence of motion. Replacing these values in Eq. 4.3, we get:

$$0 = P_a A_a - P_b A_b$$

or

$$P_b = 200 \frac{A_a}{A_b}$$

P_b is the retention pressure and remains constant during normal operation. Replacing in Eq. 4.1;

$$F = P_a A_a - 200 \frac{A_a}{A_b} A_b - f$$

or

$$F = (P_a - 200) A_a - f \quad (4.4)$$

Let

$$W = P_a - 200 \quad (4.5)$$

then

$$F = W A_a - f \quad (4.6)$$

f is generally small and can be ignored. Thus, it is concluded that

$$F \propto W \quad (4.7)$$

The operator's control panel contains several display gauges with one displaying "Feed Pressure". The readings of the gauge matched the observed W during

operation at steady state, thus justifying the validity of the assumptions suggested. For the remaining part of this thesis, W will be called "feed pressure".

Finally, we can rewrite Eq. 4.2 as

$$W_{bit} \propto W - F_{res} \quad (4.8)$$

If F_{res} remains constant, W_{bit} can be considered proportional to the feed pressure W with an amount of offset F_{res} . However, it will be further assumed that $F_{res} \ll W_{bit}$ such that

$$W_{bit} \propto W$$

or

$$W_{bit} = \beta W \quad (4.9)$$

where β is the proportionality constant.

Figure 4.11 page 49 (top) shows the pressure transducer (vertical) mounted on the hydraulic pump assembly.

Actual Rotary Speed

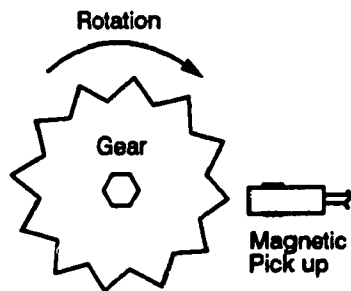


Figure 4.2: Measurement of rotary speed

The rotary speed was measured by means of a magnetic pick-up sensor facing the teeth of one gear coupling the motors to the rotating shaft, as shown in Fig. 4.2. At every tooth encounter, a voltage pulse is generated across a resistive load connected

to the magnetic pick-up terminals. Each shaft revolution generated 78 pulses, thus the rotary speed was proportional to the frequency of the generated signal. The latter was further converted to a voltage (V_n) proportional to frequency using a frequency to voltage converter signal conditioning unit. Thus, the following holds

$$N \propto V_n \quad (4.10)$$

Weight-On-Bit and Rotary Speed Set-Point

It was necessary to record the operator inputs (or set-points) to the machine to define the input-output characteristics of the system. The manual levers that the operator controls for rotary speed and weight-on-bit demand drive steel rods directly connected to the hydraulic pumps. Two Linear Displacement Transducers (LDT) had to be fixed near the pumps to measure the displacement of the steel rods as shown in Fig. 4.11 (page 49 top – the transducers are horizontal). Each transducer consists of a permanent magnet ring that slides along a six inch long waveguide. The position of the ring on the waveguide is detected by the transducer's electronics that uses the principle of magnetostriction (also known as the joule effect) [4]. However, it later became clear during field experimentation that the drill operator would use a knob for fine adjustments of feed pressure set-point, while the lever position that was monitored would be maintained at maximum position during the drilling phase! The knob position was unfortunately not monitored.

Rotary Torque

The D75K is equipped with two hydraulic motors driven by hydraulic pumps. Although several techniques exist for measuring torque in mechanical machines, one practical method here was by measuring the differential pressure at the inlet and outlet of the hydraulic motors, as depicted by Fig 4.3. The torque produced by the

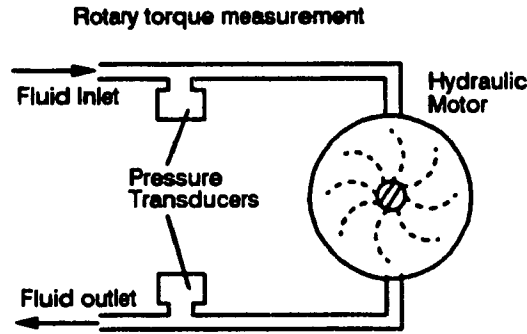


Figure 4.3: Measurement of rotary torque

motor is

$$T_m = \frac{(P_{in} - P_{out})q}{2\pi\eta} \quad (4.11)$$

where P_{in} and P_{out} are the fluid pressures at inlet and outlet, q is the geometrical displacement of the motor and η is the motor's efficiency.

The factor η is considered to be the hydraulic-mechanical efficiency that takes into account the energy losses caused by oil leakage and mechanical frictions in the motor. Since oil leakage is related to the differential pressure ($P_{in} - P_{out}$) of the system and the rotary speed of the motor, the efficiency is related to these two parameters. The efficiency varies with different motors because of different designs. For any particular motor, a performance characteristic is provided by the manufacturer showing the relationships between torque and speed at different pressure drops and oil flows. However, using such charts for each data point was considered cumbersome, and as an alternative, the following approximation was used;

$$T_m \propto (P_{in} - P_{out})$$

Let

$$P_{rot} = P_{in} - P_{out}$$

then

$$T_m \propto P_{rot}$$

or

$$T_m = K_p P_{rot} \quad (4.12)$$

where P_{rot} is the difference between inlet and outlet pressures of the rotary hydraulic motors and K_p a constant. P_{rot} will be called *rotation pressure*, consistent with the same reading displayed by a gauge on the control panel facing the driver.

T_m represents the torque generated by the motors. This torque drives the mechanical load T_{load} present at the shaft and overcomes internal friction T_{fric} and external disturbances T_{dist} . Therefore,

$$T_m = T_{load} + T_{fric} + T_{dist} \quad (4.13)$$

T_{dist} is the torque that contributes to crushing the rock and represents the variable that we wish to evaluate during experimental testing.

During motion, friction can be reduced to two main components; Coulomb friction T_{cb} that remains constant and viscous friction T_b that is proportional to rotary speed. T_{fric} may then be expressed as

$$T_{fric} = T_{cb} + T_b = T_{cb} + BN$$

where N is rotary speed and B a constant.

The mechanical load T_{load} is an inertial load. In general, to bring a load to a final steady state rotation speed, the load must be accelerated. From Newton's second law,

$$T_{load} = J_l \dot{N}$$

where J_l represents the total inertia of the load and \dot{N} is the angular acceleration. Replacing the above equivalencies in Eq. 4.13, we get:

$$T_m = T_{cb} + BN + J_l \dot{N} + T_{dist} \quad (4.14)$$

To express Eq. 4.14 in terms of pressures, divide both sides by K_p ;

$$\frac{T_m}{K_p} = \frac{T_{cb} + BN + J_l \dot{N} + T_{dist}}{K_p}$$

Using the fact that $T_m = K_p P_{rot}$ (Eq. 4.12) and assuming by analogy that $T_{dist} = K_p P_{dist}$, we may write

$$P_{rot} = \frac{T_{cb}}{K_p} + \frac{B}{K_p}N + \frac{J_l}{K_p}\dot{N} + P_{dist} \quad (4.15)$$

Rearranging the terms to compute P_{dist} :

$$P_{dist} = P_{rot} - \frac{T_{cb}}{K_p} - \frac{B}{K_p}N - \frac{J_l}{K_p}\dot{N} \quad (4.16)$$

P_{dist} can be seen as the component of P_{rot} which generates the torque at the bit-rock interface.

At steady state, $\dot{N} = 0$. Thus,

$$P_{dist} = P_{rot} - \frac{T_{cb}}{K_p} - \frac{B}{K_p}N \quad (4.17)$$

P_{rot} and N are measured, the ratios T_{cb}/K_p and B/K_p can be identified from experimental testing. This is achieved by rotating the drill's shaft-bit combination in air (no load at the bit-rock interface) and recording several observations of N and P_{rot} . In this case $P_{dist} = 0$ and Eq. 4.17 becomes:

$$0 = P_{rot} - \frac{T_{cb}}{K_p} - \frac{B}{K_p}N$$

or

$$P_{rot} = \frac{T_{cb}}{K_p} + \frac{B}{K_p}N \quad (4.18)$$

which shows a linear relationship between N and P_{rot} under assumptions used.

Subsequently, Eq. 4.17 will be used to evaluate P_{dist} , while the torque at the bit-rock interface is considered proportional to it, e.g.,

$$T_{dist} \propto P_{dist}$$

or

$$T_{dist} = \alpha P_{dist} \quad (4.19)$$

where α is the proportionality constant.

Bailing Air Pressure

The bailing air pressure was monitored by means of a pressure transducer connected to the same system as the bailing air pressure Bourdon gauge fixed onto the operator's control panel (Fig. 4.11 page 49, bottom). The transducer malfunctioned after two days of operation and could unfortunately not be replaced.

Vibration

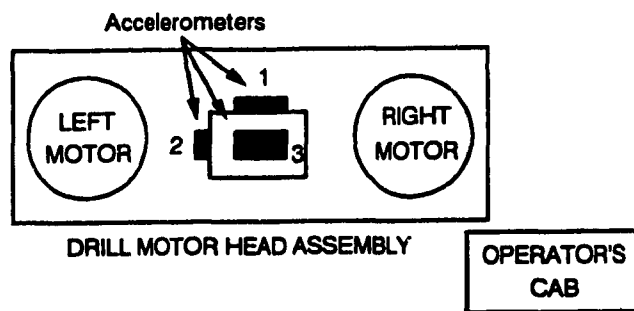


Figure 4.4: Location of vibration sensors on the drill motor head assembly

Three piezoresistive type accelerometers were fixed on the drill motor head assembly in three different orientations, as shown in Fig. 4.4. Their measurement range was $\pm 10 G$ with a frequency response of 0 – 700 Hz. However, after the field tests were completed, the analysis of the vibration data showed that frequencies below 10 Hz were not detected. The manufacturer was contacted and later acknowledged that the transducers are usually compensated at the customer's request to extend their frequency response to include the band 0 – 10 Hz.

The vibration data enables the analysis of the nature of the vibration spectrum associated with bit-rock interaction. This response may be associated to the effective coupling (sufficient weight-on-bit) between the bit and the rock or the breakage of hard versus soft rocks for a particular weight-on-bit setting. However, this topic extends beyond the scope of this thesis.

Depth and Penetration Rate

The depth was evaluated by monitoring the position of the drill motor head assembly by fixing a metallic case containing a special type of potentiometer on the upper frame of the mast. The potentiometer was driven by a steel cable having a maximum length of 500 in (12.7 m) and fixed onto the drill motor head assembly. The potentiometer operated as a voltage divider, with voltage output determined by the extended length of cable. Thus, the position of the motor head assembly was proportional to the voltage output of the potentiometer. Using this measurement, the drilling depth was then computed by correcting for the drill deck height, the maximum distance travelled by the drill motor head assembly for each steel rod and by considering the number of steel rods involved.

There was no need to monitor the penetration rate since it is the derivative of the depth signal. The following chapter describes how the penetration rate was extracted.

The potentiometer case (encircled) can be seen in Fig. 4.12 page 50 (top), fixed on the horizontal frame at the top of the drill tower.

4.3 Experimental Testing Instrumentation

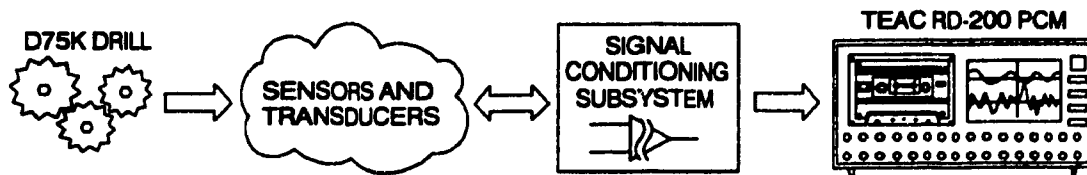


Figure 4.5: Block diagram showing experimental testing setup

The overall strategy for data measurement can be viewed in Fig. 4.5. Various sensors and transducers were installed on the drill rig to monitor the parameters of interest.

4.3.1 TEAC RD-200 PCM Data Recorder

The recording system used was a Digital Audio Tape (DAT) recorder model RD-200 PCM from TEAC (Japan). The unit records using recent DAT technology 16 analog signals of 2.5 KHz bandwidth each. When the tape is played back, the analog signals are reconstructed with minimal distortion and become readily available at the output terminals of the recorder. Each tape can store data equivalent to two hours of recording, providing a convenient mass storage medium. An additional channel is reserved for recording external comments that the user enters by speaking into a hand held microphone. The recorder was conveniently powered by the 24 V DC source available on the drill rig.

4.3.2 Signal Conditioning Subsystem

The signal conditioning subsystem (shown in Fig. 4.5) serves many purposes, namely to filter and amplify the signal outputs from the various sensors and transducers described in the previous section, before entering the TEAC DAT recorder. They also provide complete magnetic isolation, high common-mode noise rejection and easy field calibration since each module can be user-adjusted by potentiometer trimming for output zero and span.

The signal conditioning subsystem selected was part of Analog Device's 3B series line [2]. The actual physical PCB backplane was designed to accommodate 16 plug-in modules and one 24 V to ± 15 V dc-to-dc converter, used to power the modules. Furthermore, the dc-to-dc converter provided 500 V of isolation, eliminating undesirable ground loops.

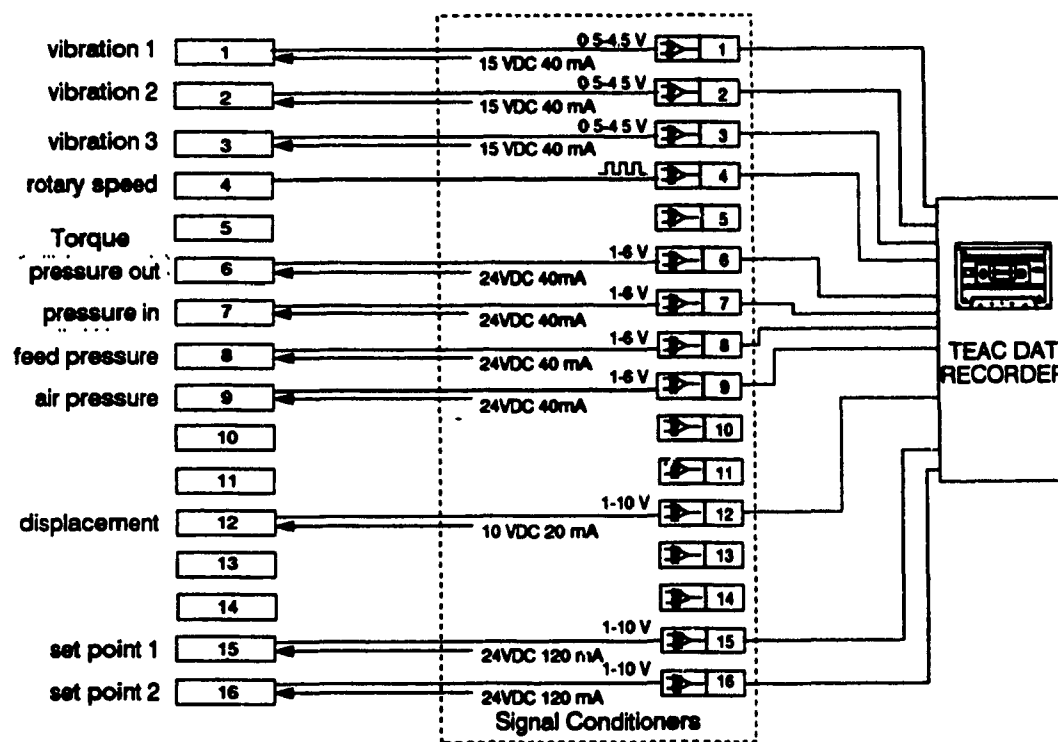


Figure 4.6: Experimental Testing Instrumentation Layout

The transducers were powered by three additional dc-to-dc converters. A voltage regulator circuit (designed and assembled by the author) was used to provide a stable 10 V source to the potentiometer measuring depth. Figure 4.6 shows the global layout of the field testing instrumentation. Also shown are the transducers excitation and output voltage levels.

The hardware described in this section was housed in a rugged fiberglass case used mainly for the transportation of photographic equipment. Figure 4.12 page 50 (bottom) shows the DAT recorder sitting on top of the fiberglass case at the test site.

Further details including transducer and equipment specifications can be found in reference [9].

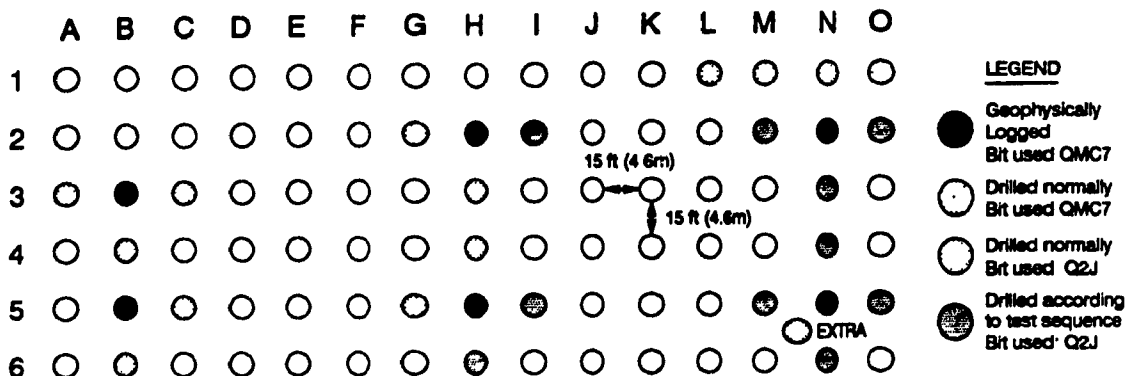


Figure 4.7: Test bench borehole layout; Delta Mine

4.4 Choice of Field Site

It had been recommended that an ideal site to conduct the field tests would be in a coal mine where, in general, there are clear strength contrasts between the different rock units. In addition, the high variability of the stratigraphy in a coal mine offered a greater challenge to the development of a functional control algorithm. Several sites were examined throughout the United States and the AMAX Delta mine located in southern Illinois was selected.

In coordination with the mine, a test area was graded and the hole locations surveyed in. The pattern measured 210 by 75 feet (64 by 23 meters) for a total of 90 boreholes on 15 foot (4.6 meter) spacings (see Fig. 4.7).

4.4.1 Geophysical Logging

In order to accurately determine the locations and types of rocks in the test area, a local geophysical company was contracted to provide gamma, density, caliper and sonic logs for this study. The first two logs would provide good discrimination of the various Coal Measures rock types and interfaces, while the sonic log would be an excellent indicator of rock hardness.

Six boreholes (see Fig. 4.7) were successfully logged and chart-strip records

provided by the contractor. Based on the interpreted geophysical logs, an accurate stratigraphic column was generated for each logged borehole to assist in locating the depths of various rock units in the adjacent monitored boreholes. The stratigraphy for borehole B3 is shown in Fig. 4.8 and is essentially the same across the test bench as indicated in both north-south (Fig. 4.9 page 47) and east-west sections (Fig. 4.10 page 48).

Some geotechnical data on rock compressive strengths (σ_c) were available from earlier testing of exploration core in other areas of the mine. The compressive strengths for the limestones and shales can be considered as reliable, while those for the sandstones are only estimates. The strengths of sandstones for the area will, however, decrease according to an increasing percentage of shaly material and matrix composition, i.e. whether silica (highest strength), calcite or clay (lowest strength). The gamma logs are good indicators of the shaly content of these rocks, by which the highest gamma response is from pure shales. The strengths of some of the mine rocks are shown next to the respective rock type in Fig. 4.8.

It was decided that experimental tests would be performed in five different rock types, at depths ranging from 70 to 122 ft (21.3 to 37.2 m). The selected rock types were:

1. Bankston Fork Limestone ($\sigma_c > 12000 \text{ psi}$)
2. Sandy Shale ($2000 < \sigma_c < 5000 \text{ psi}$)
3. Anvil Rock Sandstone ($5000 < \sigma_c < 12000 \text{ psi}$)
4. Lawson Shale ($2000 < \sigma_c < 5000 \text{ psi}$)
5. Brereton Limestone ($\sigma_c > 12000 \text{ psi}$)

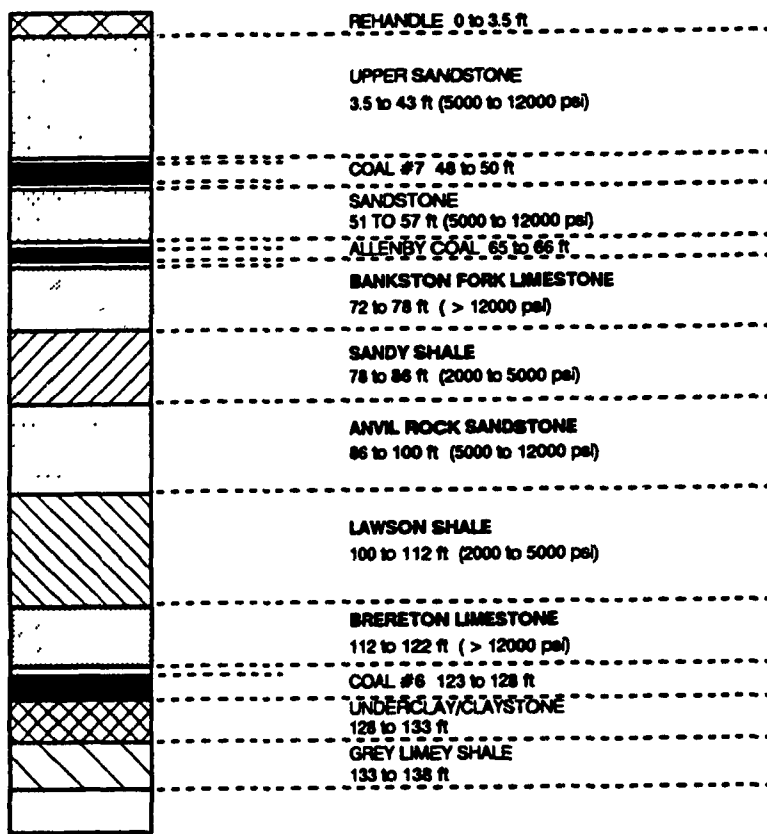


Figure 4.8: Stratigraphy for borehole B3; Delta Mine

4.5 Field Test Methodology

4.5.1 Machine Dynamics

The rotary actuator step response was recorded by conducting several step input tests while rotating the bit in air. Several step sizes were considered, some starting from zero, and others as increments from the current level of rotary speed at steady state.

The feed actuator step response was recorded by resting the bit against limestone, without rotation, and by applying step inputs to the actuator.

It was crucial that the step input amplitude be chosen so that it would not result in actuator saturation. This is because useful information can only be

extracted from step input tests if the response is (quasi-) linear. For the case of the rotary actuator, saturation would have been signaled by reaching the peak torque limit of the motor (stall conditions).

4.5.2 Bit-Rock Interface Model

Data for the bit-rock interface model and the process dynamics were gathered simultaneously in the following manner:

- Step response tests were performed to record the actuator dynamics over the operational range of rotary speed and weight-on-bit combinations in different rock types;
- The steady state values of the step response tests would be used to determine the bit-rock interface model.

The above mentioned objectives were achieved by drilling several boreholes as indicated in Fig. 4.7. The test sequence involved normal drilling until the bit reached the first layer of the five selected rock types (e.g. Bankston Fork limestone). Then drilling would proceed by increasing levels of feed pressure (starting from zero) for a constant rotary speed in the five rock types. In the same rock unit in an adjacent borehole, drilling would continue with constant feed while gradually increasing rotary speed (starting from zero). The data for all the other variables would then be analyzed with respect to the conditions of constant geology and either constant rotary speed (variable feed pressure) or constant feed (variable rotary speed). Table 4.1 summarizes the general form of the test sequences.

For these tests, it had been specified that only new bits should be used to eliminate any possible variation in drilling performance due to a worn bit.

A - To Identify Rotary Speed (N) Dynamics

| | |
|--------------------------|------------------|
| 1 - with bit clear (air) | vary set-point N |
| 2 - In soft rock | low W |
| 3 - In hard rock | low W |
| 4 - In soft rock | high W |
| 5 - In hard rock | high W |

B - To Identify Feed Pressure (W) Dynamics

| | |
|---|------------------|
| 1 - without rotation (against solid surface) | vary set-point W |
| 2 - In soft rock | low N |
| 3 - In hard rock | low N |
| 4 - In soft rock | high N |
| 5 - In hard rock | high N |

Table 4.1: Test Sequence Followed in the field

Note: "vary" implies step changes, both positive and negative, of 250 or 500 psi for feed pressure, and 10 to 30 rev/min for the rotary speed

The original bit used in the field tests was a 12.25 inch (311mm) diameter medium VAREL brand tricone bit (model QMC7). A total of 8 boreholes were drilled using this bit, which, according to the Delta mine personnel, was unable to achieve the expected penetration rates at the Delta mine.

It was therefore replaced with a 12.25 inch SMITH soft rock bit (model Q2J shown in Fig. 3.1 page 17), and used for all subsequent drilling tests. No detailed comparison of the performance differences using the two types of bits has yet been made, but will form part of any future research.

The exceptional condition of bit wear was not encountered during experimentation. According to the Delta mine personnel, for normal drill operation, bits will last in excess of 40,000 feet (12195 meters) of drilled hole. Approximately 4200 feet (1280 meters) of drilling was undertaken during the experimental tests.

The rotary motors installed on the test drill enabled normal drill rotation speeds of up to 120-125 *rev/min* to be achieved. Once the instrumentation was operational and the monitoring routine streamlined, the time required to acquire step change data from one borehole was approximately 50 to 60 minutes per 140 foot (42.7 meters) hole. This was in contrast to "normal" drilling (4 steel rods at 35 feet each, including time for steel rod changes), where using the SMITH bit a hole could be completed in about 30 minutes. Figure 4.13 page 51 shows the D75K drill rig at the Delta mine during experimental testing.

In summary, during the test period (June 1990), a total of 30 boreholes were drilled. Of these, 8 boreholes were drilled "normally" using the VAREL rock bit, in which the operator would minimize adjustments of both rotary speed and feed pressure. Subsequently, using the SMITH rock bit, an additional 12 "normal" and 10 "experimental" boreholes were drilled as shown in Fig. 4.7.

Data for normally drilled boreholes were collected for future research, where the normal operation of the drill driven by a human operator could be studied in greater detail.

4. experimental testing

47

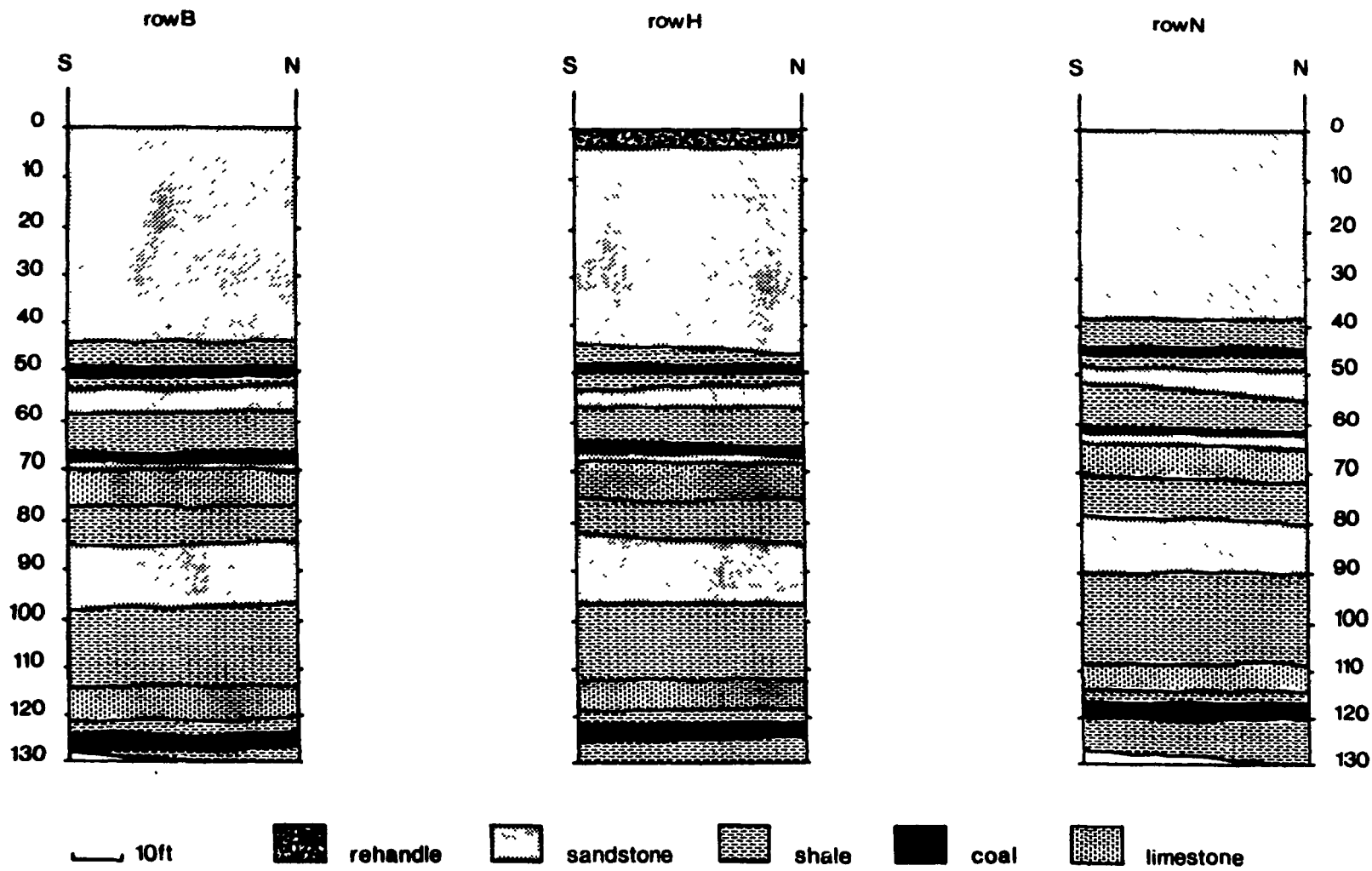


Figure 4.8: North-South sections of geology; Delta mine

4. experimental testing

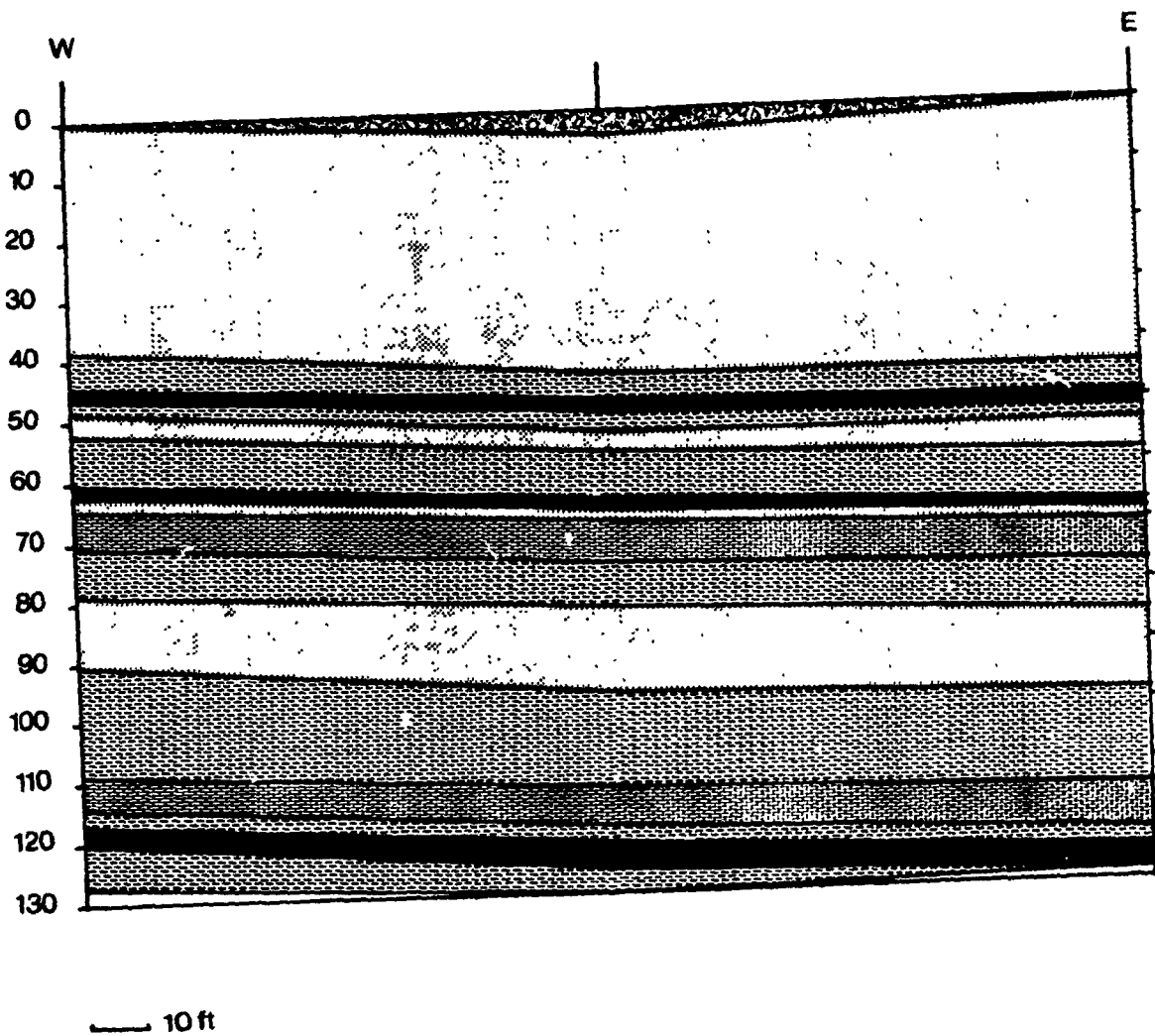


Figure 4.10: East-West sections of geology; Delta mine

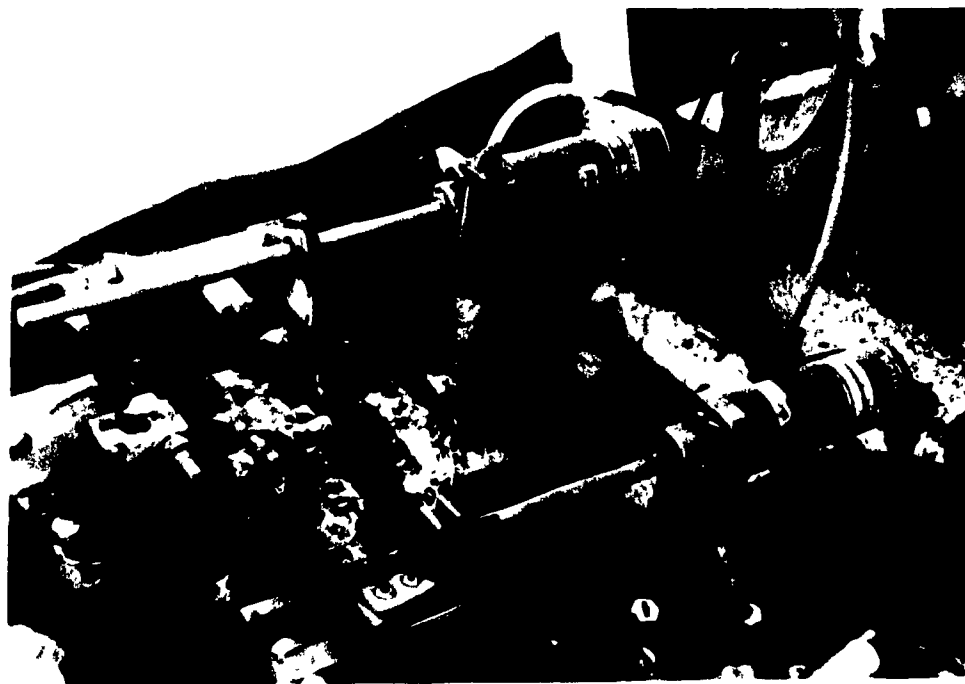


Figure 4.11: Field Instrumentation. Top: Linear displacement (horizontal) and feed pressure (vertical) transducers; Bottom: Bailing air pressure transducer.

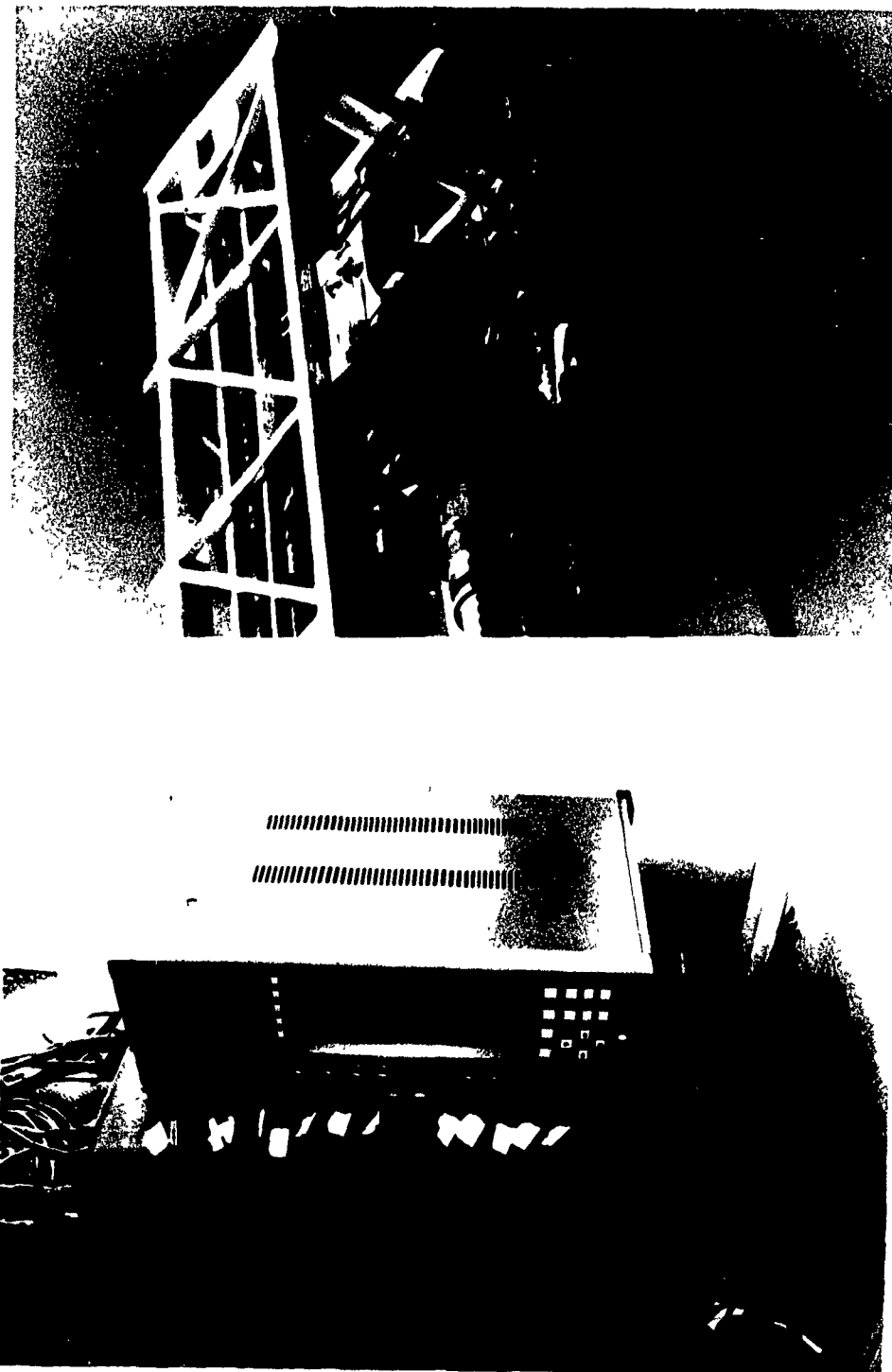


Figure 4.12: Top: Displacement transducer. (fixed on the upper horizontal frame); Bottom: The DAT recorder and the signal conditioning unit at the experiment site

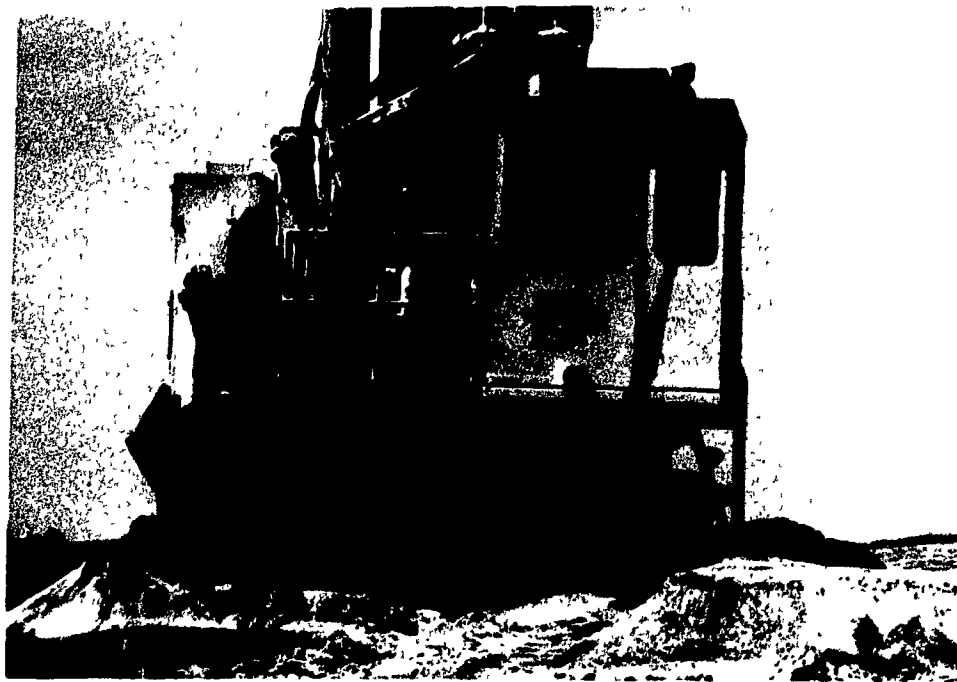


Figure 4.13: TAMROCK-DRILTECH D75K during experimental testing at the delta mine.

Chapter 5

EXPERIMENTAL DATA ANALYSIS

5.1 Analysis Environment

5.1.1 Digitization Hardware

The experimental tests data were recorded on tape using DAT technology. The tapes needed to be played back at McGill University such that the reconstructed analog signals could be digitized and channeled to a computer hard disk. The host computer used for the data acquisition was a COMPAQ II portable computer (based on Intel's 80286 microprocessor with an 80287 co-processor) equipped with 640 Kb of RAM memory, 2 Mb of extended memory, a 40 Mb hard disk, one floppy disk drive (double sided/double density), an Enhanced Graphics Adapter and a color monitor.

An Analog Device's RTI-815 [1] analog-to-digital converter board was used as the hardware interface between the host computer and external analog signals. The entire A/D board was inserted into one of the expansion slots of the computer.

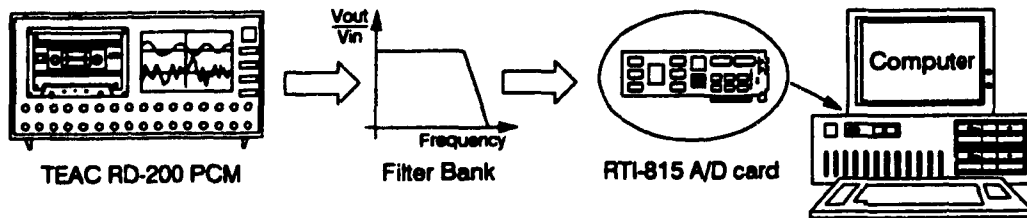


Figure 5.1: General Scheme for Office Data Digitization and Processing

Analog Filters

In order to establish steady state relationships between the drilling variables, it was desired to sample the recorded analog signals at a rate of 10 Hz. Each analog signal reconstructed by the DAT recorder was therefore filtered with a two-pole analog filter at a cutoff frequency of 3.6 Hz before entering the RTI-815 A/D board. The signals sampled at a rate of 10 Hz thus exceeded the minimum Nyquist sampling frequency of 7.2 Hz, reducing aliasing effects. The filters were built in-house, using *Texas Instruments TL081 OP-AMP* [35], and calibrated by means of a Hewlett Packard HP54504A digitizing oscilloscope. The general scheme used for digitization and processing is illustrated in Fig. 5.1.

5.1.2 Analysis Software

The data acquisition card was controlled by menu driven software that allowed the user to set up the digitization routine and specify the sampling rate. Once the digitization routine has been completed, the data were stored in binary format, complex floating point double precision so that the stored data files could conveniently be loaded into Matlab. Matlab is a powerful programming environment having a rich library of mathematical and statistical functions. It was the primary tool used for data analysis [25].

Front-End Processing

A suitable software program was needed to load the stored data files and to convert the sensors readings into the actual physical parameters that were monitored. Except for the penetration rate, the conversion between measured signals (voltages) and the actual parameters was straightforward, using calibration curves supplied with the transducers.

The program developed for this purpose consisted of a set of macros that run inside the Matlab environment.

Derivation of the penetration rate

The penetration rate could be obtained by mathematically computing the derivative of the depth signal. However, due to the nature of the drilling process and the bouncing effect at the bit-rock interface, the depth signal contained AC ripple, and consequently its derivative signal showed numerous spikes.

It was therefore necessary to rely on digital filtering techniques to filter the depth signal at a fairly low cutoff frequency, without introducing large phase lags. A 32nd order *linear phase* Finite Impulse Response (FIR) filter with a cutoff frequency of 0.1 *Hz* was designed using the window method [28]. Matlab's signal processing toolbox provided a suitable environment for the filter design.

The depth signal was then filtered and the phase error of the output signal corrected. Subsequently, the penetration rate was computed by applying a first order difference equation to the filtered depth signal.

Since the depth signal was sampled at 10 *Hz*, the computed penetration rate had a resolution of 0.1 second. For larger time resolutions, the penetration rate samples were averaged over the specified time interval.

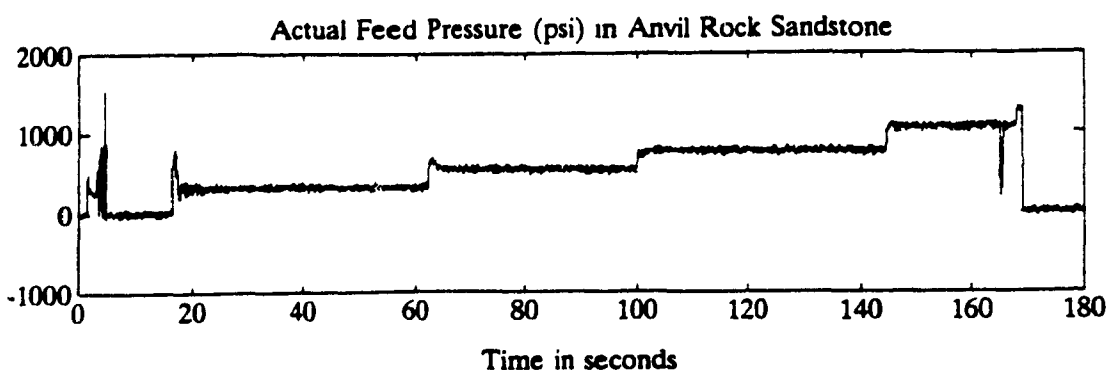


Figure 5.2: Example of test signals

Gathering observations to define the bit-rock interface model

The usual procedure during experimental tests was to maintain W (or N) constant and increment N (or W) within the same rock type. A period of 30 seconds at this level allowed the system to stabilize, before incrementing N again, with this routine continuing until the machine experienced severe vibration or the pressure valve in the rotation circuit opened ($> 3500 \text{ psi}$). The same procedure was followed by maintaining N constant and incrementing W .

One such sequence is referred to as *a test*, while the 30 second interval is called *a state* (see figure 5.2). Note that during one test, the same variable is incremented through to maximum levels.

Each state lasted 30 seconds, where in general, the first 5 seconds showed transient behaviour due to the machine/process dynamics. The remaining 25 seconds showed steady state conditions. Since the data were sampled at 10 Hz, each state is represented by 300 consecutive samples, with approximately 250 samples corresponding to the steady state interval. The steady state samples were averaged to represent one observation to be used in defining the model at the bit-rock interface.

5.2 Fitting a Model for Penetration Rate

As suggested in chapter 3, a model for the penetration rate within the same rock unit using the same bit can be described by the following equation (Eq.3.22, page 23):

$$R = KW_{bit}^x N^y \quad (5.1)$$

Replacing W_{bit} with βW (Eq. 4.9, page 32), Eq. 5.1 becomes:

$$R = K\beta^x W^x N^y$$

since β is a constant, we let

$$K\beta^x = K_*$$

The final model for penetration rate becomes:

$$R = K_* W^x N^y \quad (5.2)$$

The model equation is non linear, however it can be linearized by taking the natural logarithms on both sides:

$$\ln R = \ln K_* + x \ln W + y \ln N \quad (5.3)$$

Equation 5.3 is linear, and the use of linear regression becomes possible. It can be written in matrix form;

$$\mathbf{Y} = \mathbf{AP}$$

where

$$\mathbf{A} = [1 \ \ln W \ \ln N]$$

$$\mathbf{P} = [\ln K_* \ x \ y]^T$$

and

$$\mathbf{Y} = [\ln R]$$

The estimate \mathbf{p} of \mathbf{P} using a least squares regression is given by [11]:

$$\mathbf{p} = (\mathbf{A}^T \mathbf{A})^{-1} \mathbf{A}^T \mathbf{Y} \quad (5.4)$$

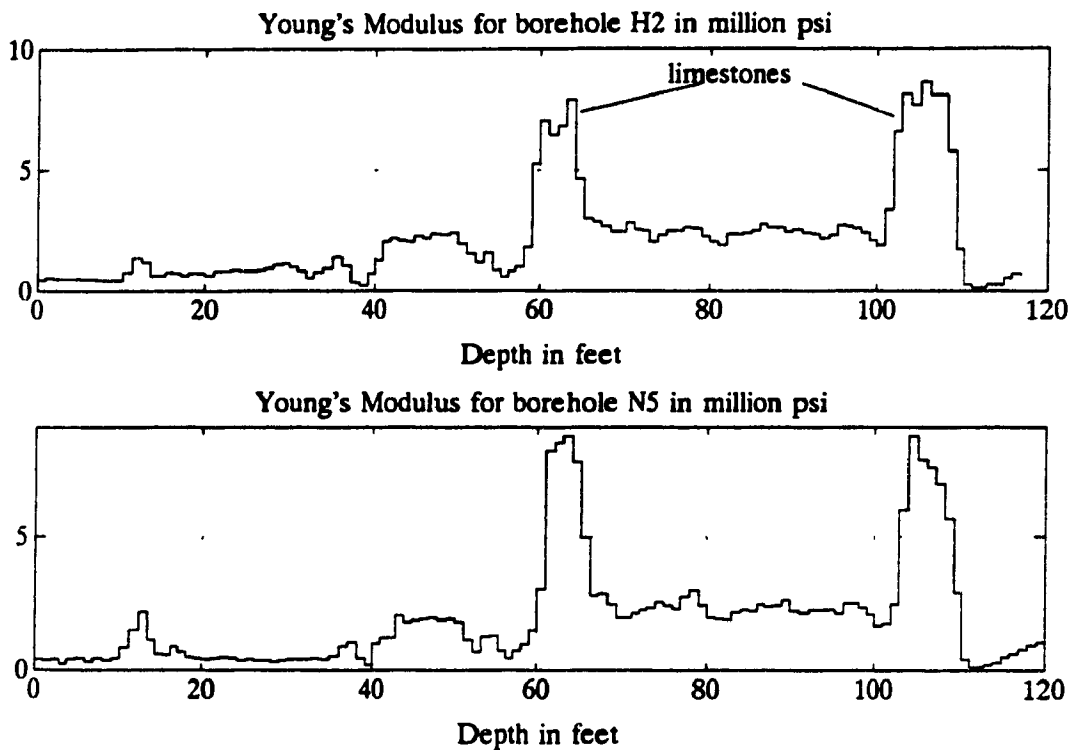


Figure 5.3: Young's Moduli for boreholes H2 and N5, as provided by the geophysical logging company

with fit quality computed by:

$$R^2 = \frac{\mathbf{p} \mathbf{A}^T \mathbf{Y} - n \bar{Y}^2}{\mathbf{Y}^T \mathbf{Y} - n \bar{Y}^2} \quad (5.5)$$

where n is the number of entries in \mathbf{Y} with mean \bar{Y} . R^2 is the proportion of total variation about the mean \bar{Y} , and is equal to 1 for a perfect fit.

Before applying linear regression, observation outliers had to be discarded. In order to appreciate the reason for data deviation, it was useful to assess the extent of nonhomogeneity within rock units. The geophysical logging company had provided data for rock Young's Moduli measured at one foot resolution from the six boreholes logged. Figure 5.3 shows the Young's Moduli plotted for boreholes H2 and N5. The graphs displayed show the variability of the ground within the same rock unit, and from one borehole to the other. This variability is clearly observed in the limestones.

| Rock Type | R fit | R^2 | % data discarded |
|-------------------------|-----------------------------------|-------|------------------|
| Bankston Fork Limestone | $R = 0.001178W^{0.9}N^{1.085}$ | 0.950 | 27.12 |
| Anvil Rock Sandstone | $R = 0.029W^{0.614}N^{1.028}$ | 0.894 | 29.16 |
| Lawson Shale | $R = 0.335W^{0.5053}N^{0.6796}$ | 0.933 | 13.15 |
| Sandy Shale | $R = 0.49012W^{0.4889}N^{0.6191}$ | 0.864 | 36.67 |
| Brereton Limestone | $R = 0.0004696W^{1.08}N^{0.982}$ | 0.969 | 20.73 |

Table 5.1: Penetration rate fit in five different rock types

Linear regression was applied to all valid observations within the same rock unit. The results are tabulated in Table 5.1. R is given in *feet/hour*, W in *psi* and N in *rev/min*. Also shown are values for R^2 and the percentage of observations not considered in the regression analysis.

Except for Sandy Shale, the values of R^2 are sufficiently high to validate the selected model for penetration rate.

5.3 Analysis of Penetration Rate Data

The penetration rate observations used in the regression analysis are plotted in Figs. 5.4, 5.5 and 5.6 which show the behaviour of penetration rate for the two cases:

- Constant feed pressure (W), rotary speed (N) varied
- Constant rotary speed (N), feed pressure (W) varied

The data related to the shales and Anvil Rock Sandstone were monitored at depths varying from 70 *ft* (21.34 *m*) and 90 *ft* (27.43 *m*), while the Bankston Fork and Brereton Limestone data were monitored at depths of 65 *ft* (19.81 *m*) and

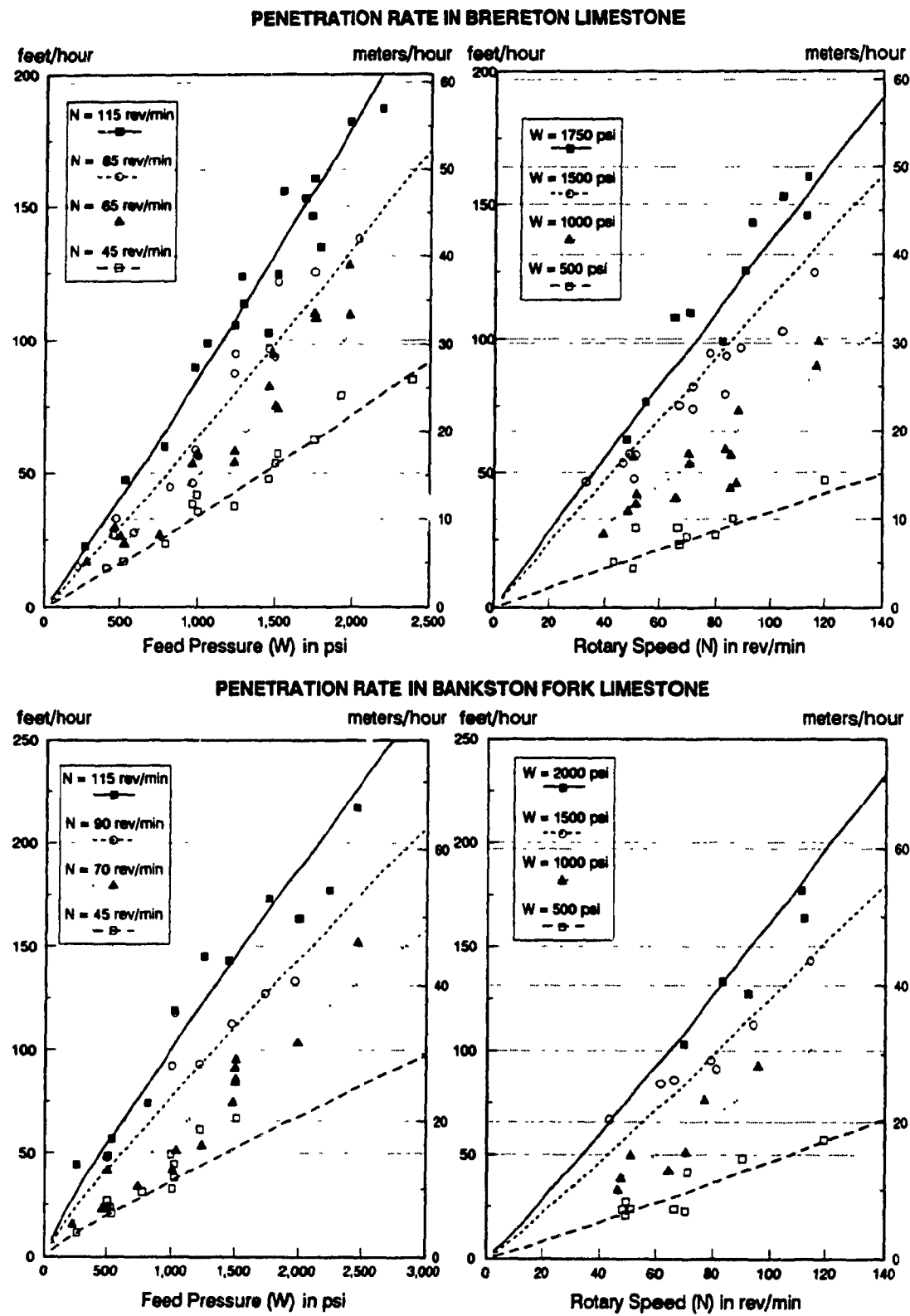


Figure 5.4: Penetration rate in Brereton and Bankston Fork Limestone plotted against feed pressure and rotary speed

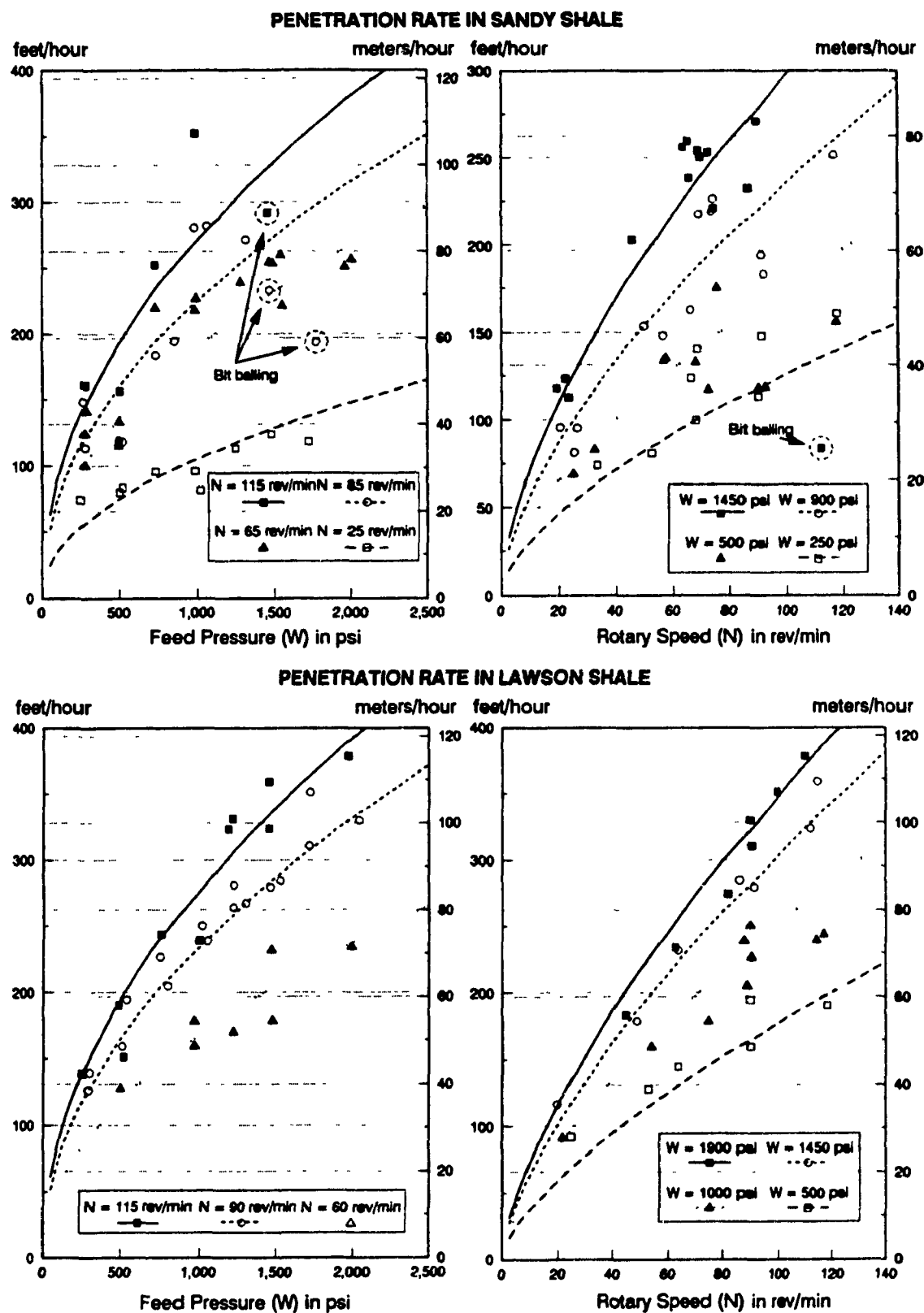


Figure 5.5: Penetration rate in Sandy and Lawson Shales plotted against feed pressure and rotary speed

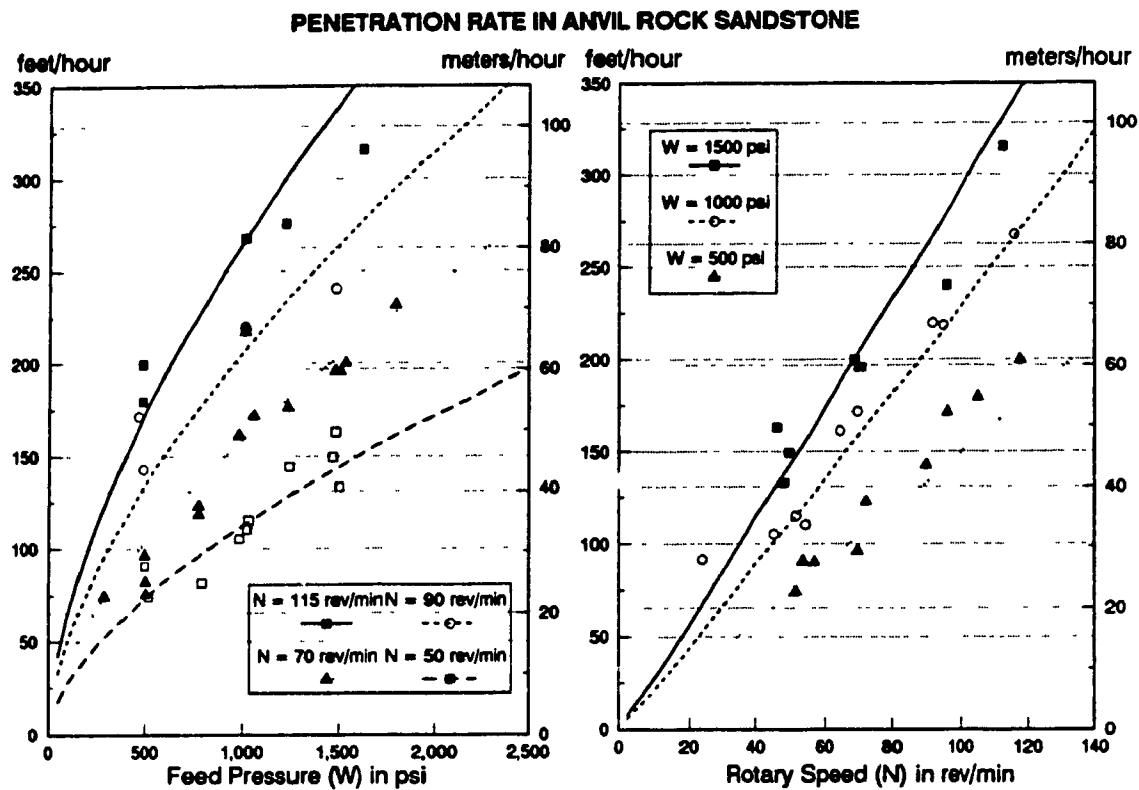


Figure 5.6: Penetration rate in Anvil Rock Sandstone plotted against feed pressure and rotary speed

115 ft (35.05 m) respectively.

The lines fitting the plotted data are computed using the equations displayed in Table 5.1. The variables displayed as "constant" in the legend are actually within $\pm 10\%$ of the specified value.

The graphs allow easy comparison of the general shape of the penetration rate with respect to feed pressure and rotary speed. It is apparent that this relationship is fairly monotonic, in that for constant feed pressure, increasing rotary speed results in an increase in penetration rate, and vice versa for constant rotary speed and increasing feed pressure. The monotonicity is more marked in the limestones and less marked in Sandy Shale. This effect is also enhanced by the low value of R^2 in Sandy Shale, even though more than one third of the total observations were discarded.

The general shape of the penetration rate versus feed pressure, and penetration rate versus rotary speed characteristics can be assumed consistent for a given material type at different rotary speeds and feed pressures, with the main change being with respect to offset of the curves. However, if within the same rock type, the constant levels of rotary speed or feed pressure were each considered as one data set, slightly different exponents for each fit (or subfit) are found, with better R^2 values. But for control purposes, generality is the aim, and therefore only one relationship for the penetration rate was estimated for the same rock type.

The penetration rate versus feed pressure characteristic shows a linear relationship between feed pressure and rotary speed in hard, homogeneous materials, eg. Brereton and Bankston Fork Limestones. The exhibited behaviour is related to the bit-rock breakage mechanism at work, where the impact-crushing mechanism predominates in hard materials in which brittle failure occurs. In such cases the energy from the bit (from both W and N) is transmitted with little attenuation to break the rock.

In Anvil Rock Sandstone, the exponent of N is close to unity while the exponent of W is close to 0.6. This suggests that in relatively soft formations where impact-crushing is less important in rock breakage, it is more important to excavate the broken rock at faster rotary speeds.

In the shales, the exponents of W and N are both less than unity, showing a curvilinear relationship, although one would expect similar trends as for Anvil Rock Sandstone since they fall into the soft rock category. However, a scraping-gouging mechanism dominates when drilling soft/shaly materials, where ductile failure occurs due to plastic deformation prior to failure. This plastic deformation results in bit energy being attenuated by the shaly rock. This may explain the difference in penetration rate behavior with respect to rotary speed observed in the shales and Anvil Rock Sandstone.

The graphs for Sandy Shale show situations described by "bit balling" in drilling terminology, where increasing feed pressure or rotary speed resulted in a decrease in penetration rate. This happens when the bit becomes deeply buried in the rock, adversely affecting cutting and chips removal. These observations were not included in the regression analysis.

From a control point of view, the graphs reviewed show that penetration rate is more sensitive to variations in feed pressure than to rotary speed. In the absence of constraints, the penetration rate theoretically can be maximized by setting rotary speed to maximum and increasing feed pressure. However in practice, increasing feed pressure indefinitely will result in torque overshoot, possible vibration build-up, bit overload, lower penetration rates and bit blocking as well as excessive bit bearing friction and possible bit failure.

5.4 Analysis of Penetration Per Revolution Data

The bit insert size is yet another factor affecting drilling and the penetration rate. The study presented by Maurer, based on single insert impact, does not consider the cases where the inserts are completely buried in rock. This is investigated here by computing the ratio of penetration rate to rotary speed ($\frac{R}{N}$) which represents the distance travelled by the bit per revolution. $\frac{R}{N}$ ratios exceeding the vertical length of the longest insert on the bit denote that all the inserts are completely buried in the rock.

It is important to understand the effect of burying the bit on the performance of the drilling process in order to develop an appropriate control action relevant to the actual drilling situation.

| Rock Type | $\frac{R}{N}$ | $\frac{R}{N} > 0.5 \text{ in}$ |
|-------------------------|--|---|
| Bankston Fork Limestone | $\frac{R}{N} = 2.35 \times 10^{-4} W^{0.9} N^{0.085}$ | — |
| Anvil Rock Sandstone | $\frac{R}{N} = 0.0058 W^{0.614} N^{0.028}$ | $W > 1200 \text{ psi}$ $0 < N < 120 \text{ rev/min}$ |
| Lawson Shale | $\frac{R}{N} = 0.067 W^{0.5053} N^{-0.3204}$ | $W > 1200 \text{ psi}$ $0 < N < 120 \text{ rev/min}$ |
| Sandy Shale | $\frac{R}{N} = 0.098 W^{0.4889} N^{-0.3809}$ | $W > 1200 \text{ psi}$ $0 < N < 120 \text{ rev/min}$ |
| Brereton Limestone | $\frac{R}{N} = 9.392 \times 10^{-5} W^{1.08} N^{-0.018}$ | — |

Table 5.2: $\frac{R}{N}$ in five different rock types

5.4.1 Computing Penetration Per Revolution

The penetration per revolution has been computed from the equations listed in table 5.1 and are tabulated in table 5.2 for the same five rock types. $\frac{R}{N}$ is given in inch/rev, W in psi and N in rev/min.

The equations show that $\frac{R}{N}$ in the limestones and Anvil Rock Sandstone is little affected by the rotary speed N , in contrast to the shales where increasing N decreases $\frac{R}{N}$ (N has a negative exponent). It is also apparent that feed pressure is the variable primarily affecting $\frac{R}{N}$.

5.4.2 Graphical Analysis of Penetration Per Revolution

Figures 5.7, 5.8 and 5.9 show the general trends of $\frac{R}{N}$ behaviour for the same two cases of:

- Constant feed pressure (W), rotary speed (N) varied

- Constant rotary speed (N), feed pressure (W) varied

The variables displayed as "constant" in the legend are actually within $\pm 10\%$ of the specified value.

The graphs of $\frac{R}{N}$ against feed pressure in Figs. 5.7, 5.8 and 5.9 clearly confirm that $\frac{R}{N}$ increases with an increase in feed pressure at constant rotary speeds. The graphs of $\frac{R}{N}$ against N in the same figures confirm that in the shales, $\frac{R}{N}$ decreases with increasing rotary speed at constant feed pressure. However it is not clear if $\frac{R}{N}$ remains constant or slightly decreases in the limestones and Anvil Rock Sandstone under the same conditions.

It is concluded that one can increase $\frac{R}{N}$ by increasing feed pressure at constant rotary speeds in the limestones and Anvil Rock Sandstone, or by *reducing rotary speed* if feed pressure is maintained constant, in shaly/sticky materials.

Bit information provided by Smith International [23] related to the Q2J model used at the experiment site showed the longest insert to be 0.5 in (12.7 mm). Although the inserts were slightly inclined with respect to the bit axis, for simplicity, the value 0.5 in was retained as the upper limit for $\frac{R}{N}$ beyond which the inserts were considered buried in rock.

The dashed boxes in Figs. 5.8 and 5.9 show the regions where the bit inserts become buried (e.g. $\frac{R}{N} > 0.5$ in).

From these graphs, approximate values of feed pressure (W) that bury the inserts at the full operating range of rotary speeds (e.g. regardless of the operating rotary speed) have been identified and are displayed in table 5.2. However, it is seen that at low rotary speeds ($N < 40$ rev/min) in the shales, feed pressures as low as 500 psi are sufficient to bury the bit inserts.

In contrast with soft formations, the inserts were never buried in the limestones. This is due to the fact that feed pressure could not be increased above certain

levels which increased the rotation pressure (P_{rot}) beyond its maximum safe limits.

Thus, it appears that in soft formations, the bit inserts are buried most of the operating time, at normal operating feed pressures and rotary speeds. In Sandy Shale $\frac{R}{N}$ is very high at rotary speeds near 25 rev/min, suggesting that high values of $\frac{R}{N}$ can by no means be interpreted as large penetration rates unless it is known that the rotary speed is large. These findings can be generalized by stating that the bit could comfortably operate in soft formations with a penetration per revolution ($\frac{R}{N}$) slightly larger than the longest bit insert, e.g. near 0.6 in (15.2 mm), i.e. 20% larger than the longest insert of the bit.

If it is assumed that $\frac{R}{N}$ increases monotonically to reach a maxima, after which it decreases sharply because of excessive feed pressures (bit balling), then by monitoring $\frac{R}{N}$ one can anticipate the occurrence of such event, and react appropriately by decreasing feed pressure. Furthermore, if one could prevent $\frac{R}{N}$ from exceeding a certain maximum value, then drawbacks at the bit level such as jamming, broken inserts, bearings and subsequently bit failure may be reduced considerably.

From a control point of view, the choice of feed pressure as the manipulable variable is justified since feed pressure is the main variable affecting both the penetration rate and the penetration per revolution ($\frac{R}{N}$). It is also clear that $\frac{R}{N}$ should be one of the feedback variables upon which the controller would base its control action.

5.5 Fitting a Model for Torque

The model for torque as described in chapter 3 (page 27) is:

$$T = \left[C_3 + C_4 \sqrt{\frac{R}{ND}} \right] W_{bit} D \quad (5.6)$$

or equivalently;

$$T = C_3 D W_{bit} + C_4 \sqrt{D} \sqrt{\frac{R}{N}} W_{bit}$$

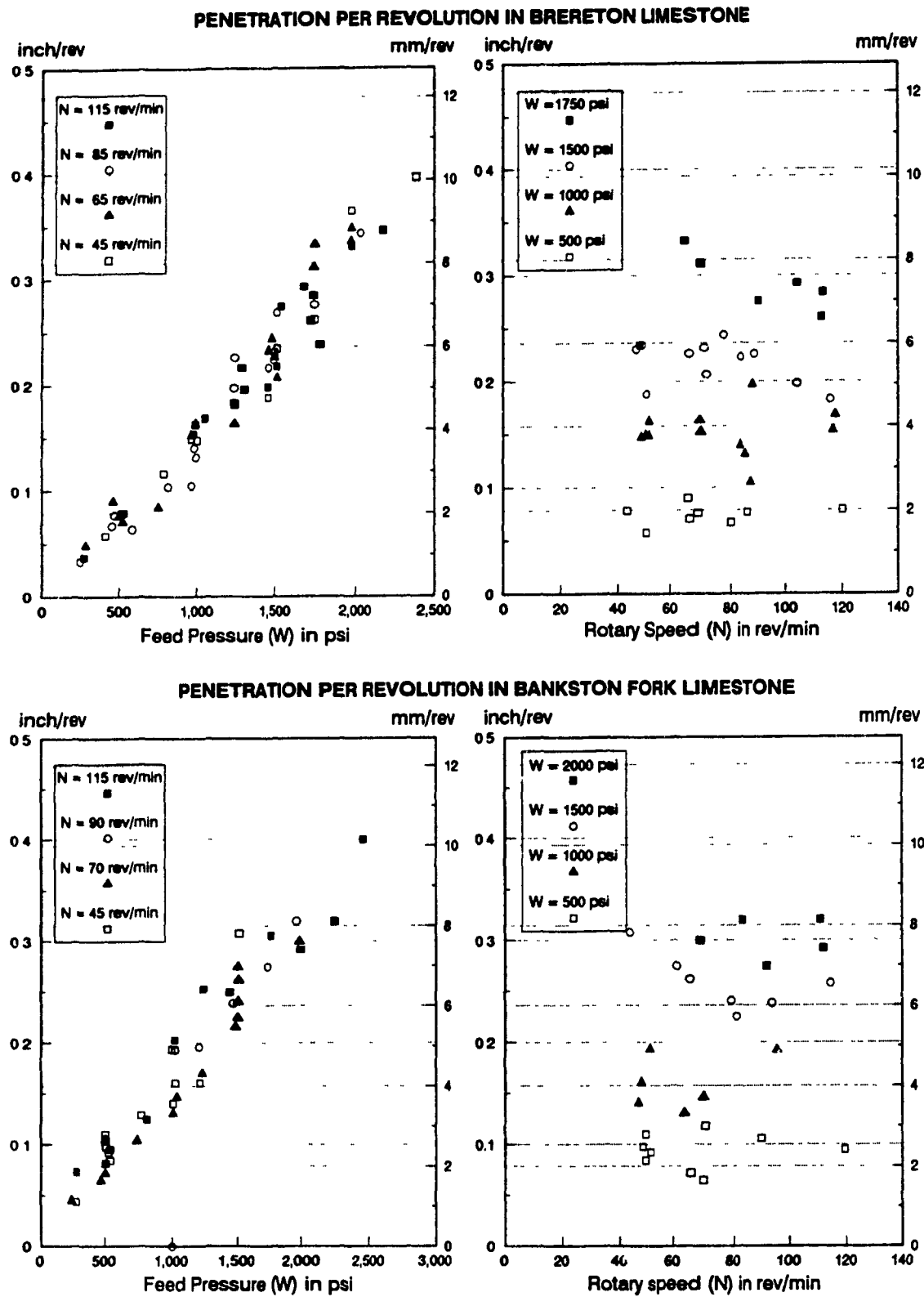


Figure 5.7: $\frac{R}{N}$ in Brereton and Bankston Fork limestone plotted against feed pressure and rotary speed

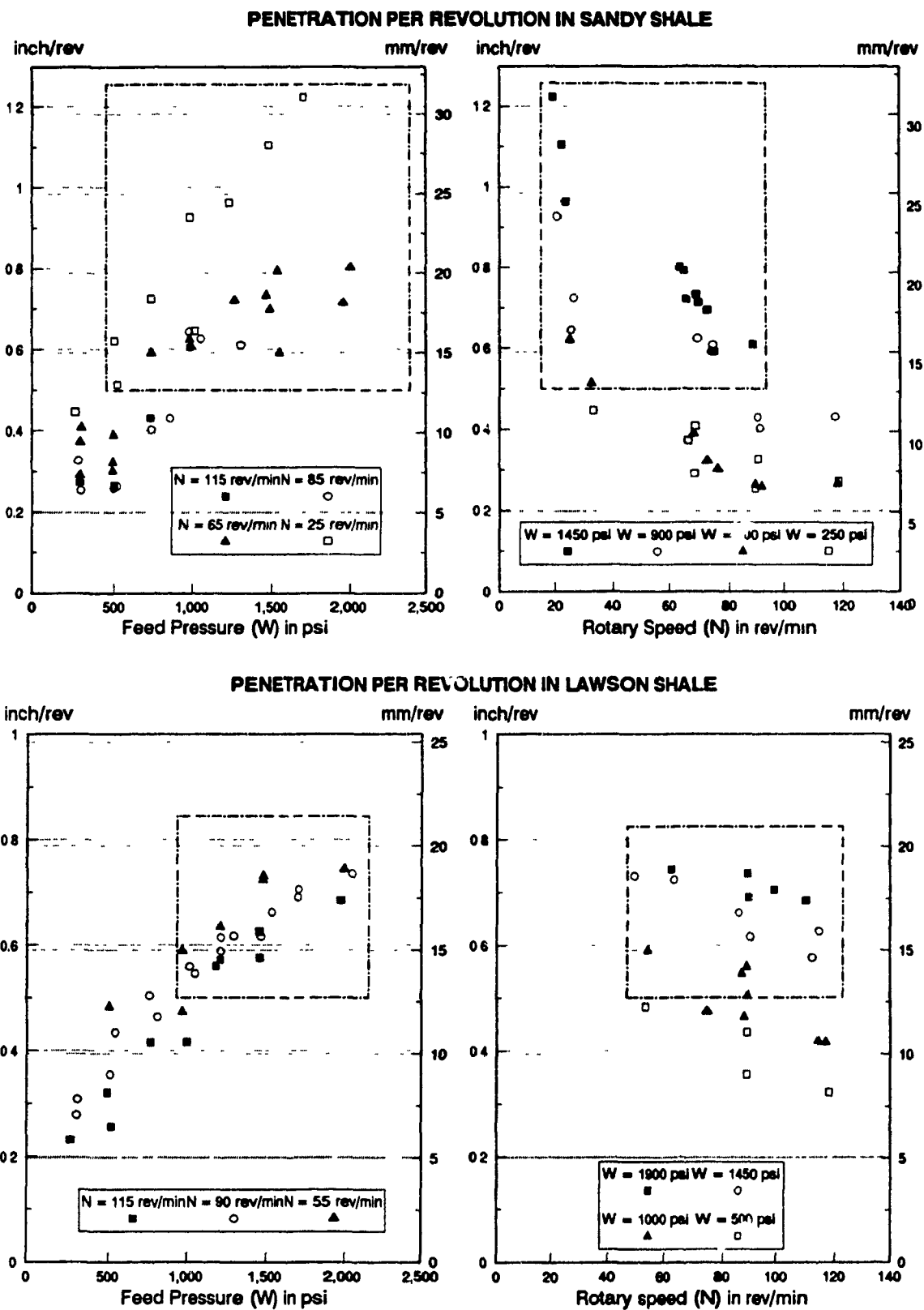


Figure 5.8: $\frac{R}{N}$ in Sandy and Lawson Shales plotted against feed pressure and rotary speed

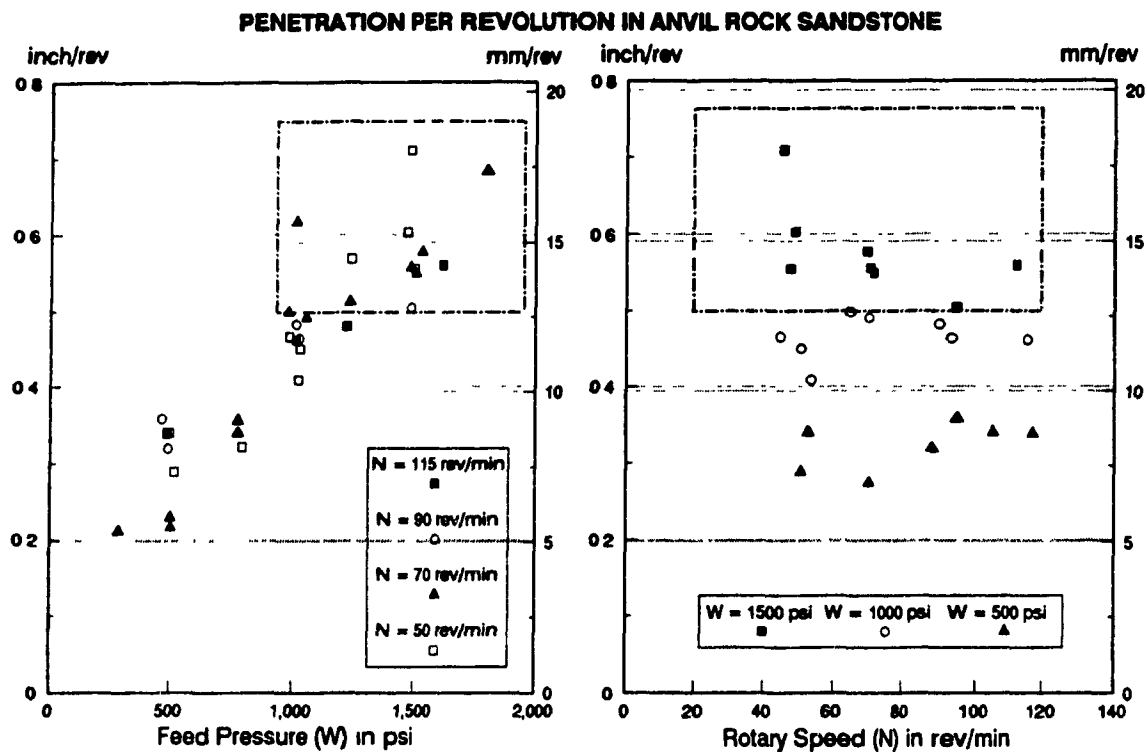


Figure 5.6: $\frac{R}{N}$ in Anvil Rock sandstone plotted against feed pressure and rotary speed

Substituting $T = \alpha P_{dist}$ (Eq. 4.19 page 36) and $W_{bit} = \beta W$ (Eq. 4.9, page 32), we obtain;

$$\alpha P_{dist} = C_3 D(\beta W) + C_4 \sqrt{D} \sqrt{\frac{R}{N}} (\beta W)$$

Dividing both sides by α , we get;

$$P_{dist} = \frac{C_3 D \beta}{\alpha} W + \frac{C_4 \sqrt{D} \beta}{\alpha} \sqrt{\frac{R}{N}} W$$

The bit diameter remains constant for the same machine, and therefore we let

$$K_1 = \frac{C_3 D \beta}{\alpha}, \quad K_2 = \frac{C_4 \sqrt{D} \beta}{\alpha}$$

therefore,

$$P_{dist} = K_1 W + K_2 \sqrt{\frac{R}{N}} W \quad (5.7)$$

Writing Eq. 5.7 in matrix form,

$$\mathbf{P} = \mathbf{B}\mathbf{K}$$

where

$$\mathbf{P} = [P_{dist}]$$

$$\mathbf{B} = \left[W \quad W\sqrt{\frac{R}{N}} \right]$$

$$\mathbf{K} = [K_1 \quad K_2]^T$$

The estimate \mathbf{k} of \mathbf{K} using a least squares linear regression is given by:

$$\mathbf{k} = (\mathbf{B}^T \mathbf{B})^{-1} \mathbf{B}^T \mathbf{P} \quad (5.8)$$

The analysis of experimental data at steady state, with bit rotating in free air has given the following coefficients for Eq. 4.18:

$$P_{rot} = 325 + 1.8443 * N$$

When the bit is coupled with rock, P_{dist} is then computed from the following 4.17:

$$P_{dist} = P_{rot} - 325 - 1.8443 * N \quad (5.9)$$

Equation 5.9 was derived using one steel rod since it was not possible to maintain the bit in air if two or more were used. It is assumed that the error introduced in Eq. 5.9 when using two or more steel rods can be neglected.

Linear regression was applied to the observed data for the five rock types, and the computed models are shown in table 5.3, along with R^2 . For Brereton Limestone, many data points were discarded, as shown in Fig. 5.10. The low values of R^2 are yet another reflection of the poor fit for the model used.

Figures 5.10 and 5.11 show the fitted model for each of the five different rock types. The y-axis represents P_{dist}/W while the x-axis represents $\sqrt{\frac{R}{N}}$. Plotted this way, the graph becomes a straight line. However, as seen in the plots, the real data does not closely confirm this expected trend.

The initial model formulated by Warren in the context of petroleum engineering related the cutting variables measured at the bit-rock interface. The discrepancy

| Rock Type | P_{dist} | R^2 |
|-------------------------|---|-------|
| Bankston Fork Limestone | $P_{dist} = [1.443 - 0.6364 * \sqrt{\frac{R}{N}}] * W$ | 0.26 |
| Anvil Rock Sandstone | $P_{dist} = [2.3376 - 1.1594 * \sqrt{\frac{R}{N}}] * W$ | 0.44 |
| Lawson Shale | $P_{dist} = [3.3326 - 2.5254 * \sqrt{\frac{R}{N}}] * W$ | 0.54 |
| Sandy Shale | $P_{dist} = [2.8638 - 1.6986 * \sqrt{\frac{R}{N}}] * W$ | 0.47 |
| Brereton Limestone | $P_{dist} = [0.9837 + 0.4108 * \sqrt{\frac{R}{N}}] * W$ | 0.21 |

Table 5.3: P_{dist} evaluated in five different rock types, using Warren's model

encountered between the presented experimental data and Warren's model may be based on the fact that the presented measurements were performed at the actuators level. As a consequence of the poor fits, alternative models had to be considered.

5.6 Analysis of Disturbance Pressure Data

In an attempt to better understand the behaviour of the disturbance pressure (P_{dist}) during the drilling process, observations of disturbance pressure data P_{dist} are plotted and displayed in Figs. 5.12, 5.13 and 5.14 which show the behaviour of P_{dist} for the two cases:

- Constant feed pressure (W), rotary speed (N) varied
- Constant rotary speed (N), feed pressure (W) varied

The graphs show that at constant levels of feed pressure, the disturbance pressure decays slightly with an increase in rotary speed, as observed in the five rock types. This phenomenon is due to linear viscous damping, related to the mechanical design of the rotary actuators since the rotation pressure produces the rotary speed.

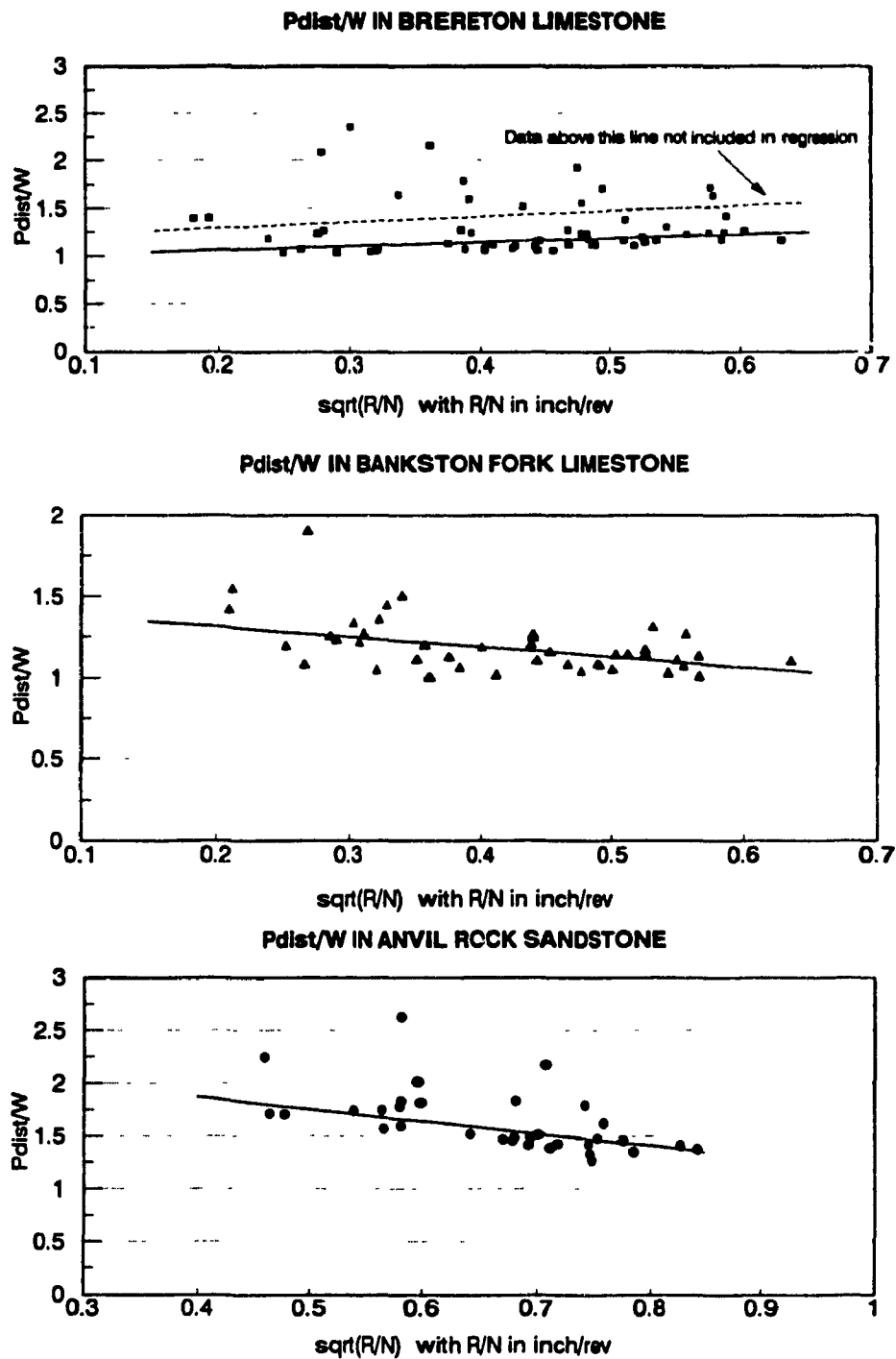


Figure 5.10: P_{dist} model for Bankston Fork Limestone, Brereton Limestone and Anvil Rock Sandstone

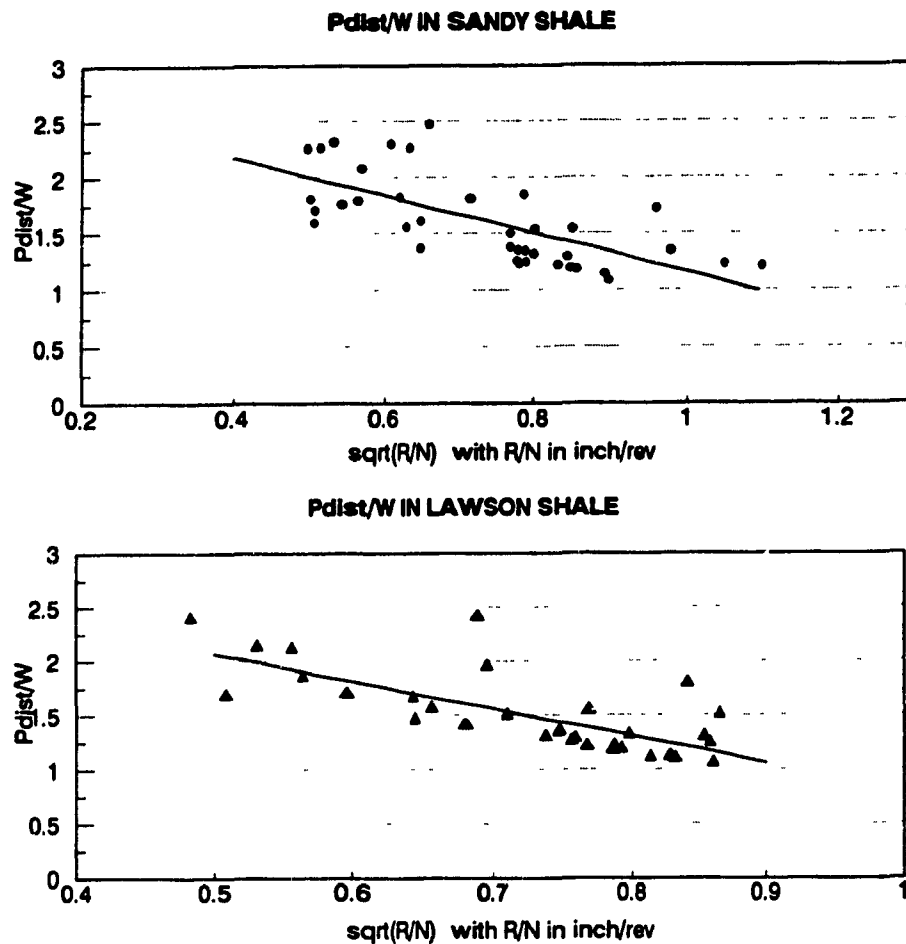


Figure 5.11: P_{dist} model for Sandy Shale and Lawson Shale

Therefore the observed relatively flat torque characteristics is specific to the rotary actuators of the D75K drill.

As a result of the relatively flat torque characteristic, the disturbance pressure becomes more sensitive to changes in feed pressure than to changes in rotary speed. This conclusion is confirmed by the graphs showing the disturbance pressure plotted versus feed pressure.

The direct relationship between the disturbance pressure and feed pressure offers an attractive solution for replacing the initial torque model suggested by Warren. A linear regression analysis similar to the method used for fitting the penetration

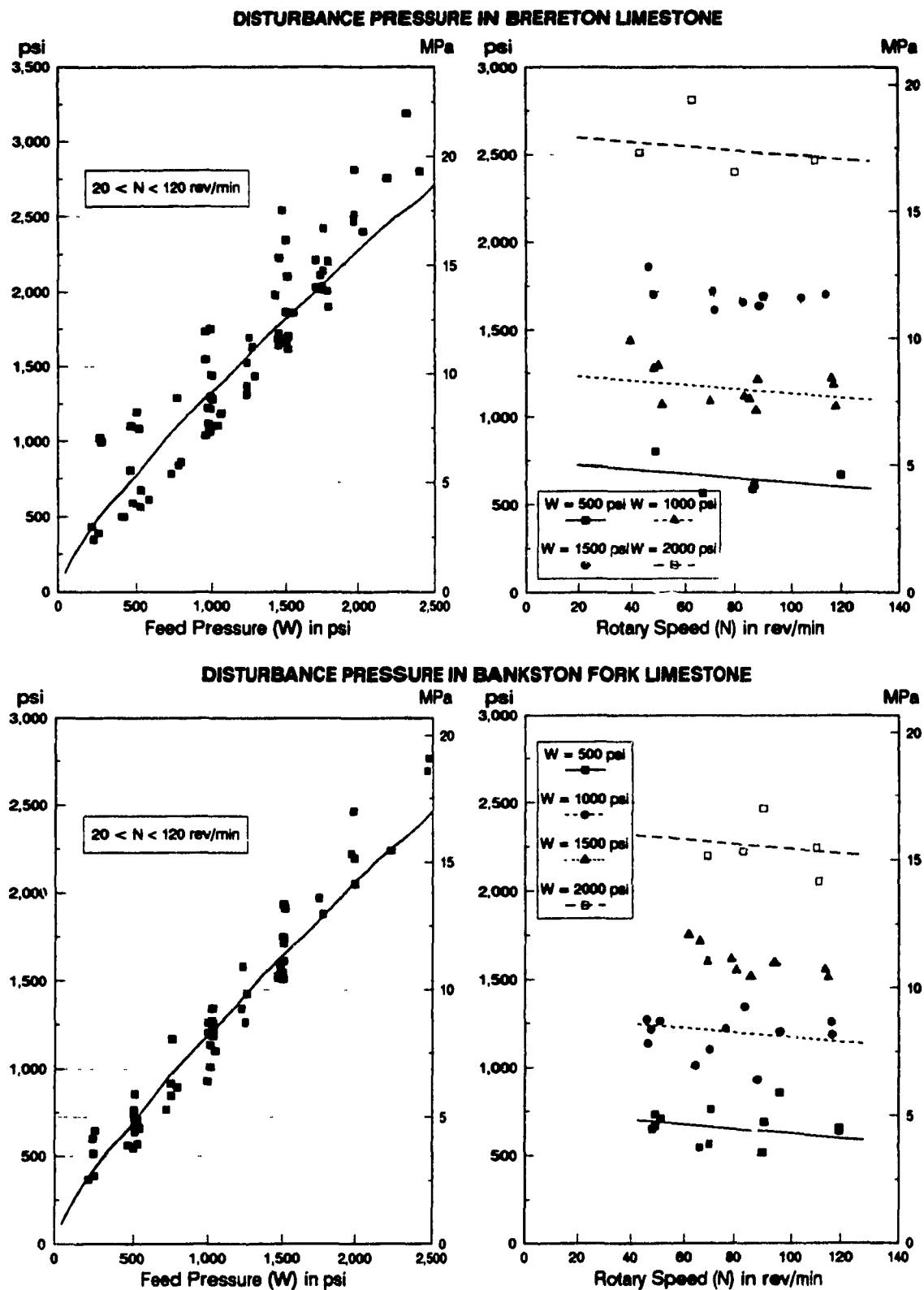


Figure 5.12: P_{dist} in Brereton and Bankston Fork Limestone plotted against feed pressure and rotary speed

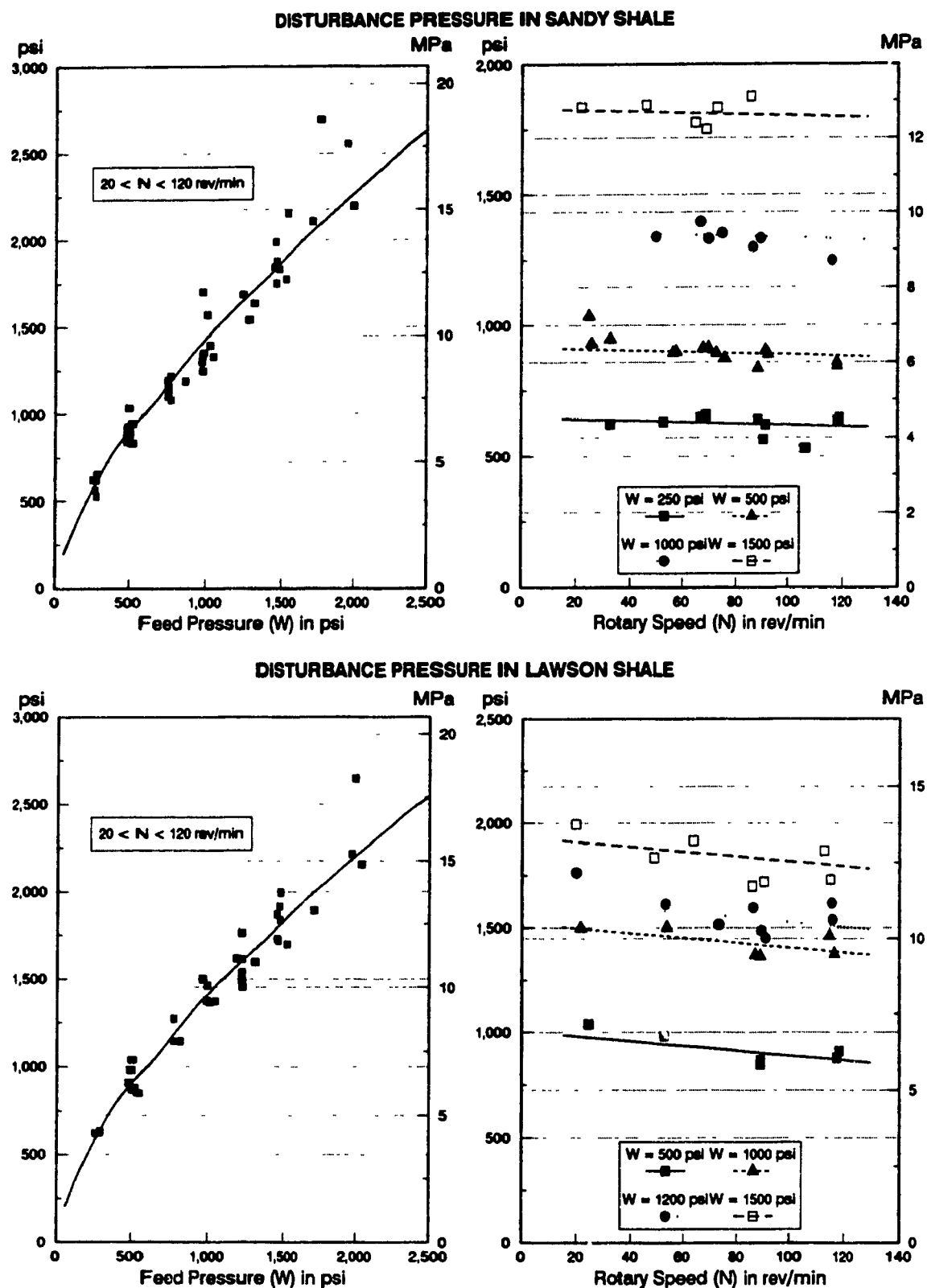


Figure 5.13: P_{dist} in Sandy and Lawson Shales plotted against feed pressure and rotary speed

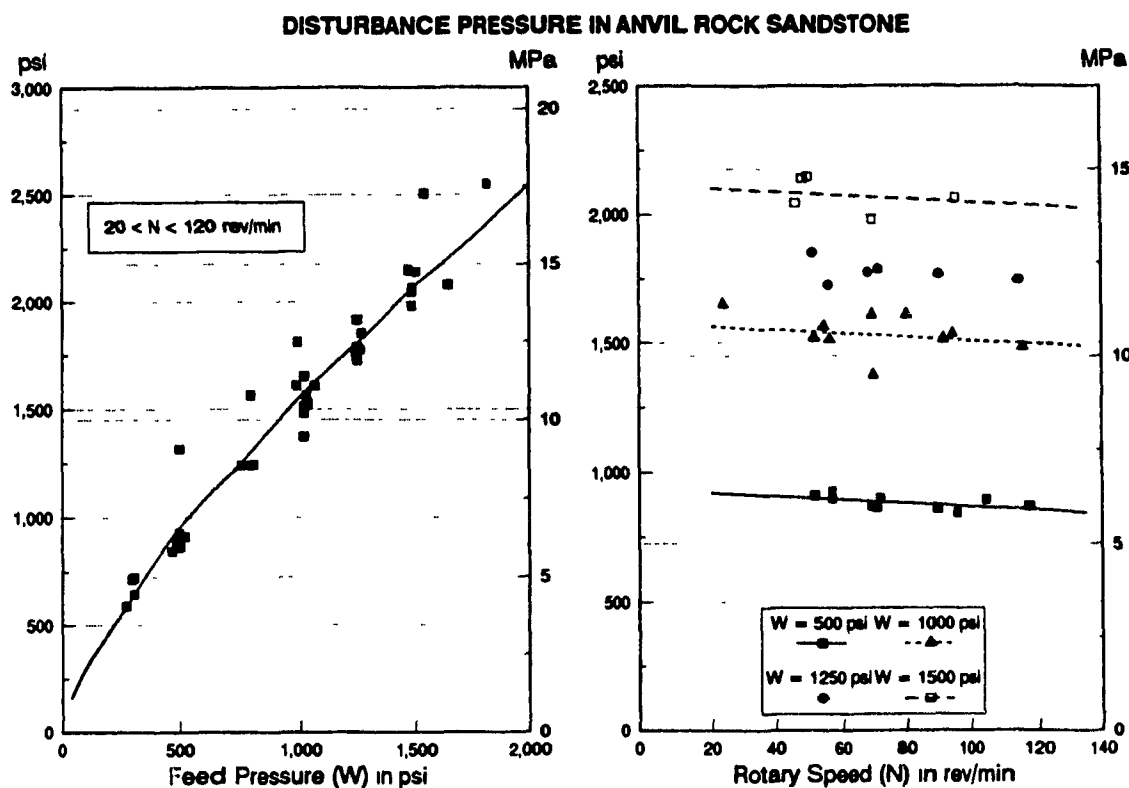


Figure 5.14: P_{dist} in Anvil Rock Sandstone plotted against W and N

rate model was applied to the P_{dist} observations. The results are tabulated in table 5.4, along with R^2 and the percentage of outliers not considered in the fit. The equations show a power relationship between P_{dist} and feed pressure, with high values for R^2 and a low percentage of outliers. The variation in the exponent of W is moderate for the five rock types, however the main change is in the coefficient of W .

From a control point of view, it is concluded that an increase in feed pressure would increase the disturbance pressure which in turn would increase the rotation pressure. Since rotation pressure is one constraint not to be exceeded, it is clear that it should be part of the feedback signals upon which the controller would base its control actions.

| Rock Type | P_{dist} | R^2 | % data discarded |
|-------------------------|------------------------------|-------|------------------|
| Bankston Fork Limestone | $P_{dist} = 5.046W^{0.791}$ | 0.93 | 0 |
| Anvil Rock Sandstone | $P_{dist} = 11.756W^{0.707}$ | 0.95 | 6.25 |
| Lawson Shale | $P_{dist} = 16.418W^{0.645}$ | 0.96 | 7.14 |
| Sandy Shale | $P_{dist} = 14.525W^{0.664}$ | 0.97 | 1.67 |
| Brereton Limestone | $P_{dist} = 6.098W^{0.779}$ | 0.81 | 8.53 |

Table 5.4: P_{dist} evaluated in five different rock types, using an arbitrary model

5.7 Conclusions

Based on the results from the current data analysis, the following points appear to be valid;

1. Penetration Rate

- The data shows the monotonicity of the penetration rate versus feed pressure and penetration rate versus rotation speed characteristics. Increasing feed pressure and rotary speed will increase the penetration rate up to the point where the bit becomes buried in rock, assuming other constraints – rotation pressure, vibration level, bailing air pressure ... – have not been violated.
- The model for penetration rate proposed by Maurer has been validated and derived for the five rock types of Brereton and Bankston Fork Limestones, Anvil Rock Sandstone, Sandy and Lawson Shales.

2. Penetration Per Revolution

- The data shows monotonicity of the penetration per revolution $\frac{R}{N}$ versus feed pressure characteristics. Increasing feed pressure increases $\frac{R}{N}$.
- In the shales, $\frac{R}{N}$ decreases with increasing rotary speed at constant feed pressure. In Anvil Rock Sandstone and in the limestones, $\frac{R}{N}$ remains nearly constant under the same conditions. As a result, $\frac{R}{N}$ can be increased by increasing feed pressure at constant rotary speeds in the five considered rock types, or by *reducing rotary speed* in the shales, with feed pressure maintained constant.
- The penetration per revolution $\frac{R}{N}$ can exceed the length longest insert on the bit by a small fraction in the soft formations, without adversely affecting the operation of the machine.

3. Disturbance Pressure

- Plots of disturbance pressure versus rotation speed behavior at constant levels of feed pressure show a relatively flat behavior, which is specific to the rotary actuators used in the D75K drill. Consequently, the disturbance pressure (P_{dist}) depends on feed pressure. Increasing feed pressure increases P_{dist} , which in turn results in a rise in the rotation pressure (P_{rot}).
- The model for torque proposed initially by Warren did not fit the data presented here. However, a direct correlation between P_{dist} and feed pressure was established, enabling the computation of the rotation pressure P_{rot} .

4. Control Considerations

- Since the penetration rate and the disturbance pressure appear to be more sensitive to feed pressure than to rotary speed, the choice of feed pressure as the manipulable variable is adequate for control.

- The results of the data analysis form a platform upon which a suitable control strategy can be formulated. The models for penetration rate and rotation pressure can be used to build a software simulator that would interface with the developed control algorithm, enabling testing, tuning and validation of the control strategy.

Chapter 6

IDENTIFYING THE D75K DRILL DYNAMICS

6.1 Objectives

In this chapter, the mechanical behaviour of the D75K drill and its dynamic response are identified. The primary tool used is Matlab's *System Identification Toolbox* and the *Control Toolbox*.

6.2 Rotary actuators dynamics

The response to step inputs of the rotary actuators is shown in Fig. 6.1. The data have been digitized from borehole N3, where several tests were run with the bit rotating in the air (no load at bit–rock interface). For good noise rejection, the analog signals were low-pass filtered at 500 Hz and sampled at 1 KHz , then further low-pass filtered digitally at 50 Hz and decimated by 5 (i.e. resampled the resulting smoothed signal at a rate of 200 Hz).

Figure 6.1 shows a delay of approximately 200 ms between the rotary speed demand and the actual response. The size of the pure delay is consistent with transportation delay between the hydraulic valve and the actuators due to long hoses. A slight overshoot is also observed before steady state is reached. Also shown is the

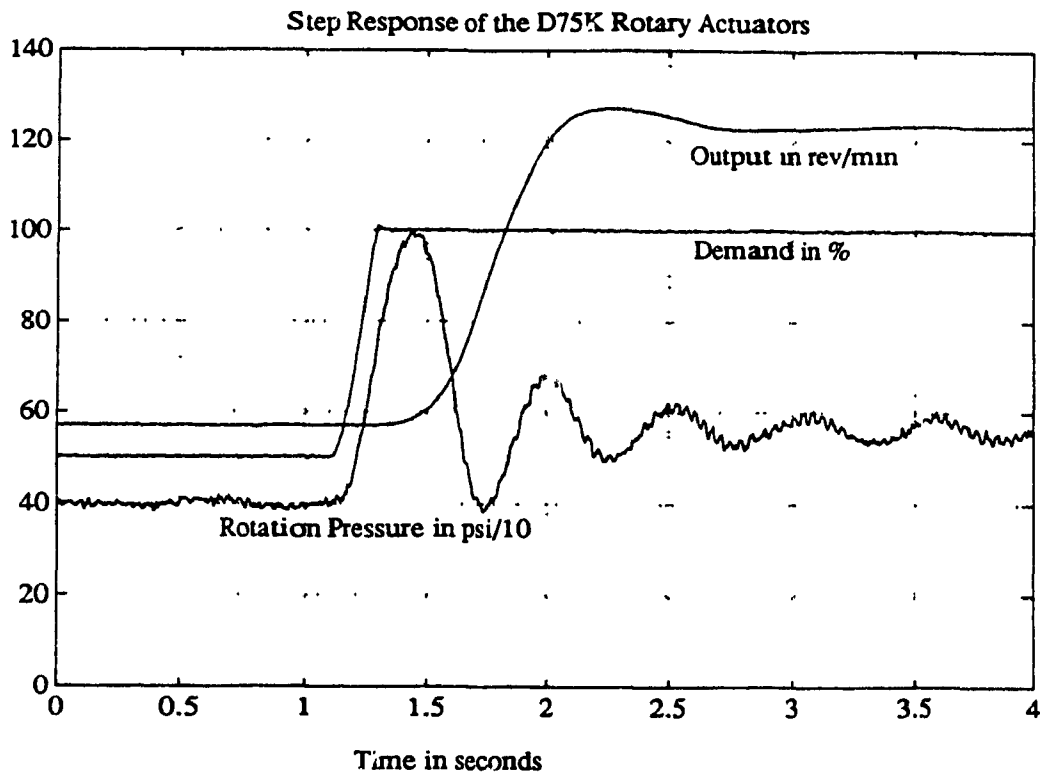


Figure 6.1: Rotary actuators response with step inputs

rotation pressure (P_{rot}) whose amplitude has been divided by 10 to fit in the same graph.

The step input has been deliberately selected to start from a non-zero steady state rotary speed to reduce stiction effects. It was decided that a second order system would be appropriate to approximate the actual input/output relationship. A second order system is described by the following transfer function:

$$\frac{Output(s)}{Input(s)} = \frac{\omega_n^2}{s^2 + 2\zeta\omega_n s + \omega_n^2} \quad (6.1)$$

where ω_n is the natural frequency and ζ the damping factor. The parameters to be identified are thus reduced to ω_n and ζ . Initial values for ω_n and ζ were selected based on the rise time and overshoot of the response and then refined by comparing the simulated response to that of the actual one.

Figure 6.2 shows the simulated response for $\omega_n = 4.7 \text{ rd/s}$ and $\zeta = 0.65$

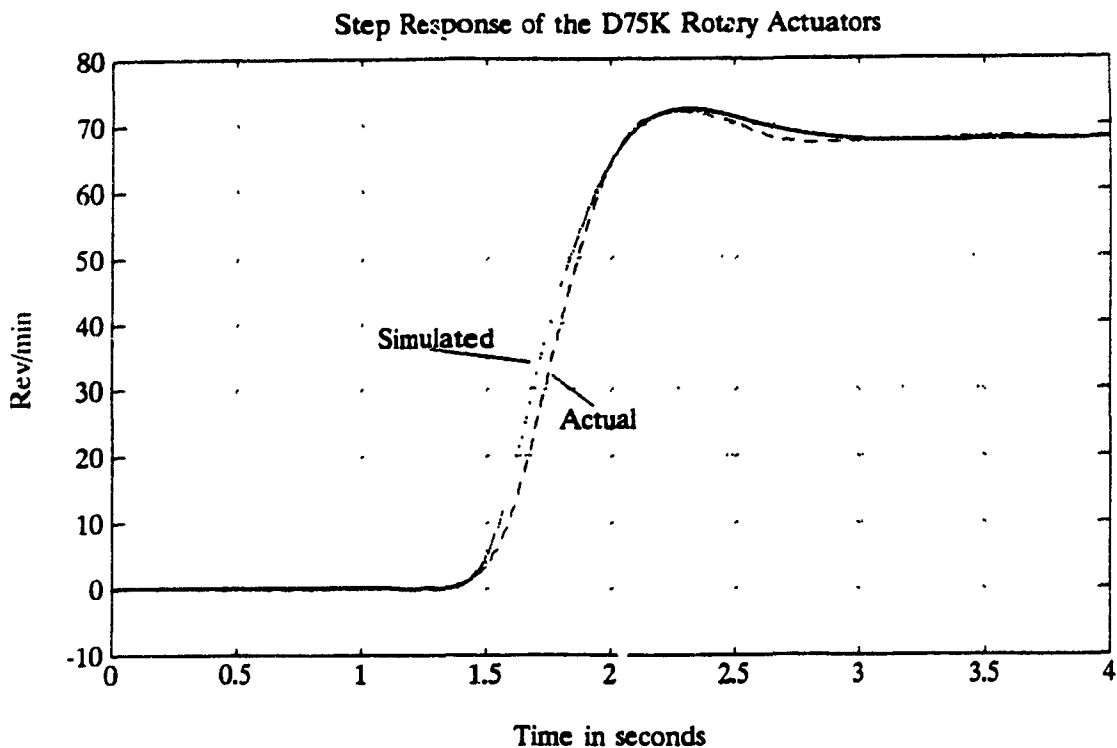


Figure 6.2: Rotary actuator response: actual and simulated

along with the actual output. The transfer function thus obtained is

$$\frac{N(s)}{N_{ref}(s)} = \frac{(4.7)^2 e^{-0.2s}}{s^2 + (2)(0.65)(4.7)s + (4.7)^2}$$

or

$$\frac{N(s)}{N_{ref}(s)} = \frac{22.09 e^{-0.2s}}{s^2 + 6.11s + 22.09} \quad (6.2)$$

The exponential term accounts for the 200 ms delay. For simulation purposes, the delay has been implemented using a 4th order Pade transfer function approximation.

6.2.1 Effect of Bit Loading on Rotary Speed

It had been observed that the rotary speed decayed slightly with increase in the rotation pressure, due to loading of the bit. Figure 6.3 shows this behaviour from data collected while drilling in Brereton Limestone. A similar behaviour has been observed in the other rock types as expected since this phenomenon depends strictly

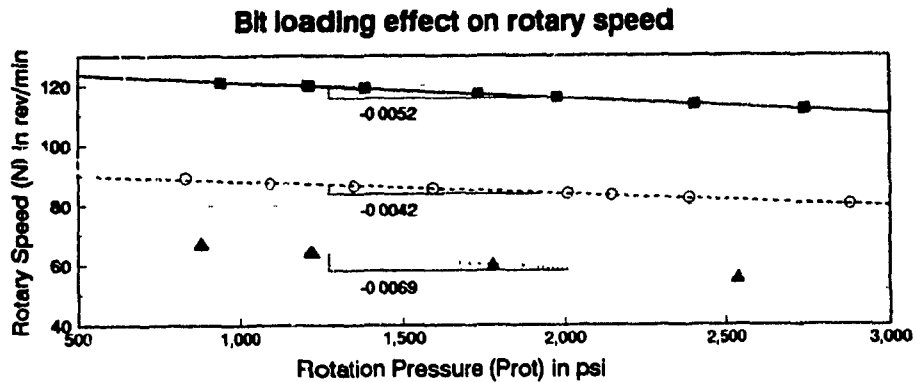


Figure 6.3: Effect of bit loading on rotary speed

on the machine mechanics. From the data plotted, the following approximation can be extracted:

$$N = N_{no-load} - 0.005 * P_{rot} \quad (6.3)$$

where $N_{no-load}$ is the rotary speed before the bit is coupled with rock.

6.3 Feed actuator Dynamics

In a drilling cycle, the bit is coupled with rock. The feed actuator response is thus examined for such conditions, for simplicity of analysis. Figure 6.4 shows the feed actuator's response in two different rock types (Hard versus Soft), at a rotary speed near 65 rev/min. Although the two rock types differ largely in hardness, their effect on the feed actuator appears to be small. It is reasonable to expect that the response be damped due to rock resisting the motion of the actuator.

A first order system approximation with a fixed time constant of 300 ms appeared acceptable. Since the operator's set-point to the feed actuator was not recorded (chapter 4), the true delay occurring between the set-point and the feed pressure could not be evaluated. However, by analogy with the rotary actuators, a delay of 200 ms was assumed since the mechanical coupling and length of the hydraulic hoses for both actuators was roughly the same.

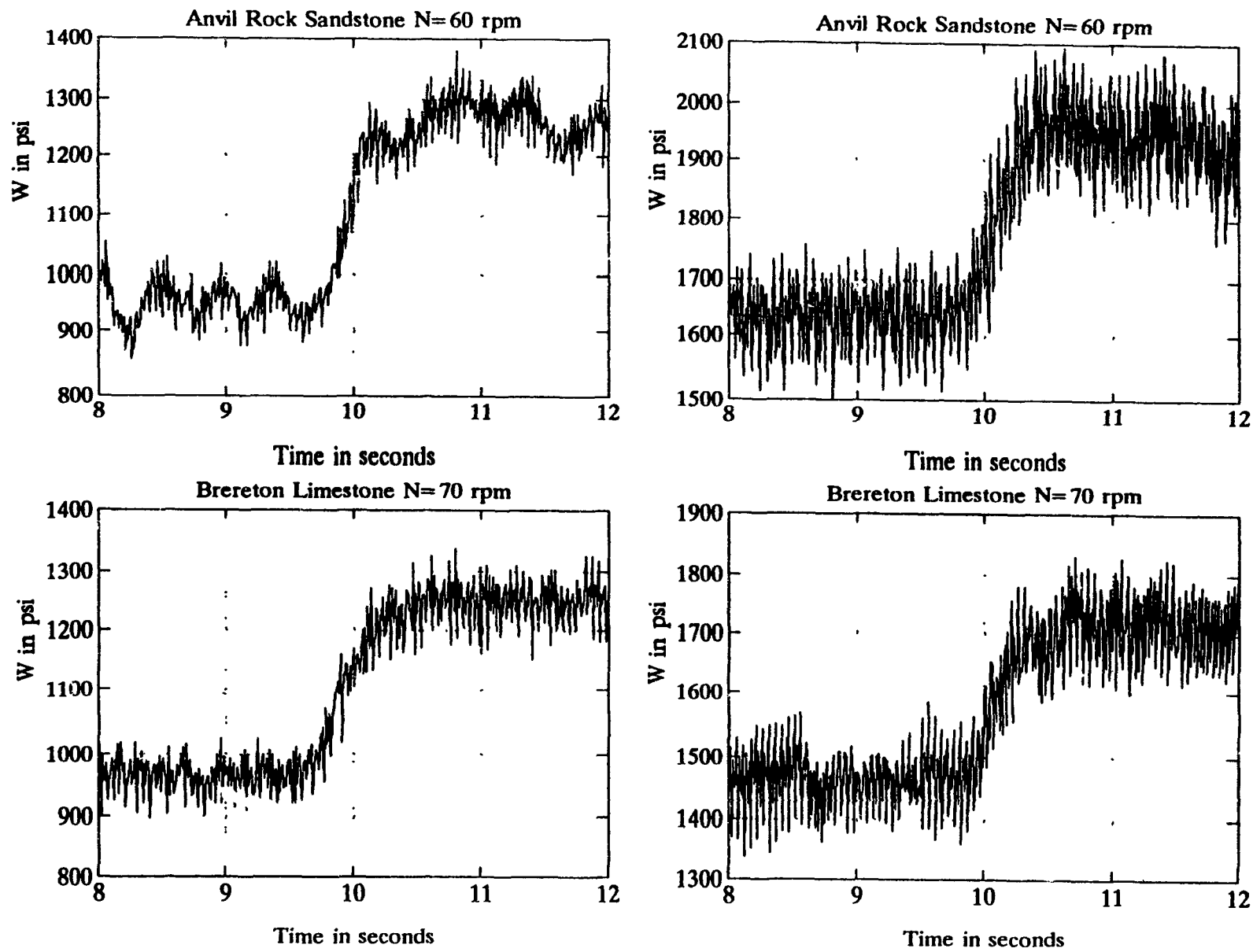


Figure 6.4: Feed actuator response in two different rock types

To summarize using equations:

$$\frac{W(s)}{W_{ref}(s)} = \frac{e^{-0.2s}}{0.3s + 1} \quad (6.4)$$

6.4 Conclusion

The machine dynamics and delays in the system have been identified. These results will be oriented towards the design of a computer blasthole drilling simulator, discussed in chapter 7.

Chapter 7

CONTROLLER DESIGN

7.1 Formulation of The Control Strategy

The drilling process in the absence of "abnormal" exceptions such as bit failure, drill string jamming, cavities or fractured rock encounters etc. can be viewed as a time-varying multivariable dynamic system, subject to various disturbances. The exceptions may be viewed in the framework of discrete events which change the characteristics of the dynamic system from "normal" to one of a finite number of structured states.

It follows from the decomposition of the controlled process into a relatively slowly time-varying dynamic system, within the larger framework of a virtually instantaneously changing discrete-event, that a two-tier control strategy needs to be adopted, as illustrated in Fig. 7.1. Although events happen instantaneously in the outer loop, they occur with much less frequency than the variations of the variables in the inner dynamic loop. Hence we can view this scheme as a high bandwidth inner control loop, around which is a low bandwidth "supervisory system". While classical control design techniques apply to the inner control loop, the outer lower bandwidth loop however requires some knowledge-based reactive strategy.

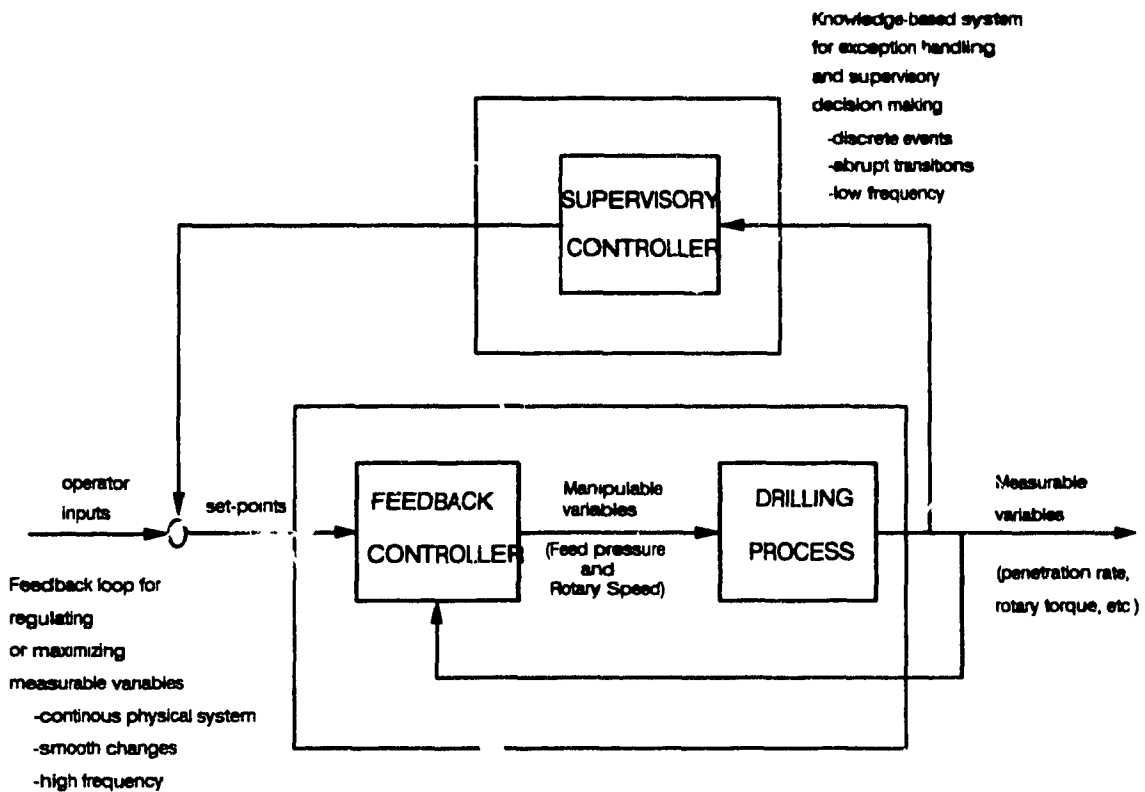


Figure 7.1: The Two Tier Control Strategy

It may be possible to use the supervisory loop to provide set-points of rotary speed and feed pressure to the inner control loop, derived from a function which attempts to minimize drilling costs. The predetermined minimum cost function would be based on bit and drill cost, labor, power, maintenance, rig life, drilling performance etc.

Although the supervisory loop has been introduced, it will not be considered in further detail in this thesis.

7.2 Formulation of The High Bandwidth Inner Control Loop

From the analysis of experimental data, discussions and observations during field tests, the following holds:

1. The feed pressure is the variable which primarily affects the penetration rate, the penetration per revolution and the rotation pressure.
2. It has been observed during experimental testing that high rotary speeds resulted in excessive vibrations, mainly in the shales. Adjusting rotary speed would not only affect penetration rate, but would affect the vibration level as well.
3. From the conclusions of chapter 5, increasing feed pressure would increase both the penetration rate and the rotation pressure. Since it was observed that the P_{dis} versus feed pressure characteristic remains fairly similar for different rock types, regulation of the rotation pressure P_{rot} at some "maximum allowable" level by continuously adjusting feed pressure appears to be adequate for maximizing penetration rate at the operating rotary speed – as long as the bit does not become buried – with vibration and bailing air pressure remaining within acceptable operating range.
4. It was observed during experimental tests that the drill operator – during normal drilling – tended to set the rotary speed at maximum levels and to maintain feed pressure greater or equal to 1500 psi as long as levels of vibration, bailing air pressure and rotation pressure were acceptable. In the event of sudden overshoot in vibration and the rotation pressure, the immediate reaction was to back off the rotary speed set-point.
5. The penetration per revolution should not exceed a maximum allowable limit, to prevent burying the bit and to reduce the occurrence of exceptional conditions.

The analysis described in the following sections will continuously refer to the above 5 points.

7.2.1 Control Philosophy

An intermediate step in drilling automation consists of reducing the manipulable variables of rotary speed and feed pressure to only one manipulable variable. From point 1, it is clear that feed pressure is the initial choice. Thus, rotary speed remains controlled by the drill operator¹. The control system should not alter the behavior or judgment of the driller. In case of sudden build up in vibrations – while feed pressure is automatically controlled – the operator should be able to damp them out by reducing rotary speed.

Thus the reduction of rotary speed should inevitably drive the machine to a state of increased stability.

7.2.2 Stability Considerations

Let us consider the state variables to consist of (N, W, P_{rot}, R, V_b) where V_b is a measure of vibration (axial and vertical). The state origin $(0,0,0,0,0)$ is obviously a stable state. Thus reducing N to achieve stability can be seen as driving the other state variables towards the origin.

Based on the analysis covered in chapter 5 and on field observations, decreasing N (by reducing the set-point for rotary speed) reduces R and V_b . Since N and W are relatively decoupled, W remains practically unaffected. Chapter 5 has shown a relatively flat torque characteristic for the D75K rotary actuators, suggesting that the disturbance pressure P_{dist} is not significantly reduced by a decrease in N . However, Eq. 4.15 page 36 shows that the rotation pressure P_{rot} depends on N and \dot{N} . During the exceptional conditions of high vibration of the drill string, while W is

¹In some mines or quarries where the rock strata is fairly homogeneous, the drill operator maintains the feed pressure almost constant all the time, and adjusts rotary speed. These mines or quarries may prefer the choice of automatic controls for rotary speed while keeping manual control over feed pressure

maintained within normal operating limits, the term $\frac{J_L}{K_p} \dot{N}$ dominates expression 4.15 and the rotation pressure would overshoot. Under such conditions of high rotation pressure and reasonable feed pressure, decreasing N would decrease P_{rot} .

To summarize, decreasing N would reduce R , V_b and P_{rot} , but W remains unaffected. For a stable implementation of automatic feed pressure control, the control system must be able to react when N is decreased by either reducing W or maintaining it equal to its current level.

7.2.3 Penetration Per Revolution Feedback Control Loop

A control strategy that respects the stability requirements consists of regulating the penetration per revolution ($\frac{R}{N}$) with respect to a preset value, to be selected by the mine. However, care must be taken to avoid the division of R by N when N is zero. The regulation of $\frac{R}{N}$ offers the advantage of preventing the bit from excessive overloading, reducing bit and bearing failure, thus prolonging bit life.

From point 1, $\frac{R}{N}$ is mainly controlled by W , justifying the choice of W as a manipulable variable. For any rotary speed demand by the drill operator, W would stabilize at a certain steady state value. The behaviour of $\frac{R}{N}$ with respect to N , as analysed in chapter 5, has shown that $\frac{R}{N}$ slightly decreases or remains constant, depending on the rock type. For example, in Brereton, Bankston Fork Limestone and Anvil Rock Sandstone, modifying N would lightly affect W , while in Sandy and Lawson Shale, decreasing N would increase $\frac{R}{N}$, forcing the control algorithm to reduce W to drive $\frac{R}{N}$ back to the preset value. This behavior in the shales may prove useful since the shales are known to be sticky and responsible for high vibrations and rotation pressures. By reducing N in the shales, the vibrations and W would be reduced. The reduction of W would also reduce the disturbance pressure P_{dist} .

The choice of a preset value for $\frac{R}{N}$ depends mainly on the length of the

longest insert on the bit in use, the rock to be drilled and the levels of $\frac{R}{N}$ that could be achieved at the specified location without exposing the machine to severe operating conditions. As mentioned in the conclusions of chapter 5, $\frac{R}{N}$ could be chosen to be 20% higher than the longest bit insert in soft formations. The first drilled boreholes could serve as a test to determine the best selection for $\frac{R}{N}$, by visually monitoring the gauges on the driller control panel and determining average operating values of W , P_{rot} and V for a particular selection of $\frac{R}{N}$.

Figure 7.2 shows a block diagram of the penetration per revolution controller. It is assumed that the bit is rotating at a rotary speed set by the drill operator. The input signal is the preset $\frac{R}{N}$ while the feedback signal is the measured $\frac{R}{N}$. The error signal is read by the controller, then a feed pressure demand W_{dem} is issued to the plant. A software saturation block prevents W_{dem} from exceeding a maximum allowable value that is preset by the mine.

The primary constraining variables are the rotation pressure (P_{rot}), vibration and bailing air pressure rise. Control of P_{rot} is discussed in the following section. Vibrations are controlled by the drill operator, by reducing rotary speed. The usual driller reaction to an increase in bailing air pressure consists of reducing momentarily the feed pressure. In the proposed control system, this task is handled by the "supervisory control loop" which after detecting such condition, would momentarily decrease the $\frac{R}{N}$ set-point to the control system, below the preset value. This would ultimately result in a reduction in feed pressure allowing the bailing air to clear the bit and prevent it from plugging. Since the "supervisory control loop" is not covered in this thesis, no further details concerning this topic are provided.

7.2.4 Rotation Pressure Controller

If the rotation pressure (P_{rot}) constraint in the penetration per revolution controller is violated, e.g. due to being in a stratum where the desired set-point is not achievable

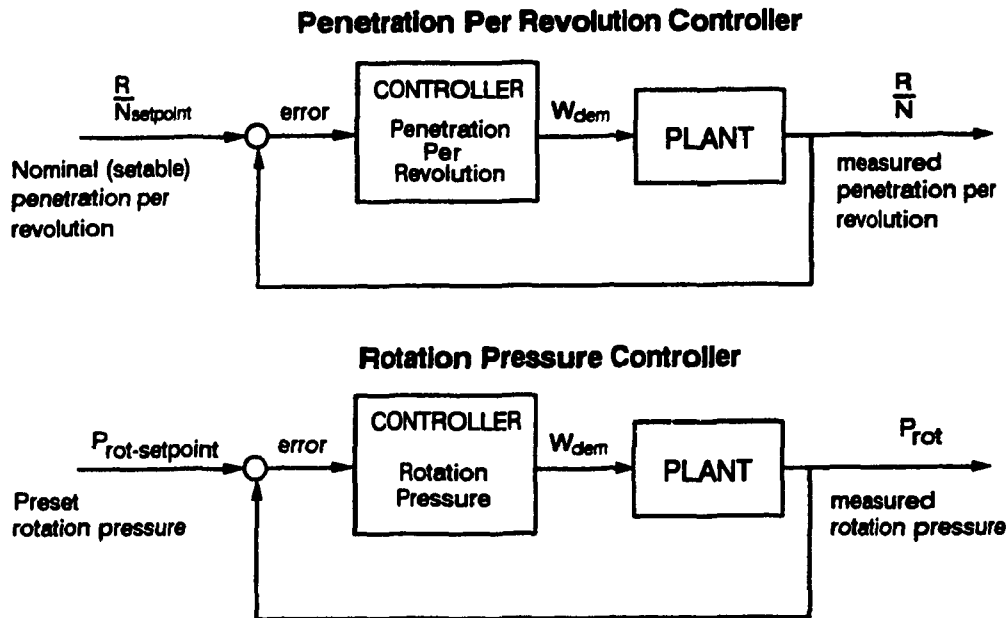


Figure 7.2: Penetration per revolution and rotation pressure controllers block diagram

within that band due to high P_{rot} (e.g. hard rock), then control switches to another loop that attempts to regulate P_{rot} to a preset level. The preset level for P_{rot} is the nominal rotation pressure that the mine desires not to be exceeded, and its selection is motivated by the degree of acceptable wear and tear of the machine. In this mode, the penetration rate is maximum at the operating rotary speed and preset P_{rot} (point 3), but the penetration per revolution is below the preset value. When the bit reaches a softer layer, $\frac{R}{N}$ increases again until it exceeds the preset $\frac{R}{N}$, at which time control is switched back to the penetration per revolution control loop.

The switching logic is described in the following pseudo-code:

```

if executing control-loop == regulate  $\frac{R}{N}$ 
  &  $\frac{R}{N} <$  preset  $\frac{R}{N}$ 
  &  $P_{rot} >$  Maximum  $P_{rot}$ 
then switch control-loop to regulate  $P_{rot}$  at preset  $P_{rot}$ 

```

if executing control-loop == regulate P_{rot}

& $\frac{R}{N} >$ preset $\frac{R}{N} + \epsilon$

then switch control-loop to regulate $\frac{R}{N}$ at preset $\frac{R}{N}$

Note that the addition of ϵ provides an optional degree of hysteresis for the second switching condition.

The executing control loop is by default regulating the penetration per revolution. Therefore, if for some reason, both P_{rot} and $\frac{R}{N}$ exceed their preset maximum values, the controller would react by reducing feed pressure to reduce $\frac{R}{N}$ back to its preset value. At the same time, P_{rot} decreases. It is only after $\frac{R}{N}$ decreases below its preset value that the controller would switch to the rotation pressure controller.

Figure 7.2 shows a block diagram of the rotation pressure controller. The input signal is the preset P_{rot} while feedback is provided by the measured P_{rot} . The feed pressure demand is computed by the controller based on the error signal. The constraining variables are vibration and bailing air pressure. Vibrations are reduced by the driller by reducing N . If bailing air pressure rises while the controller is in this mode, the "supervisory loop" would momentarily decrease the P_{rot} input to the control loop below the preset P_{rot} , ultimately reducing W .

7.3 Feedback Controllers Structure

In the general context, the function of a controller is to achieve a desired response from a system irrespective of the effect of internal (plant) and external (environmental) changes. The control objectives may be stated as [29]:

1. Minimizing steady state error

2. Minimizing settling time

3. Achieve other transient specification, such as minimizing the maximum overshoot and reduce rise-time.

For the present control problem, the primary objective is to minimize severe overshoots in the variables due to transitions between rock layers of different hardness, while keeping the steady state error close to zero.

The controllers selected for implementation are *Proportional Integral Derivative* (PID) controllers. PID controllers produce a control signal based on the error signal between the desired set-point and the actual output.

7.3.1 Proportional Control

A proportional controller generates a control signal proportional to the error signal. Proportional control gives a zero control signal for zero error. Therefore, a stable system with proportional control would reach an equilibrium in which the control signal no longer changes, allowing a constant steady state error to exist. Increasing the proportional gain reduces the steady state error but adversely affect the system's stability.

7.3.2 Integral Control

An integral controller produces a signal that is proportional to the time integral of the error. More important, the type of the system is increased by one, improving the steady state error by one order; that is, if the steady-state error to a given input is constant, the integral control reduces it to zero (provided the system is stable) [21]. However, because the system has increased by one order, it may become less stable than the original system.

7.3.3 Derivative Control

A derivative control produces a signal proportional to the derivative of the error signal. Since the derivative of the error represents its slope, derivative control can be seen as an anticipatory kind of control. For instance, large overshoots are predicted ahead of time and proper correcting effort is made. It is apparent that derivative control produces a signal *only* if the steady state error is not constant with respect to time. Therefore, derivative control should never be used alone.

7.3.4 PID Control

From the previous assertions, proportional control used with derivative control would add damping to the system, but the steady state response is not affected. Using PI control alone could add damping and improve the steady state error at the same time, but the rise time and settling time are penalized. This leads to the motivation of using a PID controller so that the best properties of each of the PI and PD are utilized.

The PID controller can be modeled as:

$$u(s) = \left[K_P + \frac{K_I}{s} + K_D s \right] e(s) \quad (7.1)$$

where u is the control signal, e the error defined as $e = u_c - y$ where u_c is the set-point reference and y the process output. K_P , K_I and K_D are the proportional, integral and derivative gains respectively.

7.3.5 Controller Implementation

Controllers connected in series with the plant are the most common because of their simplicity in implementation, depending on the nature of the process. However, they offer one degree of freedom, even though they may have more than one parameter

that can be varied. The disadvantage with a one-degree-of-freedom controller is that the performance criteria that can be realized are limited.

Controllers that are connected to the plant with a minor-loop compensation allow two-degrees-of-freedom and yield a performance that is more robust (insensitive) to external disturbance and parameter variations. The analytical model of the controller becomes:

$$u(s) = \left[K_P + \frac{K_I}{s} \right] e(s) - \frac{K_V}{1 + T_n s} y(s) \quad (7.2)$$

Note that derivative control is applied to the output y as opposed to the error e in the original form (7.1). Furthermore, the output y is filtered to avoid differentiation of the (high frequency) measurement noise [12].

The block diagram implementation of the PID controller in the simulator is shown in Fig. 7.3. Due to the nature of the drilling process, the measured output signals are noisy, and consequently the error signal is filtered with a single pole low pass transfer function. The filtered error becomes the input signal to the PI controller, which produces the control signal u . The minor loop compensator consists of a derivative controller in series with a first order low pass filter. The output signal from the minor loop is subtracted from the control signal u , adding additional damping to the oscillations in the system.

The actual controller is implemented as a software source code using Microsoft C compiler, version 5.1, and is completely transportable to commercial programmable controllers. To implement this code on the actual system would require replacement of the Input/Output functions by those appropriate to the specific software and hardware environment in which they are to execute.

The controller is implemented in digital form, with a sampling frequency of 10 Hz. The S domain transfer functions have been replaced by their Z transform equivalent at the specified sampling rate. A zero order hold (ZOH) block is inserted

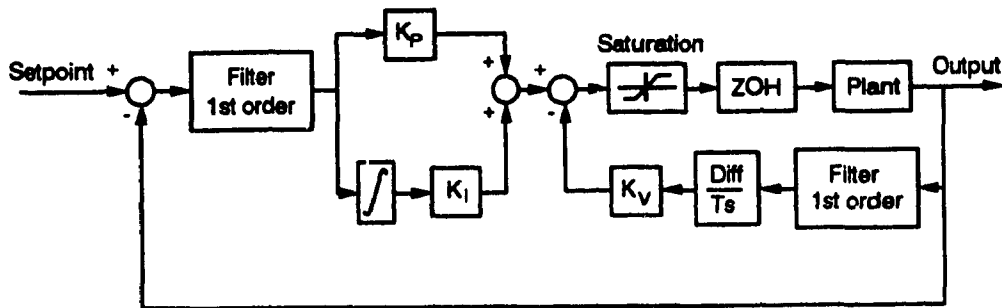


Figure 7.3: Block diagram of PID controller implementation

in series with the plant to maintain the output signal constant during the sampling interval. In addition, a multitude of extra features has been implemented, such as integral windup prevention, integral preload and derivative limiting. These features are essential to safe and effective operation in practice [3].

7.4 Controller Testing and Tuning

The controller, as developed, needed to be tested, tuned, and validated. The development of a computer simulator for the blasthole drilling process would enable one to simulate the drill's operation under various conditions. The controller developed can be tested by interfacing it with the computer simulator. The simulation results would thus allow the designer, if necessary, to modify the control architecture appropriately for achieving the desired performance.

Validation of the simulator would be done by comparing the simulation results with the corresponding field tests, reflecting a wide enough range of drilling conditions and materials.

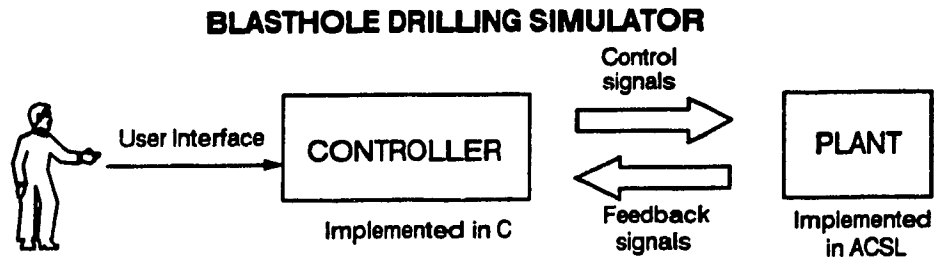


Figure 7.4: The Blasthole Drilling Simulator Block Diagram

7.5 Simulating the Plant

The simulation strategy links two environments: controller and plant. The plant is the drilling system described in chapter 3.

Normal operation of the drill requires the operator to collar the hole, then set an average level of rotary speed and initiate automatic control. The control system would send the necessary control signals to the plant. Figure 7.4 shows a block diagram of the simulator's current structure.

The bit-rock interface in the plant is inherently non-linear, and as such, the development of a simulator requires a simulation language capable of handling non-linear systems. The simulation language chosen for the plant is the *Advanced Continuous Simulation Language* (ACSL) in combination with the user-friendly interface *ACSL/PC Enhancer* (APE). Using the APE interface accelerated the iterative process of code development, testing and debugging.

ACSL is in fact a translator, which takes source code readily identifiable with the system to be simulated and converts it to FORTRAN code. This FORTRAN file is then compiled, linked and executed, resulting in the simulator outputs. The APE interface automates the sequencing of these steps through the use of pull-down menus. Compilation of the ACSL translator output was carried out using the MicroSoft FORTRAN V5.0 compiler.

The source code of the controller is written in C and compiled separately (outside the APE environment) to create an object module. The object module is then linked to the ACSL modules, resulting in one executable file.

7.6 Plant Block Diagram

The plant block diagram is shown in Fig. 7.5. The N_{ref} and W_{ref} are the control signals for rotary speed (N) and feed pressure (W). The dynamics of the machine are based on the results of chapter 6, with the addition of saturation blocks to represent the physical limitations of the actuators. The box with dotted border represents the simulated bit-rock interface, which reads as inputs rotary speed, feed pressure and an index S corresponding to a preprogrammed rock layer type.

The simulated plant estimates the penetration rate (R) and the disturbance pressure (P_{dist}) using the equations derived in chapter 5. The simulated R and P_{dist} are low pass filtered with a time constant of 0.1 s then fed back to the controller. The depth is computed for display by integrating the penetration rate, and also used as a pointer to a data structure containing the stored rock strata.

Controllers of different structures can be interfaced with the simulated plant and fine-tuned. In this manner, the behaviour of the important drilling variables can be compared with real data acquired at the Delta mine, while the drill was controlled by a drill operator.

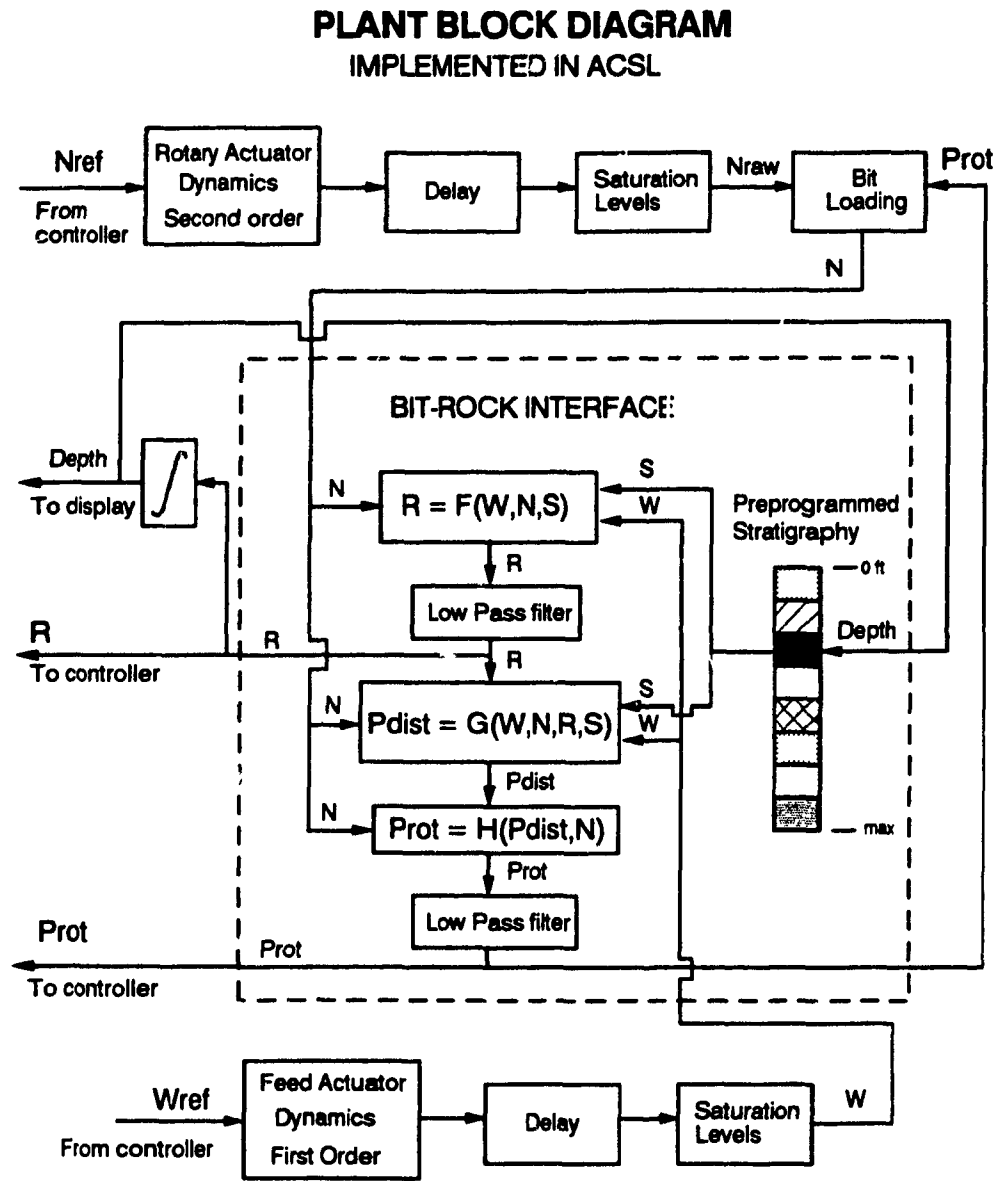


Figure 7.5: Plant block diagram

Chapter 8

SIMULATION RESULTS

8.1 Testing The Plant

Before interfacing the control system to the plant simulator, the validity of the simulated plant needed to be tested. The plant simulator was programmed to simulate drilling in Anvil Rock Sandstone, at constant rotary speed set-point of 60 rev/min, with feed pressure incremented from zero to 1100 psi. The feed pressure set-point was incremented at time intervals matching the real time intervals during actual field testing, enabling the comparison of the simulated results with actual data.

Figures 8.1 and 8.2 show the simulated and the actual variables of feed pressure, rotation pressure, rotary speed and penetration rate. The actual penetration rate data are shown as an average value at the constant feed pressure interval, as they were used in developing the penetration rate models in the previous chapters. The simulated data of feed pressure, rotation pressure and rotary speed compare well with the actual data, except at time 160 seconds, where the rotation pressure sharply increases. The operator reacted by decreasing the rotary speed at time 166 seconds. The plant simulator as implemented did not simulate exceptional situations – such as excessive vibrations, drill string jamming or slapping – which would result in rotation pressure overshoot, as was the case with the actual data. Also, the rotary speed

set-point was maintained at 60 rev/min after time 166 seconds during simulation.

The simulated penetration rate data matches the actual data except during the time interval 100—145 seconds. The actual rotation pressure data shows an unsteady behaviour during the same interval, which may indicate a non-homogeneous rock band, resulting in the penetration rate discrepancy between simulated and actual datum. The simulated penetration rate does not become zero at the beginning and end of the run because the feed pressure and the rotary speed are assigned non-zero minimum values. These small values of rotary speed and feed pressure generate the observed small penetration rate value.

8.2 Testing and Tuning Controller

After the plant simulator has been tested and validated, it was interfaced to the controller. The plant simulator was programmed to simulate drilling in five different rock type layers of one foot thickness each. The five rock types were sequenced in the same order as they actually were (stratigraphy for borehole B3, Fig 4.8 page 43), as follows: Bankston Fork Limestone, Sandy Shale, Anvil Rock Sandstone, Lawson Shale and Brereton Limestone.

The gains of the two feedback loops were adjusted and tuned after several simulation runs. The controller was set to regulate the penetration per revolution at 0.5 in/rev with feed pressure saturating at 3000 psi . The maximum rotation pressure was set to 3200 psi , which if exceeded would switch the controller to regulate the rotation pressure at 2800 psi . The controller would switch back to regulate the penetration per revolution when the latter exceeded 0.6 in under the constant rotation pressure of 2800 psi . Thus the switching condition was given a 0.1 in hysteresis to avoid oscillation between the two control modes. The rotary speed set-point is controlled through the computer keyboard, and was initialized to 50 rev/min .

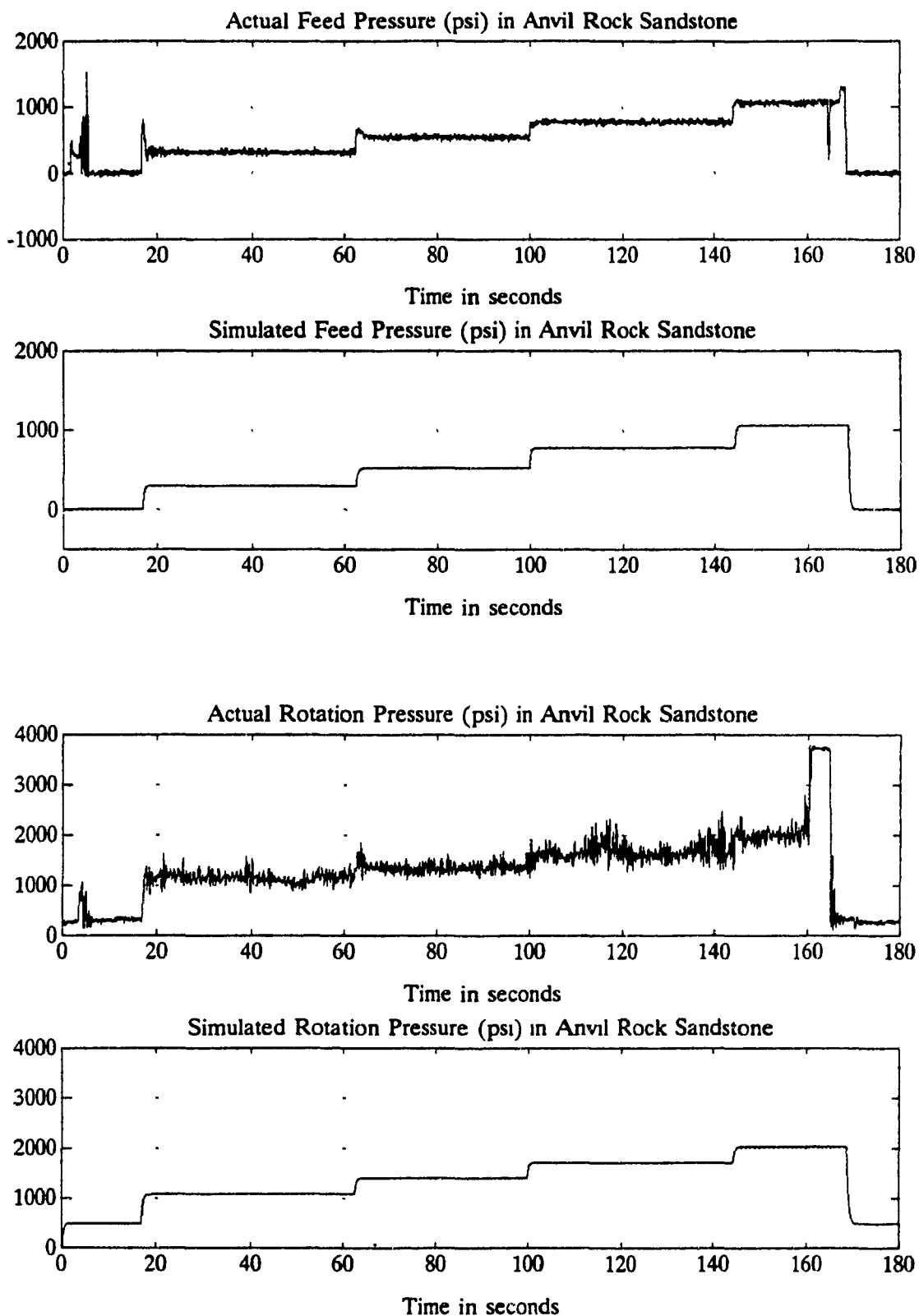


Figure 8.1: Actual and Simulated feed and rotation pressures in Anvil Rock Sandstone

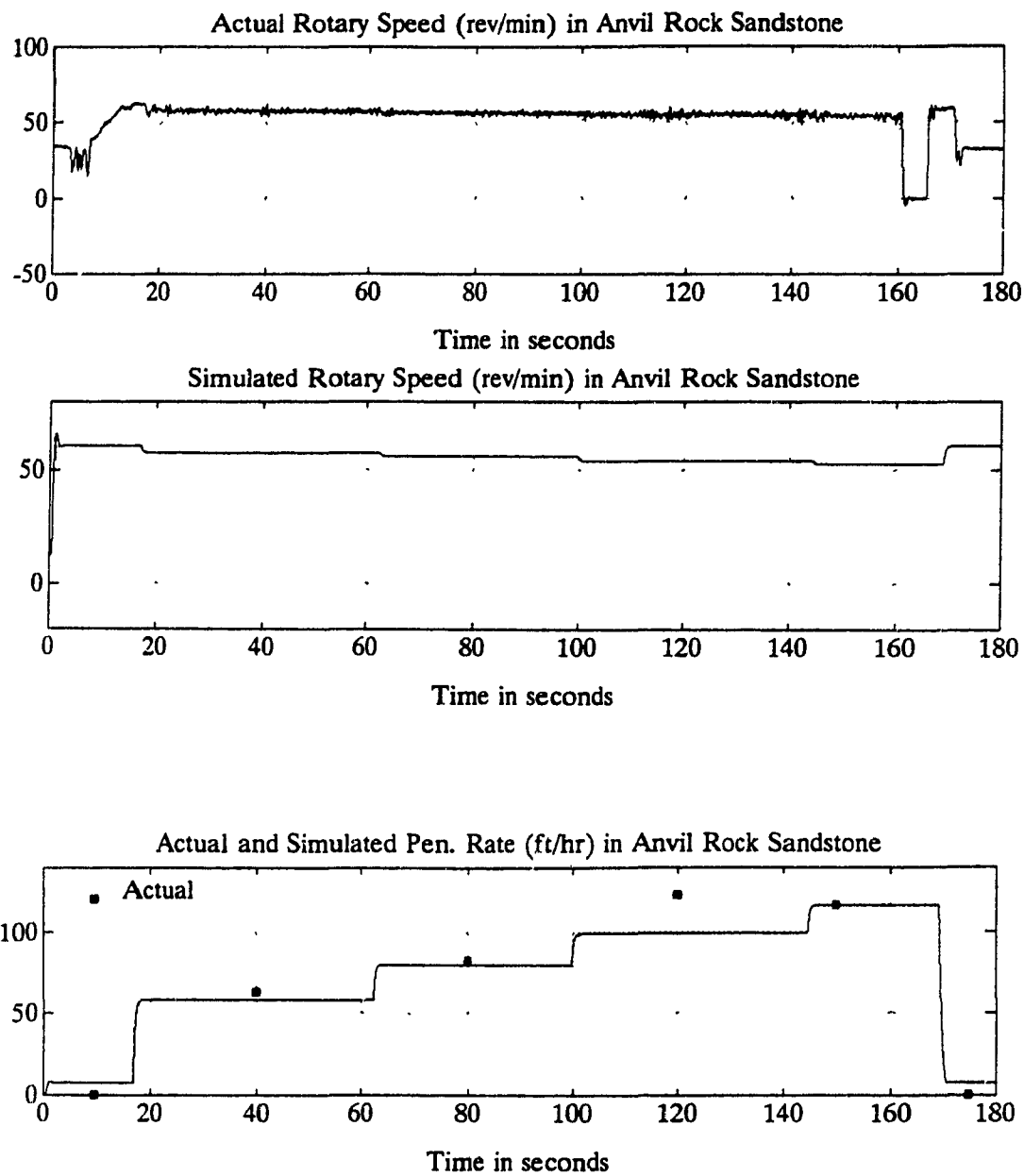


Figure 8.2: Actual and Simulated rotary speed and penetration rate in Anvil Rock Sandstone

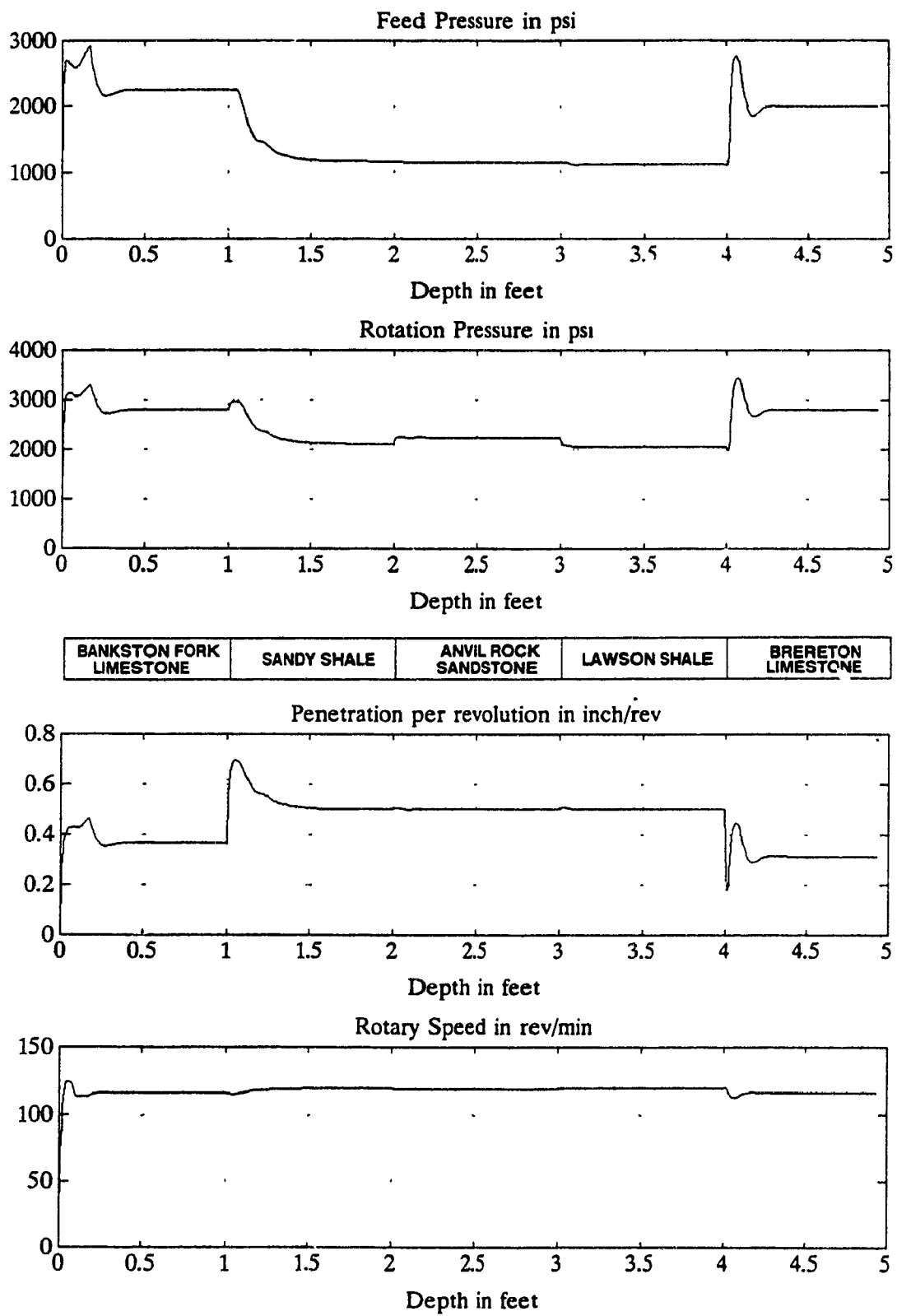


Figure 8.3: Simulation results of controller and plant at constant rotary speed, with $K_P = 4000$, $K_I = 500$ and $K_V = 50$.

The gains of the rotation pressure regulation loop were tuned as follows: $K_P = 0.05$, $K_I = 0.1$ and $K_V = 0$. They remained unchanged during the simulation runs. For the penetration per revolution regulation loop, several gain combinations are discussed.

Figure 8.3 shows the simulation results at constant rotary speed set-point of 130 *rev/min* and controller gains of $K_P = 4000$, $K_I = 500$ and $K_V = 50$. Since the first rock layer was Bankston Fork Limestone, the required penetration per revolution of 0.5 *in/rev* could not be achieved without increasing rotation pressure beyond the 3200 *psi* maximum set value. Thus at depth near 0.3 *ft*, the controller switched to regulate the rotation pressure at 2800 *psi*. When the bit reached the softer layer of Sandy Shale at the depth of one foot, the penetration per revolution increased beyond the set condition of 0.6 *in* upon which the controller switched back to regulate the penetration per revolution. However, it can be observed from the graph of feed pressure, when the latter begins to decrease, that the switching occurred at depth near 1.1 *ft*, while the penetration per revolution had reached 0.7 *in/rev*. This delay in switching is due to the filtering of the error signal – of the actual penetration per revolution and the desired set-point – since the filtered error is the variable satisfying the switching condition. The filter used had a cutoff frequency of 50 *Hz*. If necessary, the peak overshoot of the penetration per revolution can be eased by reducing the filter time constant or reducing the switching hysteresis.

Drilling proceeded smoothly until the bit reached the harder Brereton Limestone layer at depth 4 *ft*. The same remarks apply as for the Bankston Fork Limestone layer, and thus the controller switched to regulate the rotation pressure at depths above 4.1 *ft*.

Figure 8.4 shows the simulation results under the same conditions as in Fig. 8.3 but using relatively higher controller gains, with $K_P = 7500$, $K_I = 1000$ and $K_V = 200$. In the Bankston Fork Limestone layer, the controller was in rotation

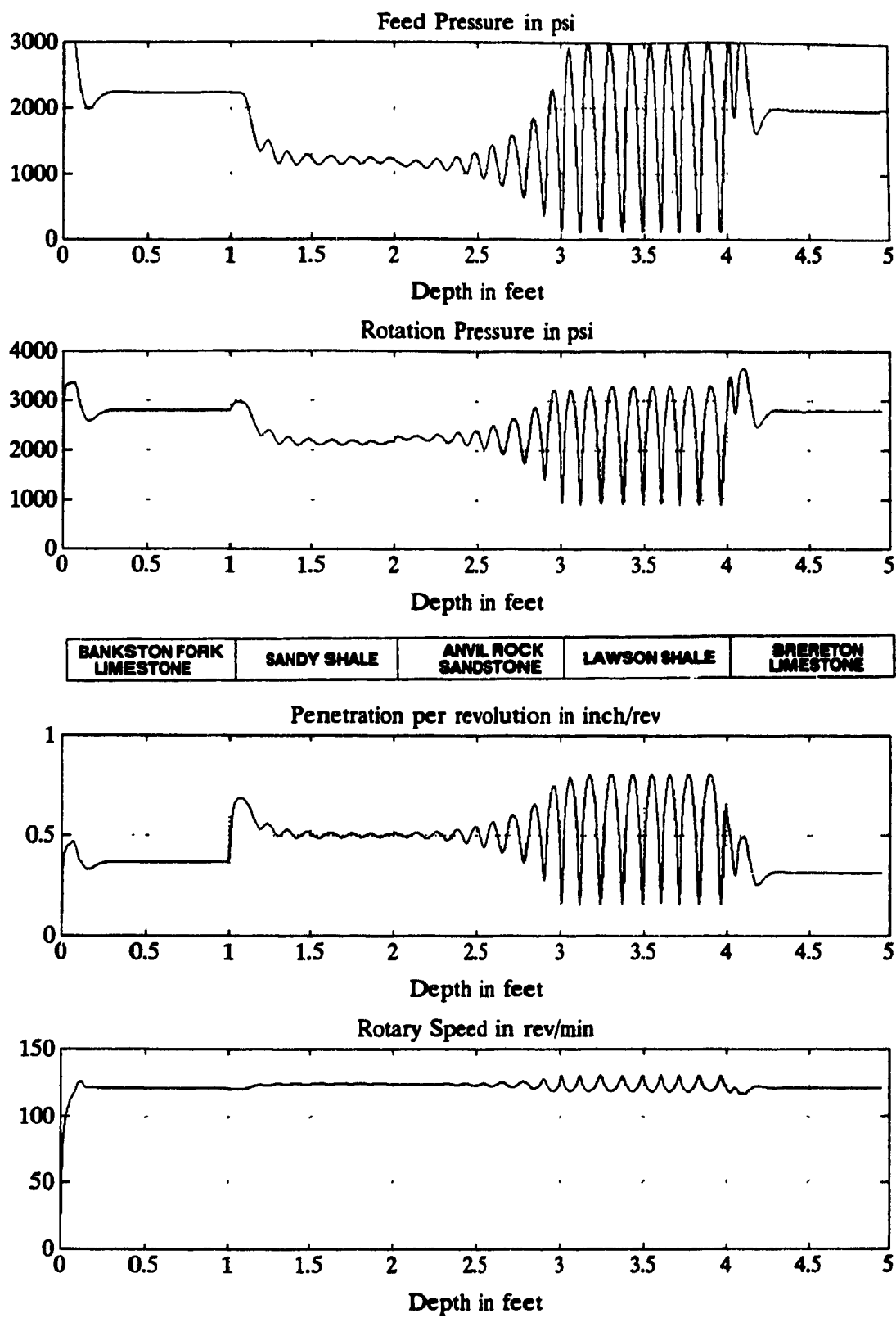


Figure 8.4: Simulation results of controller and plant at constant rotary speed, with $K_P = 7500$, $K_I = 1000$ and $K_V = 200$.

pressure regulation mode. At depth 1.1 *ft* the controller switched to penetration per revolution regulation mode. However, the settling time appears to be much longer in the current Sandy Shale layer. Once in Anvil Rock Sandstone, the system started to become unstable with a growing oscillation, until finally the system reached a limit cycle in Lawson Shale. In the Brereton Limestone layer, the controller switched again to rotation pressure regulation mode.

This result shows that controller gains that appear to be properly tuned in some rock type may result in instability in other rock formations. This is attributed to the fact that in the soft materials, where small increments of feed pressure resulted in a relatively large penetration per revolution, the gains of the closed loop system became larger than what they were when drilling in harder rock types.

Figure 8.5 shows the simulation results of the system under the same conditions and controller gains as in Fig. 8.3, however, the rotary speed set-point was varied during the simulation run. The graphs show sustained oscillation in Sandy Shale at 30 *rev/min* and instability in Lawson Shale at 45 *rev/min*;

This fact is directly related to the closed loop gain which changes according to the rock formation being drilled. Furthermore, the analysis covered in chapter 5 has shown that the penetration per revolution in the shales increased when rotary speed decreased. This behavior had the effect of further increasing the closed loop gains at lower speeds, resulting in the observed oscillations. Ironically, the same behavior was considered in chapter 7 to offer the advantage of decreasing the level of feed pressure when the drill operator decreased the rotary speed set-point. This is true for the average level of feed pressure. However, the system appears to oscillate around this average level .

Figure 8.6 shows the simulation results of the system under the same conditions of Fig. 8.5, but with relatively lower controller gains, with $K_P = 2000$, $K_I = 350$ and $K_V = 50$

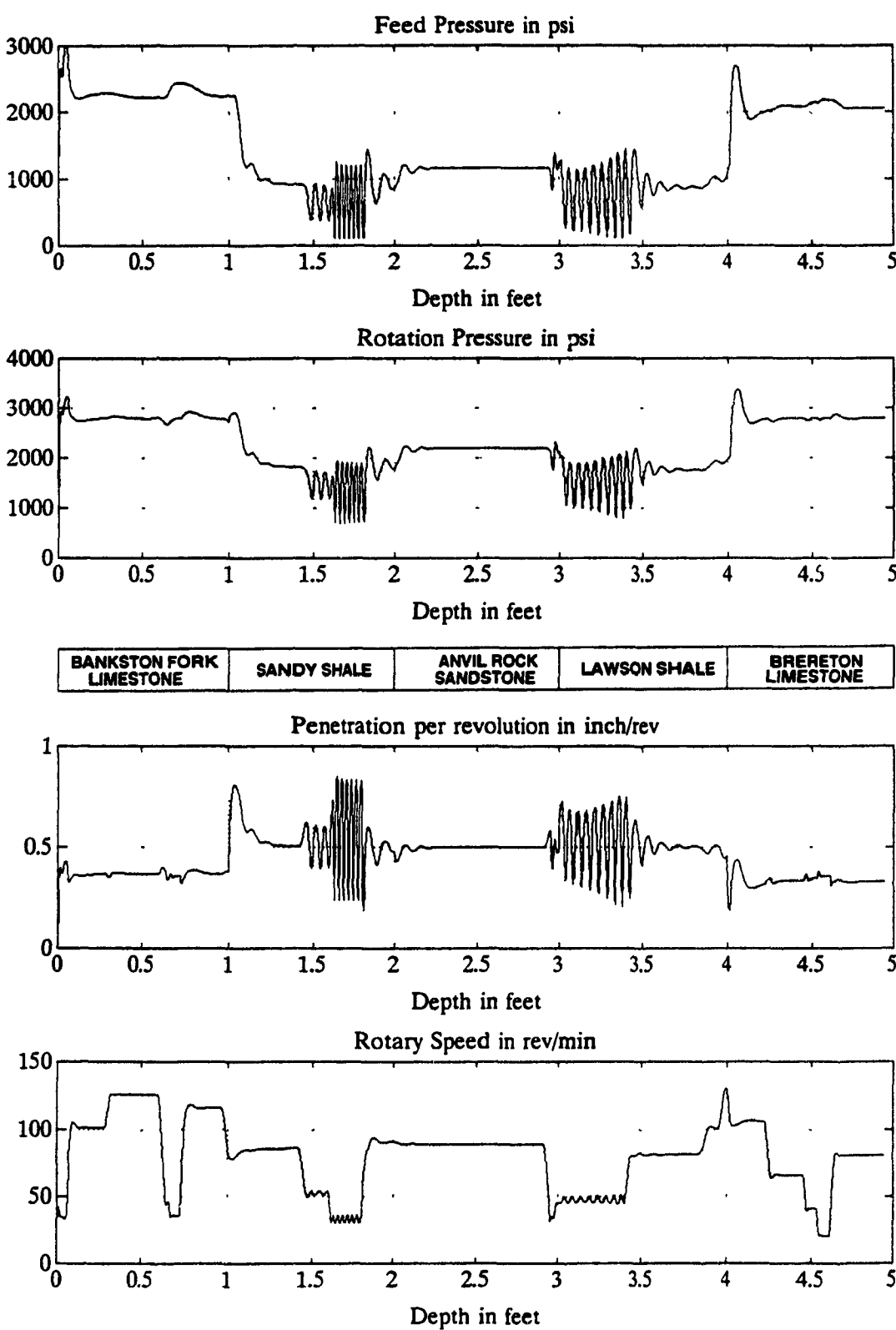


Figure 8.5: Simulation results of controller and plant at variable rotary speed, with $K_P = 4000$, $K_I = 500$ and $K_V = 50$

The graphs show an improvement at low rotary speeds in the shales where the oscillations are damped. However, the response at the interface between Bankston Fork Limestone and Sandy Shale (e.g. from hard to soft rock) has become slower, as the penetration per revolution remains close to 0.7 *in* for an approximate distance of 0.15 *ft*.

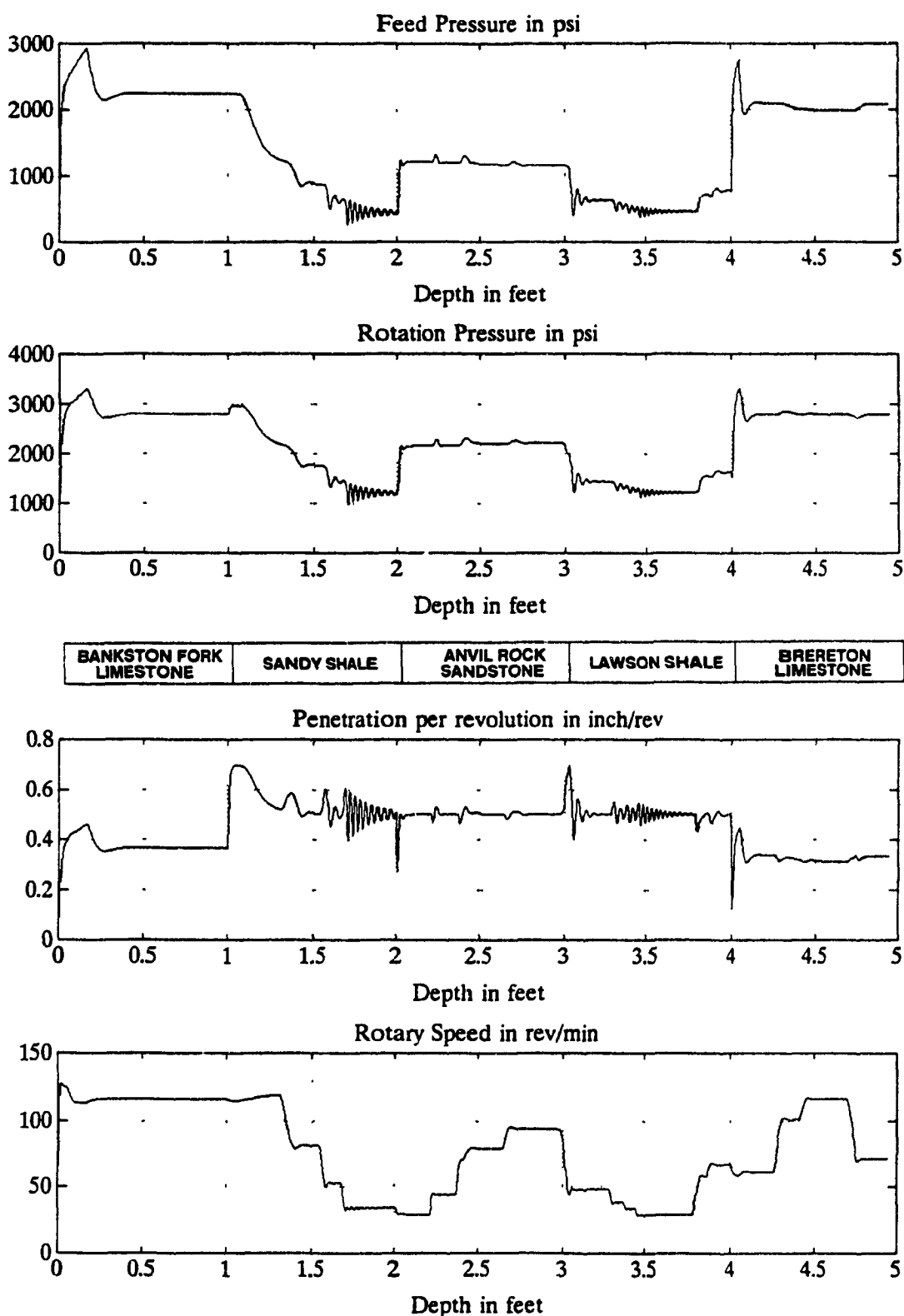


Figure 8.6: Simulation results of controller and plant at variable rotary speed, with $K_P = 2000$, $K_I = 350$ and $K_V = 50$.

8.3 Conclusion

The plant simulator built using the model equations refined in chapter 5 has been tested and validated by comparing its output to the actual data measured during field testing. It was interfaced to the controller and has proven to be an efficient tool in testing, tuning and simulating different control strategies. The plant simulator covers a range of five different rock types, from hard to soft and sticky rock types.

The controller as developed appears to work properly towards the end it was designed for. However, care must be exercised when tuning the controller gains in order to achieve the best performance at the highest system stability. The simulation has shown that the most significant disturbances occur between transitions from hard to soft rocks and drilling at low speed in shaly/sticky materials. The transition from soft to hard rock appears to be adequately handled by the controller by switching to rotation pressure regulation mode.

The oscillatory behavior observed in the shales at low rotary speed indicates the possible need for *adaptive control* for automatic drilling systems over a very diverse range of rock types, or that closed loop control of feed pressure would be disabled at low rotary speeds.

Adaptive techniques for initial tuning may also be necessary if a single controller is to be equally portable from one machine to another since the actuators and machine dynamics may vary significantly.

Chapter 9

Conclusion

9.1 Achievements

This thesis introduced a new approach for automatic rotary blasthole drilling control, based on closed loop feedback systems. The stated objectives were fulfilled by accomplishing several diverse tasks, listed below:

1. A manually operated drill rig was instrumented and tested in an open pit coal mine. The tests were aimed at refining physical models and relationships between the drilling variables. The methodology and instrumentation which were used during field testing proved adequate.
2. A comprehensive suite of software tools was developed to assist in the complicated analysis of the test results, enabling the development of the drilling model. The results were displayed in form of plots showing the variables of penetration rate, penetration per revolution and rotation pressure versus the manipulable variables of feed pressure and rotary speed in five different rock types. These plots provided a better understanding of the interaction between the drill rig and the rock in tricone bit drilling.

3. The machine actuator dynamics were identified using system identification techniques, based on field data.
4. A software simulator of the drilling process was implemented, based on the model equations derived from field testing. The simulator was validated by comparing the simulated output with actual data. It provided a flexible and powerful tool for interfacing control algorithms written in Microsoft C source code to enable testing and fine tuning them.
5. A strategy for automatic feed pressure control has been devised, based on field tests results and observations. The presented control scheme offers two regulation modes: regulation of the penetration per revolution and regulation of rotation pressure. Switching between the two modes is automatic and depends on the drilling conditions and the machine limits not to be exceeded. The control system was interfaced to the drilling simulator and tested with different controller gains. The simulation results have shown that the controller achieves the desired specifications provided the control loop gains are correctly tuned. Furthermore, the simulation has shown the possible need for adaptive control for initial tuning, and possibly for the drilling phase if the machine is drilling over a very diverse range of rock types and mainly at low rotary speeds.

9.2 Primary Research Contribution

Several empirical models relating the variables of penetration rate and rotary torque to weight-on-bit and rotary speed have been proposed in the past, however, the majority were developed in the area of oil well drilling for the petroleum industry. The models presented in the area of mining blasthole drilling were mainly derived from tests performed on homogeneous rock test slabs in the laboratory. This thesis presents new empirical models relating the same drilling variables in five different

rock types, derived from field data, where real drilling conditions were encountered.

Although automatic drilling control systems are offered by some drill manufacturers for a limited number of drill models, a new approach for automatic feed pressure control has been introduced and simulated. The simulation has proven the viability of the proposed control strategy for the problem in question. It has the merit of reducing machine wear and tear, maximizing production within the preset machine limits and prolonging the bit life by anticipating bit burying by reacting appropriately.

9.3 Industrial Relevance

Many rotary drill manufacturers have shown increasing interest in the work presented in this thesis. The presented control strategy may be adopted for their future drills, or equally serve as a basis for devising their own control strategies.

The empirical models of the drilling process and the details of building a drilling simulator can be used by the drill manufacturers to construct their own on their computing facilities. This would enable them to test their old or new control strategies. Alternatively, they can use the simulator to test the functionality of each control system they mount on a new machine.

The drilling variables relationships and interdependence presented in this thesis may prove useful to the mines themselves as they can establish some form of optimal performance criteria for the drill at the particular drilling site. The mines can thus recommend operating ranges of feed pressure and rotary speed to their drill operators, based on a a-priori approximate knowledge of the drilling bench.

The manufacturer of the bit used during field testing has also expressed great interest towards the field testing data, which relate to the bit itself and its performance. Hopefully, this contribution to their database would add improvements

in bit designs.

9.4 Recommendations for Further Work

The data acquired during field testing at the AMAX Delta mine provided a valuable database for an in-depth analysis of drilling performance in a coal mine and development of empirical models of the drilling process. However, the results were based upon a particular set of controlled field conditions, namely the drill rig, the bit type and characterized rock units at the mine.

Future work for expanding the database would focus on further field testing and analysis of the relationships between other types of rocks and bits. Also, the drilling variables could be correlated to the actual physical wear of the bit in terms of changes to insert shape/size, bearings and cone shell condition. The structural vibration of the drill rig and the drill string could be modeled as well. These additional results would be integrated into the drilling simulator.

Further in-depth theoretical synthesis of the use of adaptive control strategies for the feed pressure regulation loops could be undertaken, as well as the analysis of the stability and convergence of the adaptive schemes using applicable theory to non-linear systems.

The supervisory outer loop of the proposed strategy should be defined and simulated, mainly to test and tune it for bailing air pressure control.

Testing of the algorithms in field trials would be the next logical step. This would highlight any deficiencies in the proposed approach. Finally, an area which remains to be fully explored consists of the automatic control of rotary speed.

References

- [1] Analog Devices: *The RTI-800/815 User's Manual* 1987
- [2] Analog Devices: *The 3B Signal Conditioning I/O subsystem* 1986
- [3] Åström, K.J.:*Computer Controlled Systems* Prentice Hall 1984
- [4] Balluff inc. *Linear Displacement Transducer Series BTL; Principle of operation* 1990.
- [5] Beardsley, F. Tamrock-Driltech Internal Memorandum. Jan.9, 3p.
- [6] Cunningham, R.A.: "An empirical approach for relating drilling parameters." *Jour. Pet. Tech.* (July 1978, p.987-991).
- [7] Clausing, D. P.: "Comparison of Griffith's Theory with Mohr's failure criteria", Paper presented at Third Symp. on Rock Mech., Colorado School of Mines (1959).
- [8] Currier R.G., Project Engineer Bucyrus-Erie Company: "Status Report on Automated Drills", Presented at the O.P.M.A., Electrical Division, Annual Meeting. June 1972.
- [9] Daneshmend K.L., Peck P.J., Aboujaoude E.C., Philippe R.: *BCA Project Final Report: Research in the Control of Rotary Hydraulic Blasthole Drills* June 1991.
- [10] Doveton, J., H.:*Log Analysis of Subsurface Geology*. Wiley Interscience 1986.

- [11] Draper, N., Smith, H.: *Applied Regression Analysis, second edition* Wiley Interscience 1981.
- [12] Eitelberg, E.: "A regulating and Tracking PI(D) Controller". *Int. Journ. Control* (1987 vol. 45 pp.91-95).
- [13] El-Hadidi, M.S.M.: "The Study of Rock Properties for Prediction of Rock Drillability in Computerized Drilling Programs". M.S. Thesis, University of California, Berkeley, 1970.
- [14] Eronini, I.E.: "A Dynamic Model for Optimization and Control of Rock Drilling". Ph.D. Dissertation, Mechanical Engineering, University of California-Berkeley, 1978.
- [15] Eronini, I.E., Somerton, W.H. and Auslander, D.M.: "A dynamic model for rotary rock drilling". *Trans. ASME*, Vol.104, (June 1981), p.108-120.
- [16] Everell, M.D., Dessureault, M., Cauchon, A. and R.O. Tervo.: "A preliminary control strategy for the automatic control of an instrumented diamond drill". *Proc. 6th. Conf. Drilling and Rock Mech., Soc. Pet. Eng. AIME*, Austin, Texas, paper SPE 4235 (1973).
- [17] Fairhurst, C. and Lacabanne, W. D.: "Some principles and developments in hard rock drilling techniques", Paper presented at Annual Drill. and Blast. Symp., U. of Minnesota (1956).
- [18] Galle, E.M. and Woods, H.B.: "Best constant weight and rotary speed for lowest cost drilling". *Oil and Gas Jour.*, November 1960.
- [19] Garcia, V. M.: "Physical Properties of Mine Rock and Their Effect on Percussive Drilling", MS Thesis T-882, Colorado School of Mines (1958)
- [20] Hartman, H. L.: "Basic studies of percussion drilling", *Min. Eng.* (1959) 11, No.1.

- [21] Kuo, B.C. *Automatic Control Systems, sixth edition*, Prentice Hall, 1991. Chapter 9.
- [22] Laswell, W.M., Laswell J.L.: A three part series entitled: "The Pro's and Con's of Rotary Blasthole Drill Design", "A Supermarket of Rotary Drills", "Blasthole Drilling Doesn't Have to Be Bad". *Mining Engineering*, vol. 30 (June, July, August 1978) No. 6,7,8.
- [23] Layton Larry. Manager - Product Performance. Smith International, Ponca City, Oklahoma. Personal Communication.
- [24] Li, T.M.: "Rotary drilling with automated controls - new force in open-pit blast hole production". *Coal Age Operating Handbook of Coal Surface Mining and Reclamation*, vol. 2 (1974) Chironis, N.P, ed., McGraw-Hill Inc., New York, pp. 212-219.
- [25] Mathworks Inc. *386-Matlab user's manual* 1989
- [26] Maurer, W. C.: "Impact crater formation in sandstone and granite ", MS Thesis T-887, Colorado School of Mines (1959)
- [27] Maurer, W.C.: "The perfect cleaning theory of rotary drilling. *Jour. Pet. Tech.*, (November 1962, p.1270-1274).
- [28] Oppenheim A. V., Schafer R. W.: *Discrete-time signal processing*. Chapter 7 Prentice Hall 1990
- [29] Palm, J.W. *Modeling, Analysis and Control of Dynamic Systems* . John Wiley & sons 1983.
- [30] Simon, R.: *Collected Reports*, Drilling Research Institute (1949-1953).
- [31] Simon, R.: "Discussion of a Laboratory Study of Rock Breakage by Rotary Drilling". *Jour. Pet. Tech.* (Dec. 1959) 78A-80

- [32] Simon,R.: "Energy Balance in Rock Drilling", paper SPE 499 presented at the 1963 SPE Conference on Drilling and Rock Mechanics, Austin, TX, Jan. 23-24.
- [33] Somerton, W.H.: "A Laboratory Study of Rock Breakage by Rotary Drilling", *Trans., AIME* (1959) **216**, 92-97
- [34] Teale, R.: "The Concept of Specific Energy in Rock Drilling", *Intl. Jour. Rock Mech. Mining Sci.*, **2**, 57-73
- [35] Texas Instruments: *Linear and Interface Circuit Applications, volume 1* 1986
- [36] Warren, T.M.: "Drilling model for soft formation bits." *Jour. Pet. Tech.*, (June 1981) **33**.
- [37] Warren, T.M.: "Factors Affecting Torque for a Tricone Bit", *Jour. Pet. Tech.*, (Sept 1984) p.1500-1508.
- [38] Worsley, R.: "Energy, Impulse, and Velocity Effects in Fracturing Produced by Chisel Bits in a Limestone", MS Thesis T-908, Colorado School of Mines (1960)
- [39] Wijk, G. Atlas Copco AB. "Rotary Drilling Prediction". *Int. J. Rock Mech. Min. Sci. & Geomech. Abstr.* 1991 Vol. 28 pp. 35-42
- [40] Young, F.S.: "Computerized drilling control". *Jour. Pet. Tech.* (April 1969) p.483-496.